Winter 2021

UNMANNED AERIAL SYSTEMS (UAS) AS A TOOL FOR INVESTIGATING EDGE INFLUENCES IN NEW HAMPSHIRE FORESTS

Heather Marie Grybas
University of New Hampshire

UNMANNED AERIAL SYSTEMS (UAS) AS A TOOL FOR INVESTIGATING EDGE INFLUENCES IN NEW HAMPSHIRE FORESTS

By

Heather Grybas

B.S. Environmental science and Management, University of Rhode Island, 2012

M.S. Natural Resources, University of New Hampshire, 2015

DISSERTATION

Submitted to the University of New Hampshire

in Partial Fulfillment of

the Requirements for the Degree of

Doctor of Philosophy

In

Natural Resources and Environmental Studies

December 2021

This dissertation was examined and approved in partial fulfillment of the requirements for the degree of Doctor of Philosophy in Natural Resources and Environmental Studies by:

Dissertation Director, Dr. Russell G. Congalton, Professor of Remote Sensing and Geographic Information Systems, University of New Hampshire

Dr. Mark Ducey, Professor of Forest Biometrics and Management, University of New Hampshire

Dr. Meghan MacLean, Lecturer of Quantitative Ecology, University of Massachusetts-Amherst

Dr. Jenica Allen, Campus Living Lab Manager, Mount Holyoke College

Dr. Thomas Lee, Associate Professor Emeritus of Forest Ecology, University of New Hampshire

On August 26th, 2021

Approval signatures are on file with the University of New Hampshire Graduate School

ACNOWLEDGEMENTS

I would first and foremost like to thank my advisor, Dr. Russell Congalton, for offering me this opportunity and more during my career here. You made sure I had the equipment I needed, the drones were repaired, and that I could feed myself even when you did not have to. I would also like to thank the rest of my committee members: Dr. Mark Ducey, Dr. Meghan MacLean, Dr. Jenica Allen, and Dr. Tom Lee for your assistance with this process.

Thank you to Blue Hills Foundation Inc. for generously allowing me to conduct my research on their lands. Thank you to Philip Lovejoy for helping to coordinate my UAS data collections and George Lovejoy Jr. whose dedication to conservation resulted in the Blue Hills Foundation conservation lands where much of this research was conducted and whose backyard served as a landing area for many UAS missions. While I only had the opportunity to talk with George a few times, I could sense his love of this area and his passion. Thank you, George, for helping to leave New Hampshire with this beautiful gift.

I would like to thank my BASAL lab mates from throughout the last six years. There have been many of you; Kamini Yadav, Christine Healy, Katie Moran, Peijun Sun, Molly Yanchuck, Ben Fraser, and Jianyu Gu. You have all helped me in some way, whether it be in the field, in the lab, or at the bar with a good beer. I am especially grateful for Jianyu Gu. Your assistance with data collection and coding the last few years has been invaluable but even more so has been your friendship. I do not know where I would be right now without your willingness to drop everything and help me. I would also like to thank the undergraduate students that have supported my work,

Vincent Pagano, Hannah Stewart, and Jacob Dearborn. Sorry for the boring days watching the drone and identifying trees for me.

My friends, Christine, Rue, Katie, and Kim, the nature weirdos. Your friendship means more to me than you even know. These last few years have been hard, and you have been my steadfast supporters during the battle. Thank you for lending me your ears, beers, and cheers. You are probably the most important thing to come out of all of this.

Finally, my family. Truly, without you, none of this would have happened. The universe gifted me this amazing group of people to share my life with. You have surrounded me with love and support throughout this journey, thank you. To my parents, you have been my rock. You lifted me up during my lowest points. You have been my biggest cheerleaders throughout my whole life let alone this PhD. I love you so much. Lastly, to Khaleesi, my dog, bark bark bark bark, woof.

This research was made possible thanks to the financial assistance of the Department of Natural Resources and the Environments teaching assistantship program funded by the University of New Hampshire, the New Hampshire Agricultural Experiment Station, and by the USDA National Institute of Food and Agriculture McIntire-Stennis Project MS-77 and MS-95, and the University of New Hampshire Dissertation Year Fellowship.

TABLE OF CONTENTS

LIST OF FIGURES

LIST OF TABLES

ABSTRACT

UNMANNED AERIAL SYSTEMS (UAS) AS A TOOL FOR INVESTIGATING EDGE INFLUENCES IN NEW HAMPSHIRE FORESTS

By

Heather Grybas

University of New Hampshire, December 2021

The continued decline in forest cover across New England becomes more concerning when faced with the fact that these same forests may be playing an important role in the fight against climate change. New Hampshire, in particular, is experiencing a 0.27% annual net loss in forest cover as of 2018. Increased population growth and accompanied development has resulted in the removal of forest cover and the fragmentation of once continuous forest blocks. Fragmentation can lead to further degradation of the remaining forest stands via alterations of the biotic and abiotic process at their edges. The use of unmanned aerial systems (UAS) is becoming an important tool to ensure the sustainable management of current forests stands and may help to better understand the effects of fragmentation at forest edges. Because of the relatively recent arrival of this technology, effective and appropriate testing for accurate and efficient data collection is necessary. Furthermore, UAS have not been employed yet to detect edge effects.

This research investigated the impacts of UAS flight parameters on the accuracy of canopy height estimates made from UAS data by comparing UAS estimates across twelve combinations of

flying height and image overlap to ground measured canopy height. A multi-temporal approach to species level mapping with UAS imagery was tested by collecting multiple dates of UAS imagery from early spring to late summer and assessing whether the inclusion of one or more dates improved classification accuracy. Additional comparisons between RGB and multi-spectral cameras were carried out. Finally, UAS imagery was used to measure and assess the changes in canopy cover with increased distance from the edge. This trend was compared to trends in canopy cover measured on the ground.

The results show that flying height had no impact of the accuracy of the height estimates made from UAS data and increasing forward image overlap resulted in a significant but minor increase in accuracy. Classification accuracy was improved with the use of multi-temporal data collection but no more than three dates of optimally timed imagery was necessary. Additionally, the RGB imagery produced maps with consistently higher accuracy than the multi-spectral sensor employed in this study. Finally, we were able to detect and measure a significant trend in canopy cover that mimicked the trends found on the ground. The results of the first two parts of this dissertation will go on to provide guidance to forestry practitioners on how to collect UAS that balances accuracy and efficiency, thus reducing project costs. The final result serves as an initial demonstration of utilizing UAS for understanding edge effects and opens the door to better understanding the impacts of fragmentation over larger areas.

CHAPTER 1

INTRODUCTION

It has been increasingly recognized that New England forests are an important carbon sink in the ongoing fight against climate change (Birdsey and Heath, 1995; Goodale et al., 2002; Zheng et al., 2011; Pugh et al., 2019; Finzi et al., 2020). The land use history of the region has resulted in relatively young forest stands, still growing and sequestering carbon. The continuous decline in forest cover across New England is a serious concern in the face of this information (Zheng et al., 2010; Jeon et al., 2014; Ducey et al., 2016; Olofsson et al., 2016). New Hampshire, the second most forested state in the country, has been experiencing an increasing annual net loss of forest cover; almost doubling from 0.14% per year between 1996 and 2001 to 0.27% / year between 2010 and 2018 (Grybas et al., 2020). Much of the loss is occurring in the more urbanized counties in southern New Hampshire (Ducey et al., 2016; Grybas et al., 2020). U.S Census Data shows that these counties, Merrimack, Strafford, Rockingham, and Hillsborough County, have all seen population increases greater than 49% between 1980 and 2019 (https://data.census.gov/cedsci/). This increasing population growth has led to increased development and the fragmentation of continuous forest stands into smaller blocks, with more predicted to occur in the future (Vogelmann, 1995; Zankel et al., 2006). There are two consequences of fragmentation. First is the complete removal of the original forest and the important ecological services and communities that forest provided (Rustad et al.,

2012; Mitchell et al., 2015). Second is the potential modification of the remaining forest by exposing the forest fragment edges to conditions that alter the original ecosystem (Ranney et al., 1981; Saunders et al., 1991). It is becoming more important that we attempt to characterize and quantify the extent of these changes in the forest in order to understand the effects of future fragmentation and develop potential mitigation strategies, especially in the face of climate change, which is expected to alter these conditions further (Reinmann and Hutyra, 2017). Additionally, land managers will require detailed, accurate information on composition and structure of the remaining stands if they are to make management decisions that can help preserve the conditions/services of the remaining patches and combat the influences at the forest edges (Wilcove et al., 1986; Brosofske et al., 2014). Current advances in remote sensing technology may allow both these needs to be met more efficiently and accurately compared to traditional ground-based methods.

Exposure of the forest to the surrounding land cover matrix leads to edge influences (EI), the effect of abiotic and biotic processes at the edge that results in changes in structure, composition, and function within the forest near the edge (Chen et al., 1992; Murica, 1995; Harper et al., 2005). In general, there is greater light availability, temperature variability, and wind as well as increased access to organisms and materials like pollen and seeds immediately following the edge creation (Saunders et al., 1991; Matlack, 1993; Laurance et al., 2002; Harper et al., 2005). These direct effects of edge creation influence ecological processes (e.g., productivity, evapotranspiration, decomposition, recruitment, and mortality) which lead to changes in the forest structure (e.g., over and understory cover and density) as well as composition. Invasive species richness and cover has also been found to be positively correlated with forest edge habitat (Brothers and Spingarn, 1992; MacQuarrie and Lacroix, 2003; Pauchard and Alaback, 2006; Allen et al., 2013). Invasive plants not only out outcompete native plants, but also support fewer insect and birds species (Frappier et al.,

2003; Tallamy and Shropshire, 2009; Narango et al., 2018). The area of edge influence (referred to as forest edge habitat), is the area within a forest patch that is exposed to EIs and is thus undergoing changes (Harper et al., 2005). Edge habitat may be less suitable for many of the species that once resided in and/or relied on the non-impacted interior forest habitat (i.e., core area), effectively making the remaining forest patch smaller for them to survive in, assuming the patch is large enough to still contain core area (Murica, 1995). As fragmentation continues, patches become smaller and more irregularly shaped, causing them to be increasingly dominated by edge habitat (Ries et al., 2004). When fragmentation on the landscape scale is large enough, whole species can be pushed out of the area (Riitters et al., 2002; Fahrig, 2003; Haddad et al., 2015)

Remote sensing offers an efficient and effective opportunity to quantify the structure and composition of forests (edges and interiors) over larger spatial areas than is possible with expensive and time-consuming fieldwork. These datasets provide a means of studying ecological phenomena over broader spatial and temporal scales than fieldwork alone (Kerr and Ostrovsky, 2003; Vierling et al., 2008; Wiens et al., 2009; Anderson and Gaston, 2013; Nagendra et al., 2013). Satellite or airborne remotely sensed data have traditionally been used for these purposes, but they pose several challenges. Satellite imagery is very appealing because the extent of a single scene can be regional to global in scale and many satellites have repeat collections (Gould, 2000). However, much of the freely available imagery does not have spatial or temporal resolutions that are appropriate for many fine-scale ecological phenomena. Imagery from commercial satellites that offer higher spatial resolutions are expensive and are not collected continuously (Wulder et al., 2004; Loarie et al., 2007; Anderson and Gaston, 2013). Manned aircraft can be flown on demand and capture very-high spatial resolution imagery but require considerable planning and the acquisition costs are high (Anderson and Gaston, 2013; Cruzan et al., 2016). Recently, technological advancements have made unmanned

aerial systems (UAS) more affordable. As a result, they are experiencing a rapid adoption for remote sensing research, especially in the field of forestry (Whitehead and Hugenholtz, 2014b). The appeal of UASs lies in its flexibility. They can be deployed on demand over specific areas of interest. They are modifiable to meet user needs; one aircraft can be mounted with a multitude of different sensors to capture the information of interest. Finally, and most importantly, they can collect ultra-high spatial resolution imagery at a much lower cost relative to traditional satellite or aerial platforms (Anderson and Gaston, 2013). UAS will move remote sensing research to scales previously difficult to achieve with even the highest resolution data available (Anderson and Gaston, 2013; Cruzan et al., 2016).

Measures of forest structure and composition have been made from remotely sensed data for decades (Wulder et al., 2004). Light detection and ranging (LiDAR) data has been very popular for estimating forest structure (Næsset and Okland, 2002; Maltamo et al., 2005; Morsdorf et al., 2006). However, the cost of collecting the data and the technical skills to process it have long been barriers for wider implementation (Colomina and Molina, 2014; Puliti et al., 2015; Zielewska-Büttner et al., 2016). Photogrammetry, the process of making measurements from overlapping imagery, has been a means of extracting information about height since WWI, but has not seen widespread implementation due to a number of hardware limitations and very rigorous collection protocols (Smith et al., 2016). Recent advancement in computer vision as well as improvements in computer hardware have brought it into the 21st century through a process known as Structure-from-Motion (SfM) which allows similar 3-dimensional information to be extracted from imagery (Westoby et al., 2012). SfM outputs can include incredibly dense 3D point clouds similar to that of LiDAR (Westoby et al., 2012; Whitehead and Hugenholtz, 2014a). When the sensor is mounted on a UAS, the combination (UAS-SfM) becomes a powerful tool for studying forests (Getzin et al., 2014; Dandois

et al., 2015; Puliti et al., 2019). However, the SfM data products, while similar to LiDAR, are inherently different and highly influenced by the chosen parameters for the UAS mission (Dandois et al., 2015). The relatively recent introduction of UAS and SfM into forestry means, much like the early days of LiDAR, a thorough understanding of the impacts of how it is collected/generated and where it can be used is necessary to ensure management decisions based on the extracted information are sound.

In general, information on the species composition of a forest stand serves several important purposes such as monitoring biodiversity (Saarinen et al., 2018), assessing forest health (Michez et al., 2016b), precision forestry (Goodbody et al., 2017), or acting as inputs for species specific allometric models (Alonzo et al., 2018). Remotely sensed imagery has been a quick and efficient means to produce land cover/land use maps, including maps of forest type (Franklin and Wulder, 2002; Wulder et al., 2004). However, when mapping tree species, traditional remote sensing platforms are incapable of providing the temporal and/or spatial resolutions necessary for this scale of analysis at an affordable cost (Anderson and Gaston, 2013; Cruzan et al., 2016). Orthomosaics produced from the UAS imagery, on the other hand, have an incredibly high, up to centimeter, spatial resolution and open up an interesting opportunity to explore individual tree detection and classification to the species level (Nevalainen et al., 2017). The forests of New Hampshire, however, are highly variable and complex, making them far more difficult to classify accurately (Mickelson et al., 1998; Justice et al., 2002; MacLean and Congalton, 2013). Additionally, many UAS typically carry smaller, consumer grade cameras that sense in the visible range of the electromagnetic spectrum (i.e., blue, green, and red light) which may not be as useful for vegetation mapping at the species level (Jensen, 2016). Further, work on methodologies that help maximize the accuracy of species-

level forest maps while helping to maintain the low cost of the UAS platform would be highly beneficial to the remote sensing community as a whole.

The benefits of UAS to the forestry community are numerous. However, unlike traditional platforms that collect remotely sensed data, which have been studied and tested for decades, UAS have only recently risen to operational feasibility and come with their own limitations. While it is important to start testing applications and understanding its place in forestry, it is just as important that we investigate different methodologies and develop best practices to help ensure the accuracy of the desired products/information while maintaining efficiency (Manfreda et al., 2018). Thus, this dissertation sought to test UAS methodologies for extracting structural information and composition as well as introduce a new application of UAS. More specifically:

1. **Determine the effects of flight configuration (flying height and image overlap) on the accuracy of tree height estimates.**
2. **Investigate whether multi-temporal classification of UAS imagery, collected by both a standard RGB and multispectral camera, improves the accuracy of forest composition maps produced from both.**
    - **2.1. Investigate the optimal phenological window for improved accuracy and efficiency of data collection.**
    - **2.2. Compare the accuracy of the maps produced by RGB and multispectral imagery.**
3. **Evaluate the capability of UAS to detect and measure edge effects**

This research was accomplished through the collection of new UAS imagery and ground data across several sites. A systematic collection of several forest plots was carried out using varying combinations of flying height and image overlap. Tree height estimates were made from the imagery collected using these combinations, compared to ground data on tree height to measure accuracy, and the effects of flying height and overlap on accuracy evaluated. Multi-temporal data collection with the UAS was carried out over a complex forest stand using two different sensors. Varying combinations of dates of imagery were classified and the accuracies compared within and between the sensors used. Finally, edge effects were measured across a forest edge using both ground-data and UAS derived data on structure. The measured effects were compared between methods.

CHAPTER 2

LITERATURE REVIEW

To understand the previous work that is the basis of this study, three major bodies of knowledge will be reviewed: 1) measuring forest structure from remotely sensed data; 2) classifying vegetation from remotely sensed imagery; and 3) estimating edge influence in forested ecosystems.

Measuring Forest Structure from Remotely Sensed Data

Effective and sustainable management of forested ecosystems requires detailed and accurate information about structure (Brosofske et al., 2014). As forest management moves from the stand level to regional or operational scales, there is a need for detailed forest inventory data across large, contiguous areas; however, this need cannot be filled by traditional field inventories alone (Brosofske et al., 2014). Managers have been able to leverage the broader spatial scale of remotely sensed data to meet this need.

LiDAR is a popular source of information for structural estimates given its ability to penetrate and see into the open spaces within forest canopies (Lim et al., 2003; Wulder et al., 2008; Woods et al., 2011; Wasser et al., 2013). LiDAR is an active sensor that emits its own pulses of light or energy and registers the energy reflected back at it as a return. Based on the time between emitting the pulse and detecting the reflected energy, the elevation of that return can be calculated. Energy from the

pulse that is not reflected can continue to reflect off other surfaces so long as there are openings for it to pass through (White et al., 2013). Because of this, LiDAR is capable of capturing returns from the canopy envelope as well as within the tree crown because tree canopies are porous. LiDAR, therefore, provides 3-dimensional information about forests, both horizontal and vertical distributions of the forest structure which are highly correlated with numerous structural metrics; optical sensors can only provide horizontal (Næsset, 2002; Lim et al., 2003; Coops et al., 2007; van Leeuwen and Nieuwenhuis, 2010; ver Planck et al., 2018).

. This correlation allows estimates of forest structure to be made from the LiDAR data itself. Descriptive information about the LiDAR data, whether it be full waveform, point clouds, or raster, are used as the explanatory variables in models predicting the variable of interest (e.g., basal area, volume, above ground biomass, and height) across a larger area of interest (Lefsky et al., 1999; Næsset, 2002; Maltamo et al., 2011; White et al., 2015). Ground samples collected by traditional forest inventory or other sources act as the training/validation. Because LiDAR provides a substantial benefit to the forestry community in their efforts to properly manage their forest stands, the accuracy of LiDAR-based structural estimates and the factors that impact it have been heavily studied for some time (e.g., Næsset, 2004; Morsdorf et al., 2006; Hawbaker et al., 2010; Hamraz et al., 2016; Kükenbrink et al., 2017). Many studies have looked into the impacts of forest composition and structure (Villikka et al., 2012; Wasser et al., 2013), LiDAR specification (Næsset, 2005; Jakubowski et al., 2013; White et al., 2015), reference data sampling designs (Ruiz et al., 2014), and predictive model types (Penner et al., 2013) on estimates. In general, the process of converting LiDAR data into reliable estimate of structure are well understood (White et al., 2013). However, the high cost of the data continues to limit its operational feasibility (Wulder et al., 2008; Brosofske et al., 2014).

The recent arrival of affordable civilian UAS combined with SfM techniques has fostered new possibilities when it comes to mapping and estimating forest structural properties at a fraction of the cost (Puliti et al., 2015). Prior to SfM, the extraction of 3-dimensional information from imagery was accomplished using photogrammetry. Traditional photogrammetry could only be achieved with imagery collected by expensive, precisely calibrated (i.e., metric) cameras with rigorous flight geometry requirements (McGlone, 2013). SfM, while built upon these photogrammetric concepts, is a low-cost means of collecting similar 3-dimensional information from unordered imagery captured with inexpensive, non-metric sensors such as consumer-grade digital cameras (Snavely et al., 2008). Additionally, there are now a number of easy-to-use software packages, both free and commercial, as well as web-based applications that have automated the SfM process, making it easier to use (Micheletti et al., 2015). SfM allows researchers to overcome the issues associated with using uncalibrated, consumer-grade cameras and inexpensive GPS units for photogrammetric measurements and takes advantage of the high spatial and temporal resolution, operational flexibility, and low acquisition costs associated with the UAS platform (Lisein et al., 2013; Iglhaut et al., 2019).

By combining the UAS imagery and SfM processing, high-density, image-based point clouds that are similar to LiDAR-based point clouds can be generated quickly (White et al., 2013). It is important to note that while similar, the way the 3D information is collected/extracted by LiDAR and SfM is entirely different thus, they are not considered interchangeable. LiDAR, an active sensor, emits its own energy capable of passing through openings in the forest canopy. The SfM process is solely reliant on imagery captured by passive sensors.

The general SfM process first requires the identification of unique features in each image that are then matched using computer vision (Westoby et al., 2012). These matched points, often referred

to as tie points, are then used to estimate the interior and exterior orientation parameters of the camera for each image. Using the estimated orientation parameters, the coordinate (x,y) and the height (z) of each tie point is estimated resulting in what is known as a sparse point cloud (Dandois and Ellis, 2013; Lisein et al., 2013). The density of the result is increased using a process known as Multi-View Stereo (MVS), which carries out further feature matching, increasing the point density by orders of magnitude.

Given how important 3-dimensional measurements of forest stands have been in forestry and the greater flexibility/lower cost of the UAS platform, it is no surprise that there have been a number of studies assessing the feasibility of using UAS-SfM data in place of LiDAR. Several studies have now investigated the use of UAS-SfM point clouds to estimate forest structure, comparing their results against LiDAR-based points clouds (Dandois and Ellis, 2010; Lisein et al., 2013; Vastaranta et al., 2013; Ota et al., 2015; White et al., 2015; Wallace et al., 2016; Ni et al., 2018). Vastaranta et al. (2013) and Wallace et al. (2016) found that the UAS-SfM was just as accurate as the LiDAR at characterizing the upper canopy height and thus performed just as well at estimating several structural metrics strongly related to canopy height such as dominate height, basal area, and volume (White et al., 2013; Pitt et al., 2014). Both studies note the simplicity of the stands within which they were working, even-aged, single level, or spare forest. However, when White et al. (2015) made the comparisons in a more complex coastal forest environment, they too found the metrics to be similar.

What has become clear is the quality of the UAS-SfM point clouds has an impact on the quality of the estimations and the quality of the UAS-SfM point cloud is controlled by the UAS imagery (Iglhaut et al., 2019). The SfM process hinges on the ability to locate features in the imagery and then match them across multiple images. Several papers have discussed factors that influence the image matching and thus the SfM output (Whitehead and Hugenholtz, 2014a; Manfreda et al.,

2018; Iglhaut et al., 2019) such as image resolution, image overlap, sun-angle, surface texture, and repetitive objects. Some factors are out of the control of the UAS pilot or difficult to control/avoid, however, some such as the flight parameters entirely are. Iglhaut et al., (2019) and Manfrada et al., (2018) recently called for more research into the effects of flight parameters due to the significant impact it has on the SfM process. Research into the matter has only recently begun and so far, spans a number of different forest types, variables, and UAS platforms (Dandois et al., 2015; Torres-Sánchez et al., 2017; Ni et al., 2018; Domingo et al., 2019; de Lima et al., 2021). Furthermore, some of these studies utilize LiDAR as reference data or make comparison between UAS and LiDAR metrics rather than comparisons to field data (Ni et al., 2018; de Lima et al., 2021). Much more work is needed before any generalized recommendations can be made.

Tree Species Classification

Several studies have found great success mapping species composition of vegetation from high spatial resolution satellite and aerial imagery (Sugumaran et al., 2003; Leckie et al., 2005; Pu and Landry, 2012), but these data are expensive and not always available for the desired location or time of year (Loarie et al., 2007). The low altitudes UAS fly at are easily capable of providing centimeter level imagery that can identify individual plants whenever and wherever desired (Getzin et al., 2012; Baena et al., 2017). Additionally, the flexibility of the platform allows users to control the resolution of the imagery simply by controlling flying height, thus allowing them to tailor the scale of the data to match the scale of the phenomena or features of interest (Dandois et al., 2015). There are studies that have now employed the technology in other vegetation mapping projects. For example, UAS imagery has been used to identify individual or small groupings of invasive plants (Dvořák et al., 2015; Michez et al., 2016a; Mafanya et al., 2017; Müllerová et al., 2017), shrubs,

grasses and forbs (Laliberte et al., 2010; Lu and He, 2017; Weil et al., 2017; Komárek et al., 2018; Leduc and Knudby, 2018), and wetland vegetation (Knoth et al., 2013; Durgan et al., 2020). More studies looking into using UAS-derived orthomosaics for tree species classification are starting to appear in the literature (Lisein et al., 2015; Michez et al., 2016b; Nevalainen et al., 2017; Franklin and Ahmed, 2018; Miyoshi et al., 2020). These studies are all taking advantage of the imagery's high spatial resolution to distinguish and classify individual trees or small groupings of trees of the same species with positive results.

Besides the significantly higher spatial resolution, the flexibility of the UAS platform is another major characteristic. For one, UAS platforms can be equipped with different sensors capable of acquiring information from different portions of the electromagnetic spectrum (EMS) like the visible bands (RGB), red edge, near infrared (NIR), even thermal or microwave (Colomina and Molina, 2014; Whitehead and Hugenholtz, 2014a). There are currently sensors that can collect from one to hundreds of bands that can be mounted to UAVs. Typically, though, cost and payload weight limits restrict the sensor used (Whitehead and Hugenholtz, 2014a; Baena et al., 2017). Because of this, consumer grade digital cameras are often employed in UAS studies (Laliberte et al., 2010; Niethammer et al., 2012; Hugenholtz et al., 2013; Mafanya et al., 2017; Pádua et al., 2017a). While they are light and inexpensive, the downside of employing these cameras is that they ordinarily only capture reflectance in the visible range of the EMS (i.e., RGB cameras). Typically, most land cover classifications, especially with vegetation, require multispectral sensors (MSS) with wavelengths (bands) outside of the visible range of the EMS, frequently NIR, in order to improve the distinction between classes, especially classes that are spectrally similar in the visible range like vegetation (Jensen, 2016). Many studies have modified the spectral sensitivity of the bands in the consumer grade cameras by adding or removing filters from the camera lens, usually to capture NIR reflectance

(Hunt et al., 2010; Linchant et al., 2015; Michez et al., 2016b; Lu and He, 2017; Müllerová et al., 2017; Müllerová et al., 2017). The modified cameras are not perfect substitutes for real MSS cameras. All three bands on a consumer grade camera are sensitive to NIR energy, and thus removal of the filter blocking NIR energy from reaching the sensor can cause redundant band sensitivity or spectral overlap between bands. This spectral overlap reduces the potential for discrimination between features. Nijland et al., (2014) compared RGB imagery to color infrared (CIR) imagery (green, red, and NIR reflectance) from a modified camera for monitoring plant health and phenology and found the RGB imagery to be superior due to poor band separability with the modified camera. Lisein et al., (2015) and Michez et al., (2016b) both compared the performance of RGB imagery from an unmodified camera and CIR imagery collected from a modified camera for tree species classification and found the RGB imagery performed better. They suggest that the redundant sensitivity between the bands, after modifying the camera, reduced the ability to discriminate between species using CIR imagery. Ahmed at al., (2017) did a comparison between imagery collected from an RGB camera and a multispectral (MSS) camera specifically designed to sense wavelengths outside of the visible range for tree species classification, and found an improvement in accuracy with the MSS imagery. However, multispectral cameras can be more expensive (Whitehead and Hugenholtz, 2014a; Manfreda et al., 2018; Tmušić et al., 2020) and thus more cost-effective methods of accurately generating this information would help make UAS more operationally feasible.

Taking advantage of the UAS' temporal flexibility may help to overcome limitations in sensor spectral resolution (Key et al., 2001). The temporal flexibility of the UAS platform is considered one of its major advantages over other remote sensing platforms (Anderson and Gaston, 2013; Brosofske et al., 2014; Colomina and Molina, 2014; Manfreda et al., 2018). UAS can be flown on demand and thus flown at a temporal resolution appropriate for certain phenomena, for example phenology.

Vegetation will exhibit changes in its spectral reflectance properties as they progress through their phenological cycle. Additionally, phenology tends to differ between species (e.g., some species may start senescence earlier than others may) so, with an appropriately timed series of images, multiple species can be differentiated (Fassnacht et al., 2016). In a multi-temporal classification, multiple dates of imagery are used to create a single land cover map (MacLean and Congalton, 2013). By using multiple dates of imagery collected through the growing season, the spectral differences within and between species during this period can be used to improve the accuracy of the map; something very important in heterogeneous areas with several, spectrally similar species such as New England (Mickelson et al., 1998; Justice et al., 2002; MacLean and Congalton, 2013).

Several studies have demonstrated the advantages of a multi-temporal classification for mapping forest composition with moderate resolution satellite imagery. It should be noted that these studies are typically classifying species mixtures rather than singular species since the spatial resolution is usually larger than most tree crowns (Treitz and Howarth, 2000; Wulder et al., 2004; Fassnacht et al., 2016). Only in situations where stands match the pixel size and consist of only one species, could it then be considered species classification (Fassnacht et al., 2016). Wolter et al., (1995), Mickelson et al., (1998), Zhu and Liu (2014), and Pasquarella et al., (2018) all utilized multiple dates of Landsat imagery for species classification and found improved accuracy over using a single date (mono-temporal classification). Mickelson et al. (1998) in particular found the multi-temporal approach significantly improved the classification of forest composition in the northeastern U.S., where forests are highly heterogeneous and difficult to classify. Landsat is an appealing tool for multi-temporal vegetation classification. In addition to the imagery being continuously collected and freely available, it has a higher spectral resolution than many higher spatial resolution satellites or aerial sensors. Furthermore, at a 16-day revisit period (expected to decrease to 8 days with the

launch of Landsat 9); its temporal resolution is well within what is necessary to capture phenological changes. However, at a 30m spatial resolution, a single pixel would cover several, potentially different species creating a mixed spectral response and cloud contamination can hinder gathering enough images to properly capture phenology (Loarie et al., 2007).

The use of high spatial resolution imagery for multi-temporal species classification is uncommon (Hill et al., 2010; Immitzer et al., 2012; Tigges et al., 2013; Li et al., 2015) and the quantity of very high spatial resolution (sub-meter), non-UAS imagery is scarce, mainly due to high costs for both (Lisein et al., 2015). Key et al. (2001) used small-format 35mm true color and false color aerial photos (36cm spatial resolution) acquired across the growing season to discriminate between four deciduous species. The aerial imagery utilized in the study was very similar to that of UAS imagery in that it had very few spectral bands. They found the accuracy of the classification improved when the additional dates of imagery were added. These authors go on to state that multi-temporal classification may help to overcome limitations of spectral resolution. While several studies have taken advantage of the temporal resolution of the UAS for other applications (Niethammer et al., 2012; Lucieer et al., 2014; Du and Noguchi, 2017; Kohv et al., 2017; Pádua et al., 2017a; Torres-Sánchez et al., 2017), few have done so for tree species classification (Lisein et al., 2015; Michez et al., 2016b).

Estimating Depth of Edge Influence

Characterizing and measuring the extent of the structural changes, if any, at the forest edge is necessary in order to develop mitigation strategies as well as understand if or where non-impacted core habitat may still reside on the landscape for conservation (Ranney et al., 1981; Wilcove et al.,

1986; Laurance and Yensen, 1991). A first step in accomplishing this is to estimate the depth of edge influence (DEI) (Laurance et al., 2002; Ries et al., 2004) or the distance from the edge into the forest community over which there is a statistically significant EI (Harper et al., 2005). Once known, it is possible to then model edge habitat on the landscape scale (Ries et al., 2004).

DEI is typically determined in the field by sampling along the edge to interior gradient (Chen et al., 1992; Harper and Macdonald, 2001, 2002; Mascarúa López et al., 2006; Dupuch and Fortin, 2013; Harper et al., 2014; Eldegard et al., 2015). Transects run perpendicular to the forest edge (i.e., parallel to the gradient), with multiple transects normally collected within a patch or across multiple patches, as shown in Figure 1. The transects should be long enough that they span the full length of the gradient created by the EIs; from the edge where EIs are having the most impact, all the way to the interior forest where EIs are having the least impact. To capture this gradual change, sample plots are systematically placed along these transects (Figure 1). At each plot, one or more variables related to forest structure, composition, or processes that are believed to co-vary with distance from the edge are measured. Table 1 provides examples of some response variables that have been measured in several studies (see Harper et al., (2005) and Franklin et al., (2021) for reviews of edge influence literature). Primary responses (direct effects) result immediately or within a short time of the creation of the edge. Secondary responses (indirect effects) arise when the primary responses confound the original abiotic and biotic gradient (Harper et al., 2005).

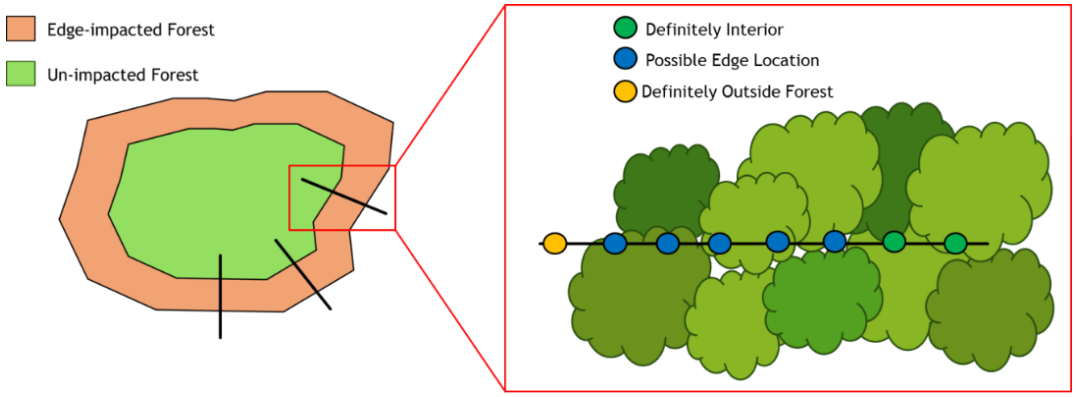

Figure 1. Diagram showing how transects and sample plots are typically set up to determine depth of edge influence.

Table 1.Some examples of commonly measured response variables used to estimate depth of edge influence from Harper et al., (2005)

Response Type	Variables
Primary	Tree Mortality
	Canopy Cover
	Snags and Logs
Secondary	Recruitment
	Canopy Growth
	Shrub Abundance
	Understory Density
	Exotic Species Abundance
	Changes in Species Composition

The structure of the forest edge plays an important role in not only the DEI but also the magnitude of edge influence (MEI), or the extent to which a particular variable differs between the edge and the reference or interior forest (Ries et al., 2004; Harper et al., 2005; Esseen et al., 2016). The structural characteristics of the edge and forest stand can alter the EI by controlling how energy, materials, and species move across the edge (Ries et al., 2004; Harper et al., 2005; Esseen et al., 2016). For example, edge maintenance, orientation, age, and species composition have been found

to alter EI at the forest edge (Matlack, 1993; Harper et al., 2005; Esseen et al., 2016). At maintained edges, the structure of the non-forest community is conserved through regular maintenance. Maintained edges usually occur where forests abut agricultural land or open fields, where regeneration is suppressed, and therefore remain open much longer. At regenerating edges, tree recruitment is not suppressed, and the edge is allowed to close up (Didham and Lawton, 1999). South facing edges typically have greater DEI than north face edges, in the northern hemisphere, due to the increased amount of light that the edge receives (Chen et al., 1992; Matlack, 1993). EI has also been shown to decrease with time since creation (Harper et al., 2015), probably as a result of forest regeneration or closure at maintained edges as a side wall of dense vegetation develops over time (Matlack, 1993; Didham and Lawton, 1999). Finally, composition may play a very important role in determining DEI. Tree species differ in terms of their tolerance to the conditions experienced at forest edges (Chen et al., 1992; Harper et al., 2005). Harper et al. (2005) suggested that landscapes with greater heterogeneity might have more pioneer, edge-adapted species present in the landscape and therefore lower DEI. Stands with abundant pioneer species are better able to withstand highly variable edge conditions, while coniferous species, especially shade-tolerant species, are less flexible (Esseen et al., 2016). In general, distinct differences in DEI have been found when comparing broad forest community types (e.g., boreal, temperate, tropical). For example, tropical forests have been found to exhibit much larger DEI than boreal forest communities (Harper et al. 2005; Franklin et al., 2021). The result is significant variation in EI over a landscape and thus variation in DEI (Pinto et al., 2010; Ibáñez et al., 2014).

These factors should be accounted for so that accurate DEI measurements and therefore reliable models of edge habitat on a landscape can be generated (Laurance and Yensen, 1991; Didham and Lawton, 1999; Ries et al., 2004). However, the variability in EI makes it difficult to accurately

measure edge depth at this scale without extensive fieldwork (Dantas De Paula et al., 2016; MacLean, 2017). Measures of forest structure, commonly used in studies of edge influences to describe forest edge habitats, have been made from remotely sensed data for decades (Wulder et al., 2004). Given the broader extent of many remotely sensed datasets, several studies have now attempted to make use of these data for investigating edge influences and calculating DEI by assessing changes in remote sensed estimates of structure with distance. MacLean (2017) took advantage of LiDAR's ability to penetrate beyond the upper canopy in order to measure changes in understory canopy cover along the edge to interior gradient. The DEI estimated from ground sampling was compared to DEI estimates based on the structural attributes collected from the LiDAR data. They found no significant difference between the estimates, indicating that LiDAR may make an effective alternative to traditional field sampling. Vaughn et al., (2014) took more of a landscape approach and utilized LiDAR to estimate impacts of fragmentation on forest canopy structure cross an 8500ha area in Hawaii. Given the extent of the data, the authors were able to investigate the effects of EI across 1060 forest fragments using thousands of pixels as individual sample points; much more than has been studied using traditional fieldwork. Similarly, Dantas De Paula et al. (2016) utilized a Landsat Tree Cover dataset (Sexton et al., 2013) to investigate changes in canopy cover with distance from a forest edge at 11 study sites across 5 continents, finding significantly lower canopy cover near edges. These studies demonstrate the usefulness of remotely sensed data for investigating edge influences and measuring DEI. However, as noted previously, LiDAR data can be expensive to collect, outdated, or lacking the specifications necessary to appropriately measure EIs (e.g., Leaf-on data would be better for capturing understory and over story density/cover). Additionally, the LANDSAT Tree Cover data or similar products like the National Land Cover Data (NLCD) Tree Cover dataset (https://www.mrlc.gov/finddata.php) are mapped at a 30m spatial resolution. At this resolution, a

pixel would cover the extent of most edge effects. For example, in a review of measured DEI for a variety of response variables, DEI, on average, was 20m to 25m for canopy and understory cover and 35m to 40m for changes in species composition (Harper et al., 2005, Franklin et al., 2021).

UAS imagery is now a source of high spatial resolution forest structural information. With image resolutions reaching down to a few centimeters, the data are well within the resolution of many measured edge effects but have yet to be utilized for this purpose. In particular, canopy cover has commonly been found to experience significant impacts due to EI (Chen et al., 1992; Matlack, 1993; Gehlhausen et al., 2000; Harper and Macdonald, 2001; Mascarúa López et al., 2006) and, as suggested by the above mentioned studies, a commonly estimated attribute from remotely sensed data. UAS-SfM can produce highly dense point clouds similar to that of LiDAR data. However, it lacks the ability to capture more of the forest's vertical structure since it is restricted to what can be seen in the imagery itself (Vastaranta et al., 2013; White et al., 2015; Wallace et al., 2016). Additionally, photogrammetrically produced point clouds can exhibit horizontal voids in the data where scene reconstruction failed (Frey et al., 2018). The orthomosaics produced from the UAS imagery can have centimeter-level spatial resolutions, opening the door to fine-scale mapping of canopy gaps based on spectral data. Much of the work on mapping vegetation cover with UAS or other very-high resolution imagery has been carried out in agricultural settings to map crop cover (Song et al., 2015; Li et al., 2018; Roth and Streit, 2018; Yan et al., 2019). While these studies achieved high accuracies, they are working in areas with considerably less structural complexity relative to forests. Several studies have implemented UAS orthomosaics for canopy cover mapping in forests and achieved high accuracies (Chianucci et al., 2016; Zielewska-Büttner et al., 2016; Bagaram et al., 2018; Jayathunga et al., 2018). The results are promising but more work is needed across a variety of forest types to assess the feasibility.

CHAPTER 3

EVALUATING THE IMPACTS OF FLYING HEIGHT AND FORWARD OVERLAP ON TREE HEIGHT ESTIMATES IN COMPLEX NEW ENGLAND FORESTS USING UNMANNED AERIAL SYSTEMS (UAS)

Abstract

Unmanned aerial systems (UAS) have recently become a promising tool for sustainable forest management by providing structural information on forests across broader spatial and temporal extents for a fraction of the coast of traditional field inventorying. In particular, Structure from Motion (SfM) processing has allowed for the generation of 3-dimensional information, similar to LiDAR, to be extracted from overlapping, UAS images collected by inexpensive, consumer grade, digital cameras. The SfM process and the quality of products produced are sensitive to the chosen flight parameters. Therefore, an understanding of the effects the choice of these parameters has on accuracy will improve the operational feasibility of UAS in forestry. This paper investigated the change in the plot-level accuracy of top-of-canopy height (TCH) across three levels of flying height (80m, 100m, and 120m) and four levels of forward overlap (80%, 85%, 90%, and 95%). Estimates of TCH were extracted for all combinations of flying height and forward overlap and compared to TCH estimated from ground data. The RMSE (root mean square error) of the TCH estimates

($RMSE_{TCH}$) ranged between 1.75m and 3.20m across all missions. Flying height was found to have no significant effect on $RMSE_{TCH}$ while increasing forward overlap was found to significantly decrease the $RMSE_{TCH}$; however, the decrease was estimated to be 4mm per 1% increase in forward overlap. The results of this study suggest that flying higher will have no significant impact on the accuracy of height estimates but will save flying and processing time. Maintaining a high level of overlap will help to improve accuracies. However, results suggest that the highest levels of overlap may not be necessary.

Introduction

Forests provide numerous environmental services as well as contribute significantly to the local and global economy. A long-term challenge associated with forest management is doing so in a sustainable manner, so that the current needs are met while maintaining healthy forest ecosystems for present and future generations (MacDicken et al., 2015; White et al., 2016). To accomplish this goal, managers require spatially detailed, accurate, and timely information on wide variety of forest structural metrics (e.g., quality and quantity of forest resources) to support operational and strategic planning and monitoring (Hilker et al., 2008; Wulder et al., 2008; Brosofske et al., 2014; White et al., 2016). Timeliness and the type of data collected becomes even more important in the face of unpredictable changes to forest structure due to biotic and abiotic factors (Goodbody et al., 2019; Iglhaut et al., 2019). This task is difficult to achieve with traditional, ground-based, forest inventory. Traditional inventory is labor-intensive, especially for remote areas, time-consuming, and increasingly expensive to carry out. (White et al., 2016; Dainelli et al., 2021). As a result, inventories typically cover small areas and limit the number and types of measurements made on the ground (White et al., 2016; Goodbody et al., 2019).

Remote sensing has offered an efficient and effective opportunity to study and quantify ecological phenomena over broader spatial and temporal scales than fieldwork alone for some time now (Loarie et al., 2007; Wiens et al., 2009; Anderson and Gaston, 2013; Nagendra et al., 2013). In the forestry community, remotely sensed data have been an invaluable tool to expand the spatial, temporal, and dimensional extent of their data collection; allowing managers to better develop and implement sustainable management strategies (Wulder et al., 2012; Brosofske et al., 2014; White et al., 2016; Guimarães et al., 2020). LiDAR remote sensing has long been the popular source of information for structural estimates, given its ability sample vegetation within the canopy. Therefore, LiDAR provides information on both horizontal and vertical vegetation distributions; optical sensors (i.e., imagery) can traditionally only provide horizontal (Lim et al., 2003). Various descriptive variables believed to relate to the forest structure are extracted from the LiDAR data and used as the explanatory variable in models predicting the structural variable of interest (e.g., canopy cover, basal area, volume, above ground biomass, height) (Lefsky et al., 1999; Næsset, 2002; Hawbaker et al., 2009; Vega et al., 2014; Arumäe and Lang, 2018). Ground samples collected by traditional forest inventory or other sources act as the training/validation. Using the developed model, the remainder of the non-sampled areas are estimated to create a wall-to-wall map of that metric (White et al., 2013).

In general, the process of converting LiDAR data into reliable estimates of structure are well understood (White et al., 2013); however, the high cost of the data continues to limit its operational feasibility, especially if repeat collection in a narrow time frame is necessary (Wulder et al., 2008; Brosofske et al., 2014; Goodbody et al., 2019). Recent technological advancements have led to a potential solution. Unmanned aerial systems (UAS) have become a reliable and affordable platform for collecting remotely sensed data. When equipped with a sensor, UAS can capture data at much

higher temporal and spatial resolutions for a fraction of the cost of traditional platforms such as satellite or manned aircraft (Anderson and Gaston, 2013). Second, advancements in computer vision have led to a process known as Structure from Motion (SfM) (Westoby et al., 2012). SfM has enabled the extraction of incredibly dense 3-dimensional point clouds from imagery captured with standard, consumer grade cameras that are very similar to LiDAR. When the sensor is mounted on a UAS, the combination becomes a powerful tool for measuring forested environments (Goodbody et al., 2019; Guimarães et al., 2020; Dainelli et al., 2021). Given the flexibility of the UAS and the importance of 3-dimentional information in forestry, there has been a rapid adoption of this technology and many studies assessing the feasibility of the technology for estimating structure. UAS derived point clouds have been used to accurately measure height (Dandois and Ellis, 2013; Lisein et al., 2013; Puliti et al., 2015; Jayathunga et al., 2018), basal area (Zhang et al., 2016; Bonnet et al., 2017), and above ground biomass (Ota et al., 2015; Zhang et al., 2016; Domingo et al., 2019). One potential reason for the success in these studies is the high reliance of the underlying models on height estimations (Dainelli et al., 2021). With this in mind, several studies have found SfM point clouds to characterize tree height as accurately as LiDAR. Vastaranta et al. (2013) and Wallace et al. (2016) found that the UAS-SfM was just as accurate as the LiDAR at characterizing the upper canopy height and consequently the accuracy of structural metrics strongly related to canopy height (dominate height, basal area, volume, etc.) were high (White et al., 2013; Pitt et al., 2014).

The SfM process to generate the point cloud relies upon the automatic detection and matching of easily identifiable features (key points) between overlapping images. Unlike traditional photogrammetry, which relies on the use of cameras with precisely known parameters, the matched points in the SfM process are used to estimate the internal and external orientation of the cameras. Once these orientation parameters are known, the coordinate and height of the feature (i.e., point) is

estimated (Dandois and Ellis, 2013; Lisein et al., 2013). Therefore, the 3-dimensional point data and the model used to estimate their values are derived from the imagery and where it overlaps. Accordingly, the characteristics and quality of the SfM point cloud is highly controlled by the quality of the UAS imagery, which in turn affects the accuracy of the estimated metrics (Manfreda et al., 2018; Iglhaut et al., 2019). Factors that influence the detection of key points within images and matching them across images effect the SfM output. Several papers now have discussed factors that influence the image matching and the SfM output (Whitehead and Hugenholtz, 2014a; Manfreda et al., 2018; Iglhaut et al., 2019) such as image resolution, image overlap, sun-angle, surface texture, and repetitive objects. Research into this matter has only been recent and so far, spans a number of different forest types, variables, and UAS platforms (Dandois et al., 2015; Torres-Sánchez et al., 2017; Ni et al., 2018; Domingo et al., 2019; de Lima et al., 2021). Furthermore, some of these studies utilize LiDAR as reference data or make comparison between UAS and LiDAR metrics rather than comparisons to field data (Ni et al., 2018; de Lima et al., 2021). More research into the effects of acquisition parameters on the SfM point clouds, especially within varying forest ecosystems and UAS platforms is necessary in order to begin determining best practices (Goodbody et al., 2017; Manfreda et al., 2018; Iglhaut et al., 2019). It is inefficient for end users to fly multiple combinations of flight parameters and assess their performance. Establishing best practices will go a long way towards making UAS much more operationally feasible.

Therefore, the objective of this study was to evaluate the effect of flying height and forward overlap on the accuracy of tree height estimates made from the UAS imagery. Four study sites were flown with every combination of three flying heights and four levels of forward overlap. Additionally, dominate tree height was measured on the ground at systematically spaced plots within each site. The photogrammetrically produced point clouds for all flight combinations were generated

using the SfM process and utilized to estimate the average dominate tree height at the sample plot locations. The accuracy of the UAS estimates relative to the ground estimates was calculated and assessed within the context of the flight parameters. The results of this study will inform best practices for UAS mission planning within the context of generating accurate tree height estimation from UAS-SfM data.

Methods

Study Area

The research and associated data collection for this project were carried out at four 150m x 150m (2.25 ha) sites. Two sites were established in the University of New Hampshire Kingman Farm Research Forest in Madbury, NH, U.S.A (Figure 2; see S1 and S2) and other two in the Blue Hills Foundation conservation lands in Strafford, NH, U.S.A **(**Figure 2; see S3 and S4). Each site was further divided into twenty-five, 30m x 30m (.09ha) square plots, 100 total, for ground data collection. These forest stands are considered transition and central hardwood- hemlock- white pine forest communities (Westveld, 1956). Eastern hemlock (*Tsuga canadensis*) and white pine (*Pinus strobus*) are the usual dominant tree species in these communities. However, they made up a very small proportion of the composition with the study sites. The study sites were predominately composed of red maple (*Acer rubrum*), red oak (*Quercus rubra*), and American beech (*Fagus grandifolia*) with black birch (*Betula lenta*), yellow birch (*Betula alleghaniensis*) and paper birch (*Betula papyrifera*) present in smaller quantities.

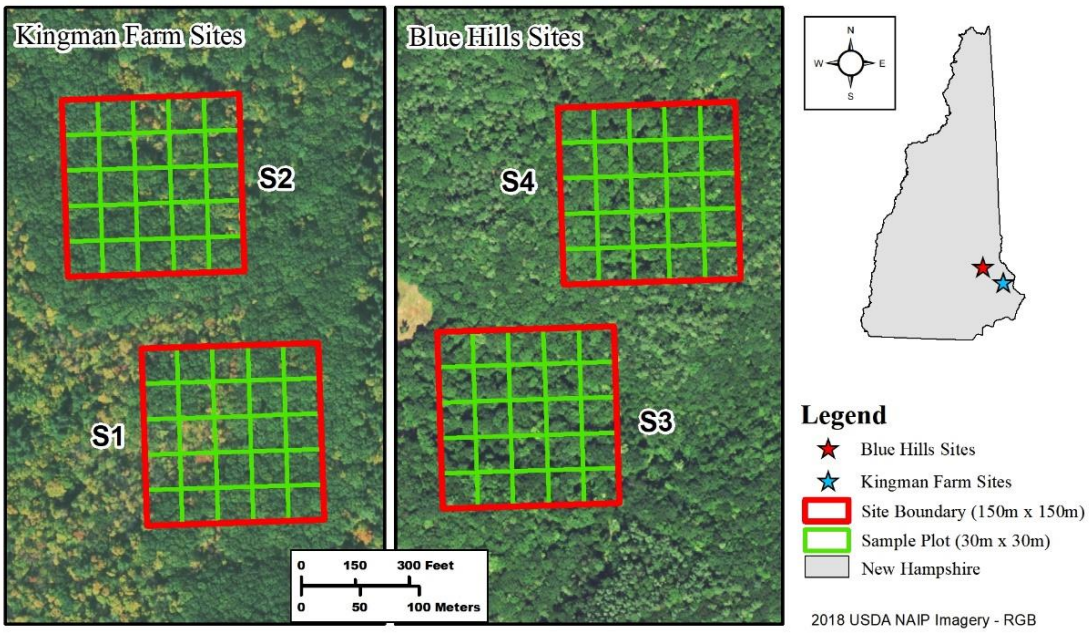

Figure 2.Map of study sites and relative location within New Hampshire. Study sites (red polygons) measure 150m x150m. The label next to each site is a unique identifier for that site. Each study site was completely imaged using all combinations of flying height and forward overlap. Sample plots within each site (green polygons) measure 30m x 30m. Ground data was collected at the center of each sample plot using variable radius sampling.

UAS Data Collection

All flights were carried out with a Sensefly eBee X fixed-wing UAS and a Sensefly Aeria X camera. The Aeria X uses a 24-megapixel APS-C sensor, an 18.5mm (35mm equivalent focal length of 28mm) focal length lens, and a global shutter. All mission planning was controlled using the Sensefly eMotion 3 software (SenseFly, 2020). A polygon of each study site was uploaded into the software. The user sets the desired flying heights and overlaps (side and forward overlap). The software then automatically determines the flight line locations, flight speed, and camera trigger time that meets the desired parameters.

In this study, three flying heights and four levels of forward overlap were tested (Table 2). Side overlap was not tested in this study as it has been found to not have a significant impact on height accuracy in similar studies (Dandois et al., 2015). Additionally, increasing the side overlap adds considerable time to the mission and data processing (Seifert et al., 2019). For these reasons, a singular side overlap of 80% was set for all missions. This value has been found through personal testing to provide reliable reconstructions under varying conditions. For each site, the UAS collected imagery using all combinations of flying height and overlap resulting in 12 missions (i.e., independent image collections at a set flying height and overlap) for each site. In total 48 missions, were carried out (3 flying heights x 4 levels of overlap x 4 study sites).

Table 2. Flying parameters tested in this study. The value in parenthesis is the nominal spatial resolution for that height given by the Sensefly eMotion Software. Every combination of flying height and overlap were tested.

Parameter	Tested Values
Flying Height (above canopy)	80m (1.69cm), 100m (2.12cm), 120 (2.54cm)
Forward Overlap	80%, 85%, 90%, 95%

Table 3 shows the collection dates for each site (S1 – S4). Data collection was conducted during the peak of the growing season and within a single day for each plot to ensure environmental conditions were consistent within the site. While weather was not a directly controlled factor in this study, it is important to note that data collection was held on either completely overcast or clear days with calm wind speeds. For collections on clear days, every effort was made to fly as close to solar noon as possible to reduce shadowing. Flight records recorded during the missions show wind speeds, as measured by the UAS while flying, were typically less than 5m/s with a peak of 6m/s on one day.

Table 3.Collection dates for the study sites

Site Location	Collection Date
Kingman Farm	7/25/2019
Blue Hills	8/2/2019 9/14/2019

UAS Image Processing

The eBee X is real-time kinematic/post-processed kinematic (RTK/PPK) enabled. Therefore, the raw GPS positions for each image can be post-processed to improve the positional accuracy. The Sensefly Flight Data Manager within the eMotion software was used to conduct the PPK post-processing with RINEX data provided by a nearby Continuously Operating Reference Station (CORS). This approach was chosen due to the inability to set ground control points (GCPs) within the study sites. Final positional accuracies reported by the eMotion software were approximately 3cm and 7cm for the imagery collected within Kingman Farm and Blue Hills areas, respectively.

The imagery was then processed using Agisoft Metashape Professional (Agisoft, 2020). Agisoft Metashape is a leading software package for implementing the SfM process. The process begins by first identifying unique features (key points) within the individual images based on image texture. The software then matches key points across the overlapping images. The matched key points, now known as tie points, are then used to estimate the camera's internal and external orientation parameters; necessary for estimating the coordinates and heights of the tie points. This results in what is known as the sparse point cloud and only includes the positions for the tie points. A second process known as Multi-view Stereo (MVS) is then run to densify the sparse point cloud and enhance the amount of information extracted. MVS works by matching pixel windows between

the overlapping imagery and similarly using the estimated orientation parameters to calculate the coordinates of the center of these matched windows (Dandois and Ellis, 2013; Lisein et al., 2013). The result of this process is known as the dense point cloud.

Each independent combination of flying height within each site (48 missions) were processed using the above process with the same parameters for consistency. The specific Agisoft workflow and parameters were as follow. 1) Align photos was run on "High Accuracy" with Generic Preselection, Reference Preselection, and Adaptive Model Fitting turned on. No key-point or tie-point limit was set due to the difficultly in generating and matching unique features in areas that are highly homogenous in texture (i.e., all trees). While decreasing this limit can increase the computation time, it allows the software to generate more key point and can improve the probability of identifying tie points. 2.) The dense point cloud creation was also run on "High Accuracy" with moderate point filtering. Each dense point cloud was normalized using a LiDAR produced digital terrain model (DTM). Photogrammetrically produced point clouds typically cannot capture information at the ground, especially in areas of dense canopy. Consequently, externally produced DTMs are commonly used to normalize the point clouds to height above the ground (Niethammer et al., 2012; Hugenholtz et al., 2013; Dandois et al., 2015). LiDAR produced DTMs covering the study sites were downloaded from the GRANIT LiDAR Distribution site (site (https://lidar.unh.edu/map/). The elevation of the ground at the pixel within which each point fell was subtracted from the elevation of the point. To ensure a comparable vertical reference was used for all four sites, the vertical datum of the DTMs were converted to NAVD88 (Geoid 12b) (current at the time of data creation) to match the UAS point clouds using the NOAA VDatum tool (https://vdatum.noaa.gov/).

Ground Data Collection

Trees were sampled at each 30m x 30m plot within the four study sites on the ground using horizontal point sampling (Kershaw et al., 2016) between January and July 2021. The center of the sample plots was located and marked on the ground using an EOS Arrow 100 GPS unit. The EOS Arrow 100 collects sub-meter accuracy when connected to a satellite-based augmentation system (SBAS) (https://eos-gnss.com/products/hardware/arrow-100; Last accessed 7/25/2021). To maximize the positional accuracy, plot centers were located during leaf-off to improve the receiver's visibility to the sky and reduce multi-path errors. Trees were determined "in" the plot using a basal area factor (BAF) of 40 for the Kingman Farm sites and 20 for the Blue Hills sites. A different BAF was required for each location due to differing stem density and diameter distributions and to achieve the goal of sampling approximate 3 - 4 trees per plot on average. Because UAS-SfM generated point clouds do not sample vegetation below dense canopies, suppressed trees, trees whose canopy receives no direct sunlight (Oliver and Larson, 1996), were not included. The height to the top of the crown of the included trees were measured with a Haglöf Vertex IV Hypsometer. Three height measurements were taken for each tree and the average recorded as the final height. The average height of all the trees within each plot was then taken as the top-of-canopy height (TCH) for that plot.

UAS-based Plot Height Estimates

For each plot in each site (100 total plots), an estimate of TCH was assessed for each flight combination to compare to the ground-based estimates. The *LidR* package (Roussel et al., 2020) in the R 4.0.2 (R Core Team, 2020) was used to process the point cloud datasets. All of the normalized point clouds for each site were clipped to the boundaries of each plot resulting in a point cloud for all flight combinations at the plot level (100 plots x 3 flying heights x 4 levels of overlap). For each plot and each flight combination (flying height and overlap), the common height-based point cloud

metrics were extracted. The point cloud metrics included average height, maximum height, and height percentiles (i.e., the height below which *p*% of the points fall) between 5% and 95% using a 5% interval. The most correlated metric with the ground estimates of TCH was chosen to represent the plot-level estimate of TCH from the point clouds. Unlike LiDAR, the SfM process can result in voids in the point cloud where features could not be reconstructed. For each flying height, the point cloud associated with the most complete DSM was chosen to run the correlations against the ground data (Frey et al., 2018). For all flight combinations, the respective DSM was exported and clipped to the site boundary. Completeness of each DSM was represented as the proportion of the pixels containing data values (i.e., was not null). As demonstrated in Frey et al., (2018), this method is superior to point density as a measure of reconstruction success as it takes into account that multiple points can exist within one pixel. Therefore, completeness gives an indication of the spread of those points across the area of interest. For each flying height, the correlation between height metrics for the point cloud with the greatest completeness and the ground was measured using Pearson's Correlation Coefficient (r). The most correlated metric was chosen as the TCH estimate for each plot within the respective flying heights.

The accuracy of the point clouds from each flight combination was assessed by calculating the root mean square error of the TCH estimates ($RMSE_{TCH}$) using the ground and UAS TCH for the plots within each site. To clarify, within a single site, the $RMSE_{TCH}$ was calculated at the plot level for all flight combinations. This analysis was repeated within each site resulting in twelve measures of $RMSE_{TCH}$ (3 flying heights x 4 levels of overlap) with four replicates (n = 48).

Statistical Analysis

The effect of flying height and overlap on the accuracy of the TCH estimates was assessed by fitting a generalized linear model (GLM). The analysis was carried out in R 4.0.2 using the *lme4* package (Bates et al., 2015). $RMSE_{TCH}$ was set as the response and the flying height and overlap as the predictors. An ID (identification number) for each site was also included as a predictor to account for the site effects. Because $RMSE_{TCH}$ values are bounded at the left side (RMSE cannot be lower than 0), a Gamma distribution with a log link function was specified for the response. Two versions of the model were generated; the first included flying height and overlap as additive effects. The second incorporated an additional interaction term between flying height and overlap to account for the relationship between the ground area covered by the overlap and flying height. An Akaike information criterion (AIC) model comparison indicated that the model without the interaction term was more parsimonious. Additionally, the interaction was not found to be significant when it was included. Based on these results, the simpler model without the interaction term chosen as the primary model for assessing the effects.

We note here that given this experimental design; an attempt was made to fit the data using a generalized linear mixed-effect model with the site set as a random effect. The model was unable to converge when a Gamma distribution was specified. Thus, the decision was made to use the GLM with the site included as a fixed effect so it was accounted for and the normality assumption for the response could be maintained.

Results

Ground Data Summary

Table 4 presents a summary of the ground data collection at each site. In total, 425 trees were measured across the four sites. It is important to note that the number of trees measured in each plot will vary based on the stem density and the DBH at the plot. Different BAFs were used to keep the sampling intensity roughly equal across the plots and the sites, which was successful based on the similarity in the average trees measured across the plots.

Table 4.Summary of ground data collection for all four sites. Standard deviation is given in parentheses.

Location	Site	Average Height (m)	Total Trees Sampled	Average Trees Per Plot
Kingman Farm	S1	28.5 (4.3)	116	4.6 (2.5)
	S2	28.9 (4.9)	88	3.5 (2.2)
Blue Hills	S3	24.5 (3.7)	100	4 (1.4)
	S4	23.0 (4.0)	121	4.8 (2.2)

Point Cloud Completeness and Correlations

The completeness of the DSMs was calculated for all flight combinations. The results are presented in Figure 3. Completeness exhibited an increase with increasing flying height, thus was the lowest at 80m and the highest at 120m above the canopy. Completeness exhibited a distinct peak at 85% overlap before dropping again. Only the 100m and 120m flying heights began to exhibit an increase again after 90% overlap.

The 85% forward overlap for each flying height was used to run the correlation between the point cloud metrics and the ground data. For each flying height, the highest correlation was found with the 85^{th} height percentile. The Pearson's correlation parameter was 0.838, 0.839, and 0.839 for 120m, 100m, and 80m, respectively. All correlations were significant at and 95% confidence interval. Thus, the 85^{th} percentile height was taken as the height estimate at each for all flight configurations.

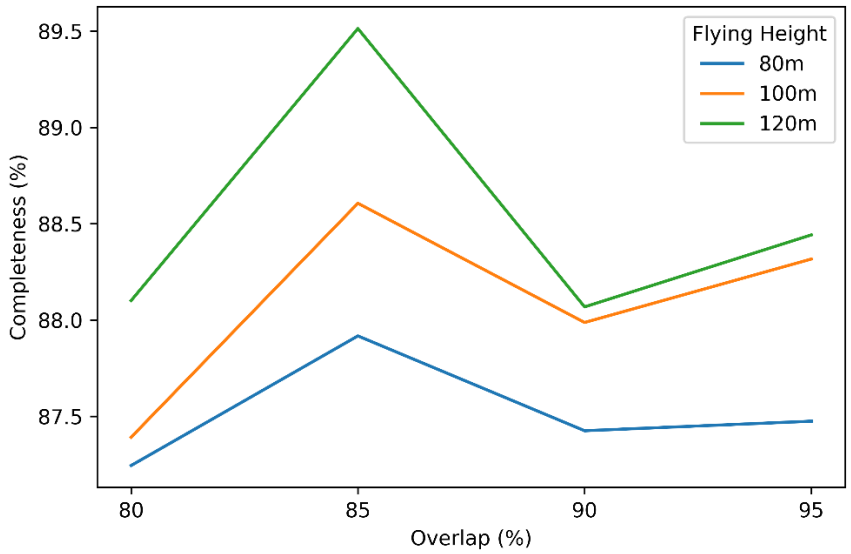

Figure 3.Change in the average completeness with forward overlap and flying height.

Effect of Flight Parameters on TCH Accuracy

The $RMSE_{TCH}$ across all sites and flight parameter combinations ranged between 1.75m and 3.20m. A comparison of the per-plot estimates to the ground reference showed consistent underestimation of the ground estimated tree height (mean error of -1.03m). The change in $RMSE_{TCH}$ with flying height and overlap are summarized in Table 5 and the coefficients and p-values of the selected GLM model are shown in Table 6. The values in Table 4 represent the average and standard deviation for the four sites. There is no consistent pattern in $RMSE_{TCH}$ with flying height. Forward overlap exhibited a slight a decrease in $RMSE_{TCH}$ with increasing overlap. The GLM model found no significant difference in $RMSE_{TCH}$ with flying height and a significant decrease in $RMSE_{TCH}$ with

increasing forward overlap. Based on the model coefficients, a 4mm decrease in $RMSE_{TCH}$ is expected with a 1% increase in overlap.

Table 5.TCH accuracy across the levels of flying height and forward overlap. Values are the mean and standard deviation (in parentheses) in $RMSE_{TCH}$ in meters for the four sites. Marginal values are row and column average $RMSE_{TCH}$

		Forward Overlap				
		80%	85%	90%	95%	
Flying Height	80m	2.40 (0.70)	2.24 (0.50)	2.26 (0.51)	2.19 (0.48)	2.36
	100m	2.40 (0.69)	2.25 (0.49)	2.29 (0.51)	2.22 (0.46)	2.29
	120m	2.39 (0.70)	2.26 (0.47)	2.28 (0.48)	2.24 (0.46)	2.29
		2.40	2.25	2.28	2.22	

Table 6. Output of the chosen GLM model. Coefficients are on the response scale. Significance of the predictor is indicated with asterisks (*)

	Coefficient	**P-value**	**Significance**
Intercept	2.37	0.000	***
Flying Height	1.00	0.672	NS
Overlap	0.996	0.041	*

** p-value < .05* **** p-value <.001* *NS – Not Significant*

Discussion

Point Cloud Completeness

The relationship between DSM completeness, flying height and forward overlap exhibited two notable trends. First, there is an increase in DSM completeness with increased flying height and second, is a distinct peak at 85% overlap for all three flying heights. The increase in completeness

with flying height is in line with the results of several studies that have investigated levels of scene reconstruction with changing flight parameters (Ni et al., 2015; Fraser and Congalton, 2018; Frey et al., 2018; de Lima et al., 2021). These studies found that reconstruction is improved by flying higher due to the decrease in image texture that occurs as the spatial resolution decreases (Dandois and Ellis, 2013; Ni et al., 2018; de Lima et al., 2021). Westoby et al., (2012) noted that reconstruction of a scene is difficult when there is a high level of homogeneity in texture across the overlapping images. This may include either highly repetitive or monochromatic texture (Bianco et al., 2018). Decreasing the texture makes it easier for the computer vision algorithms to locate unique features that can be accurately matched. In terms of the peak at 85%, increasing forward overlap has been found to increase point density (Dandois et al., 2015; de Lima et al., 2021). Increasing the overlap increases the chances of finding image matches as well as adjusts the viewing angle, which can change texture (Frey et al., 2018; Ni et al., 2018). Frey et al., (2018), however, found a continuously increasing completeness with increasing overlap. They adjusted their forward overlap by systematically removing photos along each flight line and their spatial resolution by upscaling the original imagery to courser spatial resolutions, breaking the relationship between flying height and area covered by the image overlap. In this study, each level of overlap and flying height was independently collected.

The base-to-height (B/H) ratio is the relationship between flying height and the distance between the centers of two overlapping photos. B/H has long been an important parameter in traditional photogrammetry due to its impact on the estimate of height (McGlone, 2013). Goldbergs (2021) demonstrated the importance of the B/H ratio for estimating the height and completeness, noted here as the ability to detect reference trees, using photogrammetrically derived DSMs from airborne and satellite imagery. An important conclusion of this study was that the B/H ratio had significant control on the completeness of the DSM and suggested B/H values between 0.2 and 0.3

for accurate reconstruction of the canopy in closed-canopy forests. These values approximately equate to forward overlaps between 64% and 75% with the Aeria X camera used in this study. While these values were not tested here, it is important to note that at an 85% forward overlap, every other photo on a flight line overlaps 70%, which is a B/H of 0.247. Furthermore, the B/H of the side lap utilized across all flight configurations, 80%, is also 0.247, potentially compounding the improvement. Table 4 suggests that B/H might still be important in terms of accuracy as well for UAS-SfM. $RMSE_{TCH}$ dropped when the forward overlap increased to 85% and increased at 90% forward overlap. Goldbergs (2021) found tree height accuracy was improved at optimal B/H ratios. A thorough analysis of this result is beyond the scope of the study but suggests that more work is needed to understand the relationship between B/H and the photogrammetric output with UAS as it could go a long way towards making suitable flight parameter choices.

Tree Height Accuracy

The $RMSE_{TCH}$ ranged between 1.75m and 3.20m across all sites and tested flight parameters. These values are consistent with previous studies. Lisein et al., (2013) reported an RMSE of 1.65 for dominate height estimated using a fixed wing UAS over deciduous dominated stands. Dandois et al., (2013) reported an RMSE of 3.3m for estimates over deciduous forest stands. Their errors are higher potentially because they utilized the average of the canopy height model as their UAS metric for TCH, yet their ground estimates were based on the dominate trees in their plots. Jayathunga et al., (2018) reported an RMSE of 1.78m in a complex, mixed conifer-broadleaf forest. We are taking care to note the forest type of the mentioned studies because forest type could very well have an impact on accuracy. Puliti et al., (2015) and Li et al., (2021) reported RMSEs of 0.72m and 1.01m in boreal forest stands and conifer plantations, respectively with simpler structures relative to this study.

The under estimation found in this study (mean error of -1.03m) is a commonly reported result when using UAS-SfM to estimate tree height (Lisein et al., 2013; Dandois et al., 2015; Yaney-Keller et al., 2019; Kameyama and Sugiura, 2020; Tinkham and Swayze, 2021). On the ground, tree height is typically taken as the topmost point on the canopy. It may be possible to see fine peaks, possibly branches, at the top of the canopy that could very well not be detected during the SfM process (Jayathunga et al., 2018). Furthermore, there can be substantial error when making the field measurements due to the difficultly of locating the top of the trees. Ganz et al., (2019) found height measurements taken indirectly with a Vertex Hypsometer had a mean error of -0.66m and RMSE of 1.02m when compared to direct measurements after felling the measured trees. Additionally, they found the variation in the hypsometer measurements to much higher when compared to the estimates made from remotely sensed data, including UAS-SfM products.

Flight Parameter Effects on Tree Height RMSE

The interpretation of the values in Table 5 is confirmed by the results of the GLM model (Table 6). Flying height had no significant effect on $RMSE_{TCH}$ but was found to significantly decrease with increasing forward overlap. While significant, however, the effect was minor, only a 4mm decrease per 1% forward overlap increase. Dandois et al., (2015) also implemented a fully factorial study of flight parameters on TCH over deciduous forest stands and found flying height had no significant effect while increasing forward overlap lead to a significant decrease in RMSE. Kameyama and Sugiura (2020) similarly found little change in the accuracy of individual tree height estimates with differing flying heights. Torres-Sánchez et al., (2017) also found increasing forward overlap increased the accuracy of individual tree height estimates. It is worth noting that

Torres-Sánchez et al., (2017) also show very little change in the error between forward overlaps of 80% and 95%.

Table 6 does not include the GLM results for the site variable, but a discussion of site is still relevant. A significant difference in $RMSE_{TCH}$ was found for all four sites. There are a number of reasons for this. First, the individual physical differences in the sites themselves have an impact on the structure of the forest, which was not investigated here. Second, these differences could also affect the ability to make accurate measurements on the ground. The Kingman Farm sites for example were on much flatter terrain relative to the Blue Hills sites, which was much steeper. Additionally, while an attempt was made to perform the UAS data collection under similar conditions, there are still variations in the imagery due to differences in lighting and/or wind. While these factors could impact accuracy, the utilization of site replicates lends greater credibility to the results.

The considerable effect of increased overlap is often attributed to better reconstruction of the scene due to the increased probability of locating matching features (Dandois et al., 2015; Frey et al., 2018; de Lima et al., 2021; Kameyama and Sugiura, 2021). In general, by increasing overlap, the search area for matching features is increased. Frey et al., (2018) found that the completeness of the model increased with increasing forward overlap for all spatial resolutions that were tested. (Dandois et al., 2015; Frey et al., 2018; Ni et al., 2018). Kameyama and Sugiura (2020) also noted that 3D reconstruction was more complete as overlap increased. Our study examined a narrow range of possible overlaps, less so than other studies (Dandois et al., 2015; Frey et al., 2018; Ni et al., 2018). While a significant effect was detected, the effect was minimal. Larger difference may to be measured if overlaps less than 80% are tested; however, it has been found that the estimation of the camera

parameters begins to fail as forward overlap decreases resulting in highly incomplete models (Fraser and Congalton, 2018).

The non-significance of flying height on the accuracy of tree height measurements could be the result of the narrow difference in spatial resolution within the flying heights tested. Based on the nominal spatial resolution provided by the Sensefly eMotion software, there is only a 0.85cm difference between the 80m and 120m flying height. The spatial resolution range for Dandois et al. (2015) was only 2.6cm. Frey et al., (2018) also shows that the spatial resolution of the imagery had a minimal impact on the completeness of the models at higher (> 80%) levels of forward overlap. Furthermore, TCH may not be very sensitive to flying height. Ni et al., (2018) assessed changed in the vertical distribution of the SfM point cloud across a wider range of spatial resolutions (8.6cm to 1.376m) via image upscaling and found that for high-density forests, as the spatial resolution increased, the vertical distribution narrowed but remained centered on the upper canopy. This result suggests the top of the canopy is accurately reconstructed across a number of flying heights. Structural metrics that rely on estimates from lower in the canopy, especially the ground, may find a greater effect with flying height as it has been found that lower flying heights are needed to accurately reconstruct the lower levels of the canopy (Dandois et al., 2015; Frey et al., 2018; Ni et al., 2018).

Limitations

This study only investigated the effects of forward overlap and flying height the accuracy of canopy height. Additionally, the composition of the forest across the plots were similar. Other factors such as light condition, wind speed, camera type, slope, etc. with known impacts on the 3D reconstruction were not investigated (Colomina and Molina, 2014; Dandois et al., 2015; Cruzan et

al., 2016). It is also important to note the UAS utilized in this study. It has been suggested that UAS with gimbals are useful because they stabilize the camera during the mission, better ensuring the imagery is nadir (Cruzan et al., 2016). The eBee X, like many fixed wing UAS, lacks a gimbal and thus the imagery was often off-nadir (i.e., non-vertical or oblique) due to crosswinds. The user defined overlap is only achieved when images are vertical, thus oblique images change the realized overlap across the mission area. However, these images may present an advantage when estimating tree height as it has been suggested that the inclusion of oblique imagery can improve the accuracy of forest structural estimates by providing more angles of the individual trees (Swayze et al., 2021).

The distance between successive photos on a flight line decrease with decreasing flying height and increasing forward overlap. As the distance between photos decreases, the UAS must slow down to ensure the previous image is captured and stored before reaching the location of the next. A fixed wing UAS must maintain a certain speed, however, to guarantee proper flight capabilities. Therefore, if the UAS cannot slow down enough, photos are either skipped or taken later than planned. The inability to achieve certain levels of overlap may explain why the completeness of the DSMs at an 80m flying height did not improve again after 90% forward overlap like the 100m and 120m flying heights. The distance between two photos is only 3.3m at a flying height and forward overlap of 80m and 95% respectively. With a minimum cruise speed of 11m/s, it would take the eBee X used in this study 0.3 sec to reach the next photo under perfect conditions.

Furthermore, the RTK capability of the Sensefly eBee X allows for far more precise estimates of the image locations compared to recreational grade UAS, which typically only have standard GPS receivers onboard. In these cases, GCPs would be required to improve the accuracy, but would be difficult to collect in dense forests and labor intensive, especially in remote areas (Tomaštík et al., 2019).

Implications

Based on the results of this study, two suggestions can be made about the choice of flight parameters. We note here that these results should be considered within the context of this study (i.e., UAS type, parameters tested, forest type). Flying with higher levels of forward overlap will increase the accuracy of the height estimates from the SfM point cloud; however, the increase is potentially minimal. While completeness was not a focus of this study, the results of both the $RMSE_{TCH}$ and the completeness investigations suggest that perhaps the highest overlap is not necessary. This is especially helpful at lower flying altitudes where the distance between photos is shorter. Additionally, flying height can be set higher without any significant impact on accuracy of dominant height measurements. Unlike a rotary wing UAS, flying heights for fixed wing UAS are more restrictive due to the nature of how it flies. For example, fixed wing UAS perform banking turns, placing it closer to the canopy. Additionally, a fixed wing UAS cannot stop mid-flight in the event of an obstruction, so the user must set a safe flying height. The ability to fly higher without sacrificing accuracy is a benefit both is terms of time and safety. The combination of a lower overlap and flying higher would save time both flying and processing the data by decreasing the number of images that need to be collected.

Conclusions

UAS have the potential to be an important tool in our efforts to conduct more sustainable forest management by providing 3- dimensional information about a forest in a timelier manner and with significantly reduced costs relative to traditional remote sensing platforms. A useful approach to extracting this information is through the SfM process, which makes use of overlapping images

and optical geometry to extract the height of features within the imagery. The ability to create 3-D data with simple aerial imagery rather than expensive LiDAR sensors is a significant advantage, but the SfM process, while it produces data that are similar to LiDAR, is inherently different from LiDAR. Because the SfM process relies on the ability to detect matching features within the overlapping sections of the imagery, it is sensitive to the quality and geometry of the imagery and its collection. The effects of environmental and operational factors at the time of collection are just now being recognized and more studies investigating these effects are necessary to start building our knowledge of best practices.

The objective of this study was to investigate the effects of flying height and overlap on plot level estimates of top-of-canopy height (TCH). Three flying heights and four levels of forward overlap were flown across four predominately deciduous forest plots. Estimates of TCH for each combination of flight parameters were compared to ground estimates. It was then determined if either parameter had a significant effect on the RMSE of the TCH ($RMSE_{TCH}$) estimates.

Across all flight configurations and sites, the $RMSE_{TCH}$ ranged between 1.75m – 3.20m. Tree height was typically underestimated by the UAS; however, this could be an effect of measurement error on the ground or the inability of the SfM process to properly detect and reconstruct the very tops of trees. There was no significant effect of flying height on accuracy and a significant, but minor, effect of forward overlap. There was very little variation in the spatial resolutions of the imagery based on the flying heights studied. Additionally, it is possible that reconstruction of the tops of trees is robust to the spatial resolution used. Increasing the forward overlap has been shown to improve reconstruction due to providing more overlap between images for feature matching.

Based on the results, higher forward overlap would increase the accuracy of the results. The improvement would be minor, however, and this study provided some indication that the highest

level of overlap may not be necessary. Furthermore, for estimating top of canopy height, flying higher would have no effect on accuracy; however, it could save substantial time on data collection and image processing. These suggestions might change if the parameter of interest was more dependent on 3-dimential information from the lower canopy like volume or average height.

CHAPTER 4

A COMPARISON OF MULTI-TEMPORAL RGB AND MULTISPECTRAL UAS IMAGERY FOR TREE SPECIES CLASSIFICATION IN HETEROGENEOUS NEW HAMPSHIRE FORESTS

Abstract

Unmanned aerial systems (UAS) have recently become an affordable means to map forests at the species-level, but research into the performance of different classification methodologies and sensors is necessary so users can make informed choices that maximize accuracy. This study investigated whether multi-temporal UAS data improved the classified accuracy of 14 species, what is an optimal time-window for data collection, and compared the performance of a consumer grade RGB sensor to that of a multispectral sensor. A time series of UAS data was collected from early spring to mid-summer and a sequence of mono-temporal and multi-temporal classifications were carried out. Kappa comparisons were conducted to ascertain whether the multi-temporal classifications significantly improved accuracy and whether there was significant difference between the RGB and multispectral classifications. The multi-temporal classification approach significantly improved accuracy; however, there was no significant benefit when more than three dates were used. Mid to late spring imagery produced the highest accuracies, potentially due to high spectral heterogeneity between species and homogeneity within species during this time. The RGB sensor exhibited significantly

higher accuracies; probably due to the blue band, which was found to be very important for classification accuracy and lacking on the multispectral sensor employed here.

Introduction

Detailed maps of forest composition are necessary for effective and efficient forest management (Brosofske et al., 2014; Fassnacht et al., 2016). Maps depicting species-level composition serve a number of applications such as monitoring biodiversity (Turner et al., 2003; Saarinen et al., 2018), forest health assessments (Michez et al., 2016b; Klouček et al., 2019), conducting precision forestry (Goodbody et al., 2017; Gülci, 2019) or as inputs for species-specific allometric models (Alonzo et al., 2018). Remotely sensed imagery has been used to decades as a quick and efficient means to produce continuous, large area maps of forest types (Franklin and Wulder, 2002; Wulder et al., 2004). However, traditional remote sensing platforms such as satellite or aerial imagery are incapable of providing the temporal and/or spatial resolutions necessary for species level mapping at an affordable cost (Anderson and Gaston, 2013; Cruzan et al., 2016). Thanks to recent technological advancements, unmanned aerial systems (UAS) have become an affordable alternative, capable of providing the flexibility and resolution necessary to accurately map forest species composition (Whitehead and Hugenholtz, 2014a; Fassnacht et al., 2016).

UAS are easily capable of providing centimeter level imagery that can be used to identify individual plants (Getzin et al., 2012; Baena et al., 2017). Many studies have now employed UAS to map individual or small groupings of invasive plants (Dvořák et al., 2015; Müllerová et al., 2017; Wijesingha et al., 2020; Brooks et al., 2021), shrubs, grasses, and forbs (Laliberte et al., 2010; Lu and He, 2017; Weil et al., 2017; Komárek et al., 2018; Leduc and Knudby, 2018), and wetlands

(Knoth et al., 2013; Durgan et al., 2020). More studies are now evaluating UAS-derived orthomosaics for tree species mapping (Lisein et al., 2015; Michez et al., 2016b; Nevalainen et al., 2017; Franklin and Ahmed, 2018; Miyoshi et al., 2020). All are taking advantage of the imagery's high spatial resolution to distinguish and classify individual trees or small groupings of trees of the same species with positive results.

Besides the significantly higher spatial resolution, the flexibility of the UAS platform is another major characteristic. For one, UAS platforms can be equipped with different sensors capable of acquiring information from different portions of the electromagnetic spectrum (EMS) like the visible bands (RGB), red edge, and near infrared (NIR) (Colomina and Molina, 2014; Whitehead and Hugenholtz, 2014a). Typically, though, cost and payload weight limit the sensor used (Whitehead and Hugenholtz, 2014a; Baena et al., 2017; Manfreda et al., 2018). As a result, consumer grade digital cameras are often employed in UAS studies (Laliberte et al., 2010; Niethammer et al., 2012; Hugenholtz et al., 2013; Mafanya et al., 2017; Pádua et al., 2017a). The downside of employing these cameras, however, is that they ordinarily only capture reflectance in the visible range of the EMS (i.e., RGB cameras). Typically, most land cover classifications, especially with vegetation, require multispectral sensors capable of sensing beyond the visible range of the EMS, frequently NIR, in order to improve the distinction between classes, especially classes that are spectrally similar in the visible range like vegetation (Jensen, 2016; Hernandez-Santin et al., 2019). Many studies have modified the spectral sensitivity of the bands in the consumer grade cameras by adding or removing filters from the camera lens, usually to capture NIR reflectance (Hunt et al., 2010; Michez et al., 2016b; Müllerová et al., 2016; Lu and He, 2017; Müllerová et al., 2017). The modified cameras, however, are not perfect substitutes for real multispectral cameras. All three bands on a consumer grade camera are sensitive to NIR energy, and thus removal of the filter blocking NIR energy from

reaching the sensor can cause redundant band sensitivity or spectral overlap between bands. This spectral overlap reduces the potential for discrimination between features. Several studies have found the RGB imagery performed better compared to the CIR imagery from a modified camera (Nijland et al., 2014; Lisein et al., 2015; Michez et al., 2016b) and have suggested that the redundant sensitivity between the bands, after modifying the camera, reduced the ability to discriminate between species using CIR imagery. Franklin at al., (2018) found the imagery collected by an actual multispectral camera outperformed the RGB imagery for tree species mapping. However, multispectral cameras can be more expensive (Nijland et al., 2014; Whitehead and Hugenholtz, 2014a) and thus more cost-effective methods of accurately generating this information would help make UAS more operationally feasible.

Taking advantage of the UAS' temporal flexibility may help to overcome limitations in sensor spectral resolution (Fassnacht et al., 2016). The much higher temporal resolution of the UAS platform is considered one of its major advantages over other remote sensing platforms (Anderson and Gaston, 2013; Brosofske et al., 2014; Manfreda et al., 2018). In a multi-temporal classification, multiple dates of imagery are used to create a single land cover map by taking advantage of the spectral differences within and between species during this period to improve the accuracy of the map (MacLean and Congalton, 2013). With an appropriately timed series of images, multiple species can be differentiated (Fassnacht et al., 2016). In highly heterogeneous forests with many species of trees, like those characteristic of New England, spectral separability is crucial (Mickelson et al., 1998; Justice et al., 2002; MacLean and Congalton, 2013).

Several studies have demonstrated the advantages of a multi-temporal classification for mapping forest composition with moderate resolution satellite imagery (Wolter et al., 1995; Mickelson et al., 1998; MacLean and Congalton, 2013; Pasquarella et al., 2018). However, it should

be noted that these studies are typically classifying species mixtures rather than singular species since the spatial resolution is usually larger than most tree crowns. The use of high spatial resolution imagery for multi-temporal species classification is uncommon (Hill et al., 2010; Immitzer et al., 2012; D. Li et al., 2015) and the use of very high spatial resolution (sub-meter), non-UAS imagery are scarce, mainly due to high costs for both (Lisein et al., 2015). While several studies have taken advantage of the temporal resolution of the UAS for other applications (Niethammer et al., 2012; Lucieer et al., 2014; Du and Noguchi, 2017; Kohv et al., 2017; Pádua et al., 2017a), few have done so for tree species classification (Lisein et al., 2015; Michez et al., 2016b).

As the availability and access to high, and now very-high, spatial resolution imagery increased, there was a shift away from traditional per-pixel image processing for detecting and mapping features of interest to and object-based approach (Blaschke, 2010; Blaschke et al., 2014). Object-based image analysis was a move towards integrating more spatial information into the classification/feature detection process in an effort to try and mimic human photointerpretation (Hay and Castilla, 2008). As of late, improvements in computer hardware have made deep learning algorithms like the popular convolutional neutral networks (CNN) a viable tool. Deep learning looks to train computers to think like humans and automatically identify features in an image (Lang et al., 2018). Deep learning CNN has performed well with very-high resolution imagery, but, as pointed out by Bhuiyan et al., (2020a), can only utilize three spectral bands. User's typically must choose a limited subset of all the available bands (Bhuiyan et al., 2020a; Bhuiyan et al., 2020b; Cai et al., 2021) which would limit the use of multi-temporal datasets which contain numerous bands. Furthermore, deep learning approaches perform best with a large quantity of reference data and require substantial computing power, (Kattenborn et al., 2020). Meanwhile, computationally efficient machine learning algorithms such as Random Forest are readily available in many coding languages

such as R and Python and have been found to perform well with high-dimensional, multi-temporal datasets (Breiman, 2001; Lisein et al., 2015; Belgiu and Drăgut, 2016; Michez et al., 2016b).

The integration of UAS into the field of remote sensing is very recent and given the inherent differences between UAS and traditional remote sensing platforms/data, there is a need to explore how UAS perform in a variety of applications and environments to better inform end-users on how to best employ them. This study sought to investigate whether multi-temporal classification of RGB and multispectral UAS imagery improved the accuracy of species-level forest composition maps in a highly heterogeneous forest in New Hampshire, U.S.A. Additionally, an optimal phenological window for data collection was investigated and the accuracy of the maps produced from RGB imagery were compared to those produced from the multispectral imagery. This study will inform users on data collection strategies that may help to optimize accuracy in these complex environments.

Materials and Methods

Study Area Description

This study was conducted at Kingman Farm in Madbury, NH, U.S.A (Figure 4). The property is owned by the University of New Hampshire (UNH) and is comprised of both agricultural fields and research support buildings for the NH Agricultural Experiment Station as well as 101 ha of forest which are managed by the UNH Office of Woodlands and Natural Areas for the purpose of education, research, and conservation. From this point forward, any reference to Kingman Farm, or just Kingman, will be used to indicate the forested lands on the property. The Kingman Farm forests are an example of a Hemlock-Beech-Oak-Pine forest community (Westveld, 1956), dominated by white pine (*Pinus strobus*), Eastern hemlock (*Tsuga canadensis*), red maple (*Acer rubrum*), red oak

(*Quercus rubra*), and American beech (*Fagus grandifolia*). The land use history of property and surrounding region combined with the ongoing management practices within the woodlot has resulted in a considerable mix of species. A recent inventory of the property conducted in 2017 as part of the UNH Continuous Forest Inventory (CFI) Program detected 16 different species of trees on the property.

It is important to note several characteristics within the study site that may potentially affect the within-species spectral response. Hemlock woolly adelgid and beech bark disease are widespread throughout the study site. Infected Eastern hemlock and American beech trees may exhibit differing spectral patterns compared to uninfected individuals. Additionally, the study site encompasses a range of hydrologic conditions, from dry uplands to permanently saturated swamps. Facultative species like red maple tend to exhibit wide variability in phenology due to their ability to tolerate a multitude of conditions (Klosterman and Richardson, 2017).

In order to adhere to Part 107 of the U.S. Federal Aviation Administration Regulations (Small Unmanned Aircraft Systems, 14 C.F.R. Part 107) and to maintain the safety of the research team and others, only a portion of the Kingman Farm was covered by the UAS as indicated in Figure 4. The far eastern half of the property is within a Class E to Surface airspace belonging to the Pease International Airport, off limits to UAS, and was thus removed from the study area. Additional limits were placed on the UAS mission area to ensure the pilot and visual observers could maintain visual line of site as well as a constant radio connection with the UAS while flying.

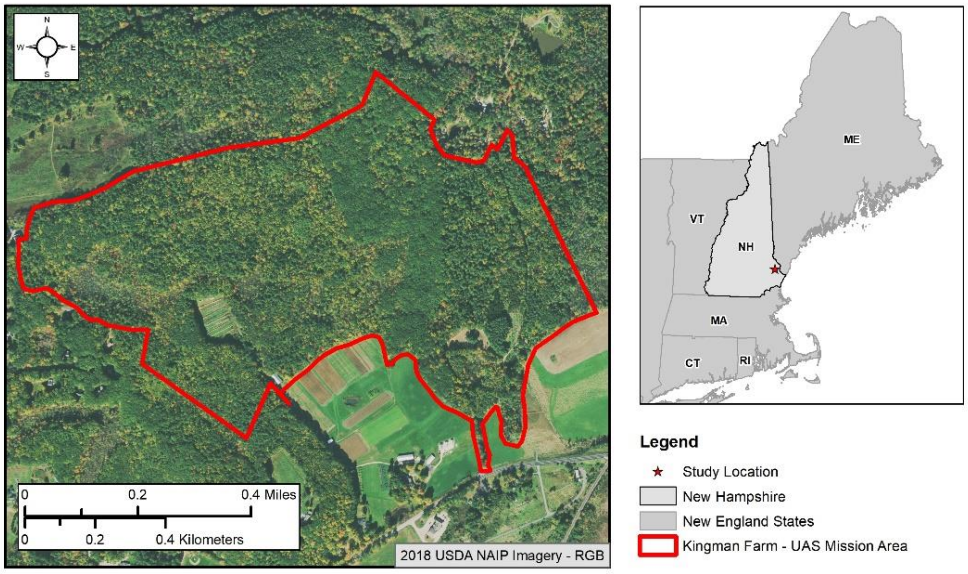

Figure 4. Study area location relative to New Hampshire and surrounding New England states. Red boundary indicates the area covered by the UAS for all data collections.

UAS Data Collection

All flights were carried out with a Sensefly eBee X fixed-wing UAS and the eMotion 3 mission planning software (SenseFly, 2020). Two sensors, the Sensefly Aeria X and the Parrot Sequoia, were flown to collect the RGB and multispectral imagery, respectively. The specifications for each camera are provided in Table 7.

Table 7.Camera specifications for the Sensefly Aeria X and Parrot Sequoia.

	Aeria X	**Parrot Sequoia MSS**
Shutter	Global	Global
Sensor	APS-C	Multispectral sensor
Resolution	24 MP	1.2 MP
Focal length	18.5 mm	3.98 mm
Spectral bands with ranges	Blue Green Red	Green (510 nm–590 nm) Red (620 nm–700 nm) Red edge (725 nm–745 nm) Near infrared (750 nm–830 nm)

The Aeria X is a standard DSLR camera and employs a common APS-C sensor capable of capturing normal color (RGB) imagery. The Parrot Sequoia is a multispectral sensor specifically designed for vegetation mapping and monitoring. As such, it captures spectral information in the green, red, red edge, and NIR portions of EMS. While the Sequoia camera does carry an additional RGB sensor, this sensor is not optimized for the generation of the orthomosaics and was not utilized (Fraser and Congalton, 2018).

Imagery was collected over Kingman farm between April 2019 and June 2020. The goal was to fly bi-weekly from the very beginning for the growing season through to the end in order to capture the full phenology of the forest with both sensors. There was a preference to fly on cloudy days to maintain consistent illumination across all the images and to avoid shadows. When not possible, the imagery was collected on clear or nearly clear conditions and as close to solar noon at possible. All missions were collected 100m above the trees (approx. 120m above the ground) with an 80% latitudinal overlap and an 85% longitudinal overlap. The Sequoia requires an additional radiometric calibration prior to each flight using a calibration target with a known albedo.

Table 8 shows the collection dates for both cameras with a seasonal descriptor. Due to weather, flight constraints, and equipment malfunctions, it was not possible to collect all the imagery within a single growing season. Within sensor collections were largely within the same year (2019 for the Aeria X and 2020 for the Sequoia) with the exception of the first and last date of collection for the Aeria X. Every effort was made to keep the between sensor collections as close as possible in order to avoid large differences in phenology when comparing sensors. Weather conditions between 2019 and 2020 were similar. May and June 2020 were roughly two degrees warmer, and June 2020 received two more inches of rain compared to June 2019. A visual inspection of the imagery did not show significant differences in phenology, however.

Table 8.Collection dates for each sensor with seasonal description. Description is based off regional trends in phenology and not any particular date ranges.

Season	Aeria X (RGB)	Parrot Sequoia (MSS)
Early spring	26 April 2020	28 April 2020
Mid-spring	16 May 2019	15 May 2020
Late spring	30 May 2019	29 May 2020
Early summer	12 June 2019	10 June 2020
Mid-summer	27 June 2020	26 June 2020

Imagery Pre-processing and Orthomosaic Generation

Due to the high canopy cover in the study area, it was not possible to set ground control points (GCPs) across the woodlot to improve the positional accuracy of the orthomosaics. The eBee X, however, is real-time kinematic (RTK) enabled and thus the raw GPS positions for each image could be PPK post-processed. All the raw UAS imagery were pre-processed using the Sensefly Flight Data Manager built into the eMotion 3 software. The Flight Data Manager extracts the geotags for all the images stored in the mission flight logs and then post-process kinematic (PPK) corrects the positions. A CORS station located approximately 3.85 km from the center of the study area (Station ID: NHUN) was used for all PPK processing. Once corrected, the software then geotags the images with the corrected positions.

Each date of collection was processed in Agisoft Metashape Professional (formally Agisoft Photoscan) (Agisoft, 2020). Agisoft utilizes the Structure from Motion (SfM) and Multi-view Stereo (MVS) processes to generate a georeferenced orthomosaic, or ortho. Points representing different features within each image are detected and then matched across multiple overlapping images. The matched points, called tie points, are then utilized to estimate the interior and exterior orientation parameters for the camera at each image. The reprojection error for all models ranged between .448 and 1.28 pixels. The original point cloud, or sparse point cloud, from the tie points is densified by

matching pixel windows between successive image pairs using the estimated camera orientations (Dandois and Ellis, 2013; Lisein et al., 2013). A digital surface model (DSM) is generated from the dense point cloud which is them used to orthorectify the images. The rectified images are then mosaicked together to form the final orthomosaic. Specifically, within the Agisoft software, the Align Photos tool was run on "High Accuracy" with Generic preselection, Guided image matching, and Adaptive camera model fitting turned on. The dense point cloud generation was run on high quality with mild filtering.

While all the missions were flown with the same parameters, the different focal lengths of the two sensors resulted in very different spatial resolutions for the resulting orthomosaics. The coarsest spatial resolution of the Aeria X and Sequoia orthos were 2.7cm and 11.9cm respectively. In order to eliminate spatial resolution as a factor when comparing the performance of the two sensors, all the orthos were exported at a 12cm spatial resolution from Agisoft. They were then georeferenced to improve the positional agreement. The June 27th, 2020, Aeria X orthomosaic was chosen as the base ortho. The remaining orthomosaics were then registered to the base ortho using several well-dispersed structural features across the study site and rectified using an affine transformation and nearest neighbor resampling.

Reference Data Collection

The dense point cloud from the June 27th, 2020, Aeria X imagery was exported and converted into a DSM with a 12cm spatial resolution to match that of the orthomosaics. The DSM was then normalized using a digital terrain model (DTM) produced from a 2011 leaf-off LiDAR collection for coastal New Hampshire and downloaded from the GRANIT LiDAR Distribution site

(https://lidar.unh.edu/map/) to produce the canopy height model (CHM). Due to the inability of photogrammetrically-produced point clouds to accurately capture the ground, externally produced DTMs, typically from LiDAR, are commonly used to normalize those produced from the imagery (Niethammer et al., 2012; Hugenholtz et al., 2013; Dandois et al., 2015). Based on the land use history of the site, there was no concern about the about the age of the DTM. A 3x3 cell Gaussian filter was then applied to the CHM to reduce the noise in the original model (Khosravipour et al., 2014). Pixels with a height less than 5m were considered non-forested and subsequently masked from the CHM.

A local maximum filter was used to generate points representing treetops for the entire study area (Hyyppä et al., 2012; Nevalainen et al., 2017). Kingman farm has a high stand density with highly variable crown widths. To ensure smaller crowns were appropriately captured, a 7 cell, or 84cm wide, circular window was applied. This window size was chosen based on the smallest measured crown width from a 2017 CFI inventory of the Kingman Farm woodlot. While smaller window sizes will over segment larger crowns (Ke and Quackenbush, 2011), this is preferable to under segmentation which could result in the canopies of different species being grouped together and has been found to improve classification accuracies (Gao et al., 2011; M. Belgiu and Drăguţ, 2014).

An initial set of reference trees were selected from the 2017 CFI inventory. For each sampled tree, the distance and azimuth from the plot center to the center of the stem at breast height was recorded in addition to the tree species. This information was used to map the location of each sampled tree stem. Each mapped tree was first, carefully inspected to determine whether the tree could visually be seen in the fully leaf-on imagery and CFI trees that were obscured by taller trees were removed. Next, for trees that are leaning, the location of the center of the stem will not match

that of the highest point of the crown so a visual inspection of the UAS imagery in Agisoft was used to select the local maximum for the remaining trees.

Based on the species represented in the chosen CFI trees, 14 were chosen for classification (Table 9). These species were determined to have a high enough occurrence within the study area to ensure a representative number of reference samples could be gathered. To improve the efficiency of the reference data collection, a random forest (RF) classification (Breiman, 2001) was performed, using the chosen CFI trees as training data. Each local maximum was assigned a preliminary classification based on the average spectral information from the June 26th, 2020, Sequoia orthomosaic occurring within a 0.5m buffer around each point. This preliminary classification was used to perform a stratified random sampling. Each selected point was then carefully inspected using the high-resolution orthomosaics and adjusted as necessary. Field reconnaissance was carried out for those reference samples that were too difficult to photo interpret. One hundred samples per class (species) were collected per the recommendation of Congalton and Green (2019). These reference samples were then randomly divided into two independent groups, one for training the classification algorithm and the other for validation, with half the samples assigned to each.

A marker-controlled watershed (MCW) segmentation was performed to delineate individual tree crowns. In a traditional watershed segmentation for tree crown delineation, a single banded image, typically representing height, is treated as a topographic surface (Blaschke, 2010; Ke and Quackenbush, 2011). The values are inverted so that local maximums (i.e., potential treetops) become local minimums and the catchment basins (i.e., crown boundaries) around all the local minima within the image are delineated. MCW segmentation requires an additional input, markers or points representing the local minima of interest. The basins associated with non-marker minima are converted to plateaus within the image and not delineated. The result is a one-to-one relationship

between markers and basins, which reduces over-segmentation. In this study, the local maximums representing the tree crowns in the study area were used as the markers and the CHM was used to define the crown boundary.

Table 9. Scientific and common names of tree species classified in this study.

Scientific Name	Common Name	Abbreviation
Fagus grandifolia	American Beech	ab
Betula lenta	Black Birch	bb
Quercus velutina	Black Oak	bo
Tsuga canadensis	Eastern Hemlock	eh
Betula papyrifera	Paper Birch	pb
Populus grandidentata	Big-toothed Aspen	pg
Populus tremuloides	Quaking Aspen	qa
Acer rubrum	Red Maple	rm
Quercus rubra	Red Oak	ro
Carya ovata	Shagbark Hickory	sh
Acer saccharum	Sugar Maple	sm
Fraxinus americana	White Ash	wa
Pinus strobus	White Pine	wp

Tree Species Classification

A series of mono-temporal (single date) and multi-temporal (multiple dates) classifications were carried out for each sensor using an object-based classification approach, whereby groupings of pixels (image objects) are classified instead of the individual pixels. An object-based approach performs better than a traditional pixel-based approach when classifying high-spatial resolution imagery since it can better handle the higher intra-class spectral variability that occurs as the spatial resolution increases (Conchedda et al., 2008; Johansen et al., 2010; Blaschke et al., 2014). The previously created tree crown segments acted as the image objects for this study.

The RF classifier was employed for all classifications. RF is a robust, non-parametric classification algorithm used often for classification an employed in other multi-temporal species classification studies (Rodriguez-Galiano et al., 2012; Michez et al., 2016b; Weil et al., 2017; Goodbody et al., 2018) The per-band average spectral value of the training tree segments was used to train the RF classifier. Each RF model was grown using 500 trees and the square root of the number of spectral bands included in the model as described below. The resulting model was then applied to the independent validation tree segments to assess its accuracy.

Each single date of imagery for each sensor was classified. Additionally, a series of multi-temporal image stacks were classified using varying combinations of the single date orthomosaics for each sensor. Image stacks started with every combination of two dates of imagery. The number of dates of imagery included in the stack was then increased incrementally until all dates of imagery are included (i.e., 3-date stack, 4-date stack, 5-date stack). In total, 62 combinations were generated, 31 per sensor (Table 10).

Accuracy Assessment

The accuracy all the classifications was assessed using the validation tree segments and an error matrix approach (Congalton et al., 1983). The ground classification of each validation tree was compared to its respective map classification and the results tallied in a matrix with the columns and the rows of the matrix representing the sample's ground and map classification, respectively. For each matrix, the overall accuracy (OA) was calculated by dividing the sum of the major diagonal (total agreement) by the total number of samples. The accuracy of the individual classes was determined by calculating the User's (UA) and Producer's (PA) accuracy (Story and Congalton,

1986). PA is calculated by dividing the number of correctly classified samples for each class by the total number of samples for that class. UA is calculated by dividing the number of correctly classified samples for each class by the total number of samples classified as that class. UA and PA were then used to calculate an F-Measure (F; Eq. 1) as a way to summarize UA and PA in a single metric.

$$F = 2 * \frac{(UA * PA)}{(UA + PA)} \quad (1)$$

Due to the randomization approach implemented by the RF classifier, the accuracy of no two RF models will be the same. To account for this, 30 RF models were generated for each date combination in Table 10. Each model was validated and the OA, UA, PA, F, calculated. These results were then averaged together to calculate a mean accuracy result for each combination.

Feature Importance

A feature importance investigation was carried out for both sensors. A RF classifier was trained using the training tree segments and all the bands for all dates of imagery and validated using the independent validation tree segments to establish a baseline accuracy. One at a time, each band included in the image stack was removed, the model retrained and validated, and difference in overall accuracy taken as the measure of importance for that band.

Statistical Comparisons

Table 10.All single and multi-date image stacks for classification. The Index column is a unique identifier assigned to each combination within a sensor.

		Aeria	Sequoia
One Date	1	4-26-20	4-28-20
	2	5-16-19	5-15-20
	3	5-30-19	5-29-20
	4	6-12-19	6-10-20
	5	6-27-20	6-26-20
Two Dates	6	4-26-20 + 5-16-19	4-28-20 + 5-15-20
	7	4-26-20 + 5-30-19	4-28-20 + 5-29-20
	8	4-26-20 + 6-12-19	4-28-20 + 6-10-20
	9	4-26-20 + 6-27-20	4-28-20 + 6-26-20
	10	5-16-19 + 5-30-19	5-15-20 + 5-29-20
	11	5-16-19 + 6-12-19	5-15-20 + 6-10-20
	12	5-16-19 + 6-27-20	5-15-20 + 6-26-20
	13	5-30-19 + 6-12-19	5-29-20 + 6-10-20
	14	5-30-19 + 6-27-20	5-29-20 + 6-26-20
	15	6-12-19 + 6-27-20	6-10-20 + 6-26-20
Three Dates	16	4-26-20 + 5-16-19 + 5-30-19	4-28-20 + 5-15-20 + 5-29-20
	17	4-26-20 + 5-16-19 + 6-12-19	4-28-20 + 5-15-20 + 6-10-20
	18	4-26-20 + 5-16-19 + 6-27-20	4-28-20 + 5-15-20 + 6-26-20
	19	4-26-20 + 5-30-19 + 6-12-19	4-28-20 + 5-29-20 + 6-10-20
	20	4-26-20 + 5-30-19 + 6-27-20	4-28-20 + 5-29-20 + 6-26-20
	21	4-26-20 + 6-12-19 + 6-27-20	4-28-20 + 6-10-20 + 6-26-20
	22	5-16-19 + 5-30-19 + 6-12-19	5-15-20 + 5-29-20 + 6-10-20
	23	5-16-19 + 5-30-19 + 6-27-20	5-15-20 + 5-29-20 + 6-26-20
	24	5-16-19 + 6-12-19 + 6-27-20	5-15-20 + 6-10-20 + 6-26-20
	25	5-30-19 + 6-12-19 + 6-27-20	5-29-20 + 6-10-20 + 6-26-20
Four Dates	26	4-26-20 + 5-16-19 + 5-30-19 + 6-12-19	4-28-20 + 5-15-20 + 5-29-20 + 6-10-20
	27	4-26-20 + 5-16-19 + 5-30-19 + 6-27-20	4-28-20 + 5-15-20 + 5-29-20 + 6-26-20
	28	4-26-20 + 5-16-19 + 6-12-19 + 6-27-20	4-28-20 + 5-15-20 + 6-10-20 + 6-26-20
	29	4-26-20 + 5-30-19 + 6-12-19 + 6-27-20	4-28-20 + 5-29-20 + 6-10-20 + 6-26-20
	30	5-16-19 + 5-30-19 + 6-12-19 + 6-27-20	5-15-20 + 5-29-20 + 6-10-20 + 6-26-20
All	31	4-26-20 + 5-16-19 + 5-30-19 + 6-12-19 + 6-27-20	4-28-20 + 5-15-20 + 5-29-20 + 6-10-20 + 6-26-20

A kappa analysis was conducted to statistically compare the best single-date and multi-date classifications for each sensor. The kappa statistic, KHAT, is another measure of how well the classification agrees with the reference data that does not assume the land cover classes are independent and utilizes the information in the entire error matrix, not just the diagonal (Congalton et al., 1983). The KHAT statistic for two error matrices can be statistically compared to determine whether there is a significant difference between methodologies (Congalton and Green, 2019). Several KHAT comparisons were conducted. First, within each sensor, the best mono and multi-temporal classifications were compared to determine not only whether a multi-temporal classification was significantly better than a single date classification, but also whether there was a significant difference between how many dates were used. Next, between-sensor KHAT comparisons were conducted for each date of imagery to compare the classification performance of the RGB imagery to that of the multispectral imagery.

Results

Within-sensor General Classification Results

Figure 5 presents the results of the three best performing classifications for the single and multi-date image stacks based on OA. The OA for all the classifications performed can be found in the Appendix (Table 12 and Table 13). Overall classification accuracies were highly varied, ranging from 24.8 % to 61.1% for the Aeria and 27.0% to 55.5% for the Sequoia. Across the individual date groups, the mono-temporal classifications had the lowest overall accuracies, reaching a maximum OA of 37.3% and 36.2% for the Aeria and Sequoia respectively. Generally, the inclusion of additional dates resulted in the accuracy of all classifications to improve. However, there is a distinct leveling

off in OA as the number of dates included in the multi-temporal classification increases, reaching the peak OA for the 5-date classification (Aeria) and for the 4-date classification (Sequoia).

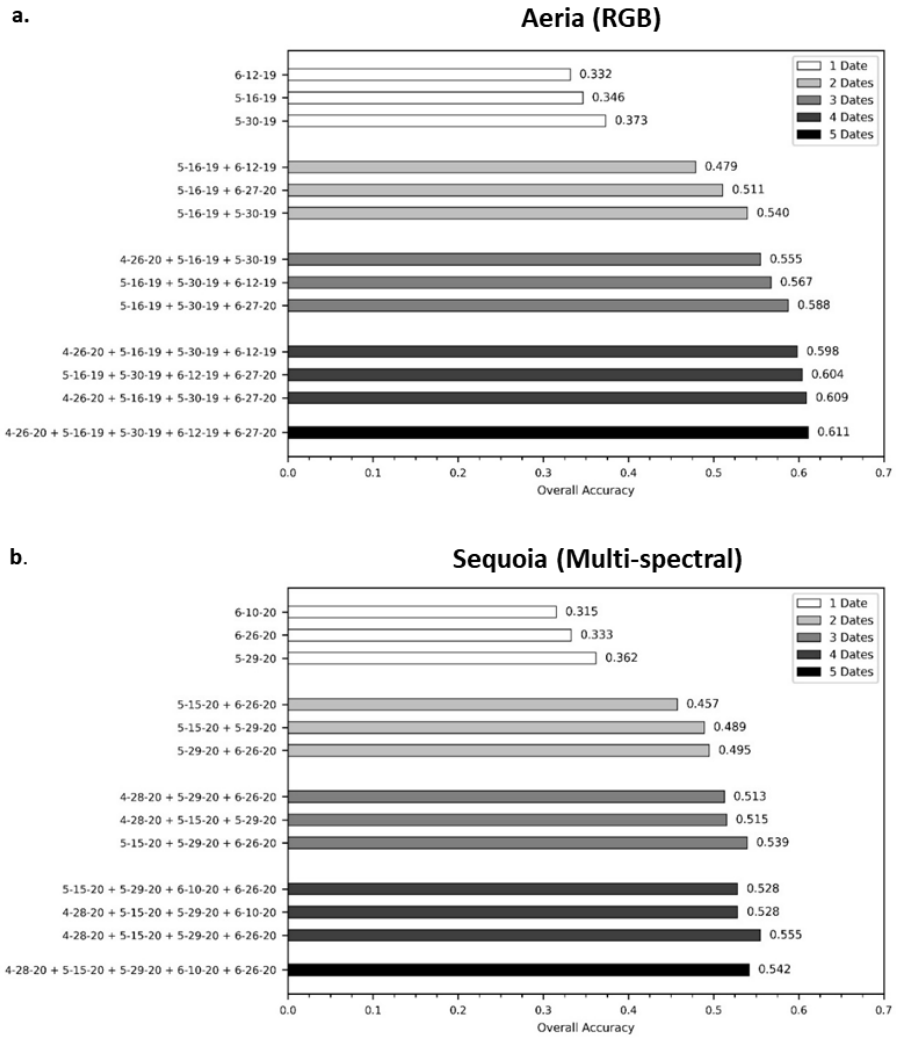

Figure 5. The three best single and multi-date image combinations based on overall accuracy for (a) the normal color Aeria sensor and (b) the multispectral Parrot Sequoia sensor. The bars are grouped by the number of images in the image-stack.

For the top performing combinations (Figure 5), the mid and late May imagery were consistently chosen. The best mono-temporal classification for both sensors also occurred at the end

of May, late-spring. For the multi-temporal classifications, the best date combinations varied slightly between the sensors, but mid and late-spring imagery were frequently utilized, especially for the 2 and 3-date combinations for which there was 10 combinations for each.

Mono versus Multi-temporal Classification

The results of the pairwise comparison between the mono and multi-temporal classification for both sensors are given in Table 11. For each pairing, the 30 individual classifications were compared, and the number of significantly different classifications totaled. Both sensors exhibited the same trend in the number of significantly different classifications. The best 2-date multi-temporal classification was always significantly better than the best mono-temporal classification. Between two and 3-dates, the number of significantly different classifications decreased considerably. After three dates of imagery, there was no significant difference in the classifications.

Per-species Classification Result

The UA, PA, and F for all species and all classifications are presented in Figure 6 and Figure 7 for the Aeria and Sequoia, respectively. The accuracy of eastern hemlock (eh) and white pine (wp), the only coniferous species in this study, were consistently better than that of the deciduous species across all combinations. The F of both were often > 70%, peaking at 88% for eastern hemlock (Aeria) and 80% for white pine (Sequoia). White ash (wa), red maple (rm), and American beech (ab), were consistently poorly classified, never achieving Fs greater than 50%. The performance of the

remaining species varied with the number of dates included and the specific dates in the combination for each sensor.

Between-sensor Classification Results

The best performing based on OA, Aeria and Sequoia classifications for each mono and multi-temporal classification group were statistically compared. For each pairing, the 30 individual classifications were compared, and the number of statistically significant results summarized. The results of the comparisons are shown in Figure 8. When compared to the Aeria, the Sequoia consistently under performed in terms of OA. The smallest difference was seen in the mono-temporal classifications (OA difference of 1.1%) while the greatest occurred with the 5-date classification (OA difference 6.9%). None of the mono-temporal classifications was found to be significantly different. Each of the multi-temporal pairings had some significantly different results, the number of which increased with the number of added dates. Almost all of the 5-date comparisons were found to be significantly different.

Feature Importance

The results of the feature importance analysis are presented in Figure 9. Feature importance here is measured as the decrease in overall accuracy relative to a baseline model (the 5-date combination), when that feature or band is removed. Positive values indicate that the model accuracy decreased when the band was removed while negative values indicate that the model accuracy improved. For the Aeria, the blue bands are considerably more important, than the other spectral bands. Furthermore, the mid and late-spring imagery, regardless of the spectral band, were also

important. The Sequoia had numerous bands indicated as having negative impacts on performance. The mid and early spring green and red bands were predominately the most important. The red-edge and NIR bands were consistently the least important.

Discussion

This study sought to investigate (1) whether a multi-temporal approach improved the accuracy of species-level forest composition mapping with UAS imagery in a highly heterogeneous forest, and in doing so determine whether there is an optimal phenological window within which to collect imagery and (2) compare the performance of RGB imagery collected via a consumer grade DSLR to that of a multispectral camera. A series of mono-temporal and multi-temporal classifications of 14 different species was carried out for both sensors and validated with an independent set of reference samples and error matrices. Kappa comparisons were then conducted between the best performing mono and multi-temporal classifications within each sensor and then between sensors to determine whether multi-temporal was significantly better than mono-temporal classifications and whether there was significant difference between the classifications produced by the RGB and multispectral sensors.

While the underlying goal of this study is to inform users on data collection strategies, it is important to note that this study was conducted in a single stand in one point of the globe. The results of this study should be interpreted within the context from which they were derived. Geographic variation in phenology aside, results may vary even with geographically close locations simply due to differences in site, lighting, and composition, most of which are difficult to control.

Tree Species Classification Accuracy

This study achieved a maximum overall accuracy of 61.1% and 55.5% for the Aeria and Sequoia respectively. These OAs are lower compared to comparable studies that performed similar investigations to this (Lisein et al., 2015; Michez et al., 2016b; Gini et al., 2018). Both Lisein et al. (2015) and Michez et al., (2016b) conducted multi-species level forest mapping in mixed forest stands using both multi-temporal RGB and multispectral UAS imagery. These studies achieved maximum accuracies of 91.2% (based on RF out-of-bag errors) and 84.1% respectively. It should be noted that these studies, while similar, varied in two important ways. First, both studies only included 5 classes. Some were species while others were groupings representing specific genera (e.g., birches). This study included individual 14 species of trees. The greater number of species employed here lead to greater spectral confusion, especially for species exhibiting similar phenology across the time period investigated (Michez et al., 2016b). This study chose to represent the diversity of the study site as is rather than choosing a subset of species exhibiting the best separation, thus expanding the generalization of these results to similar conditions (Fassnacht et al., 2016; Weil et al., 2017).

Table 11. Results of the mono versus multi-temporal kappa comparisons for the Aeria and Sequoia. The date combination with the highest overall accuracy within each sensor was used for each comparison. The value represented the number of iterations out of 30 that were found to be significantly different at the 95% confidence level.

	Number Significant	
Comparison	**Aeria**	**Sequoia**
One date vs. two dates	30	30
Two dates vs. three dates	5	3
Three dates vs. four dates	0	0
Four dates vs. five dates	0	0

Second, these studies employed additional derivative layers that were not utilized here, mainly spectral indices and textural metrics. Additional derivative information, especially texture,

has been found to significantly improve the accuracy of forest classification in a number of settings (Rodriguez-Galiano et al., 2012; Gini et al., 2018; Ferreira et al., 2019) and other vegetation mapping studies as well (Laliberte and Rango, 2011; Feng et al., 2015). This study establishes a baseline for the performance of these two sensors based on spectral properties alone. Given the resolution these UAS sensors are capable of achieving, a great deal of information on crown texture can be extracted. The benefits of textural metrics for mapping stands such as this an interesting topic in need of additional research.

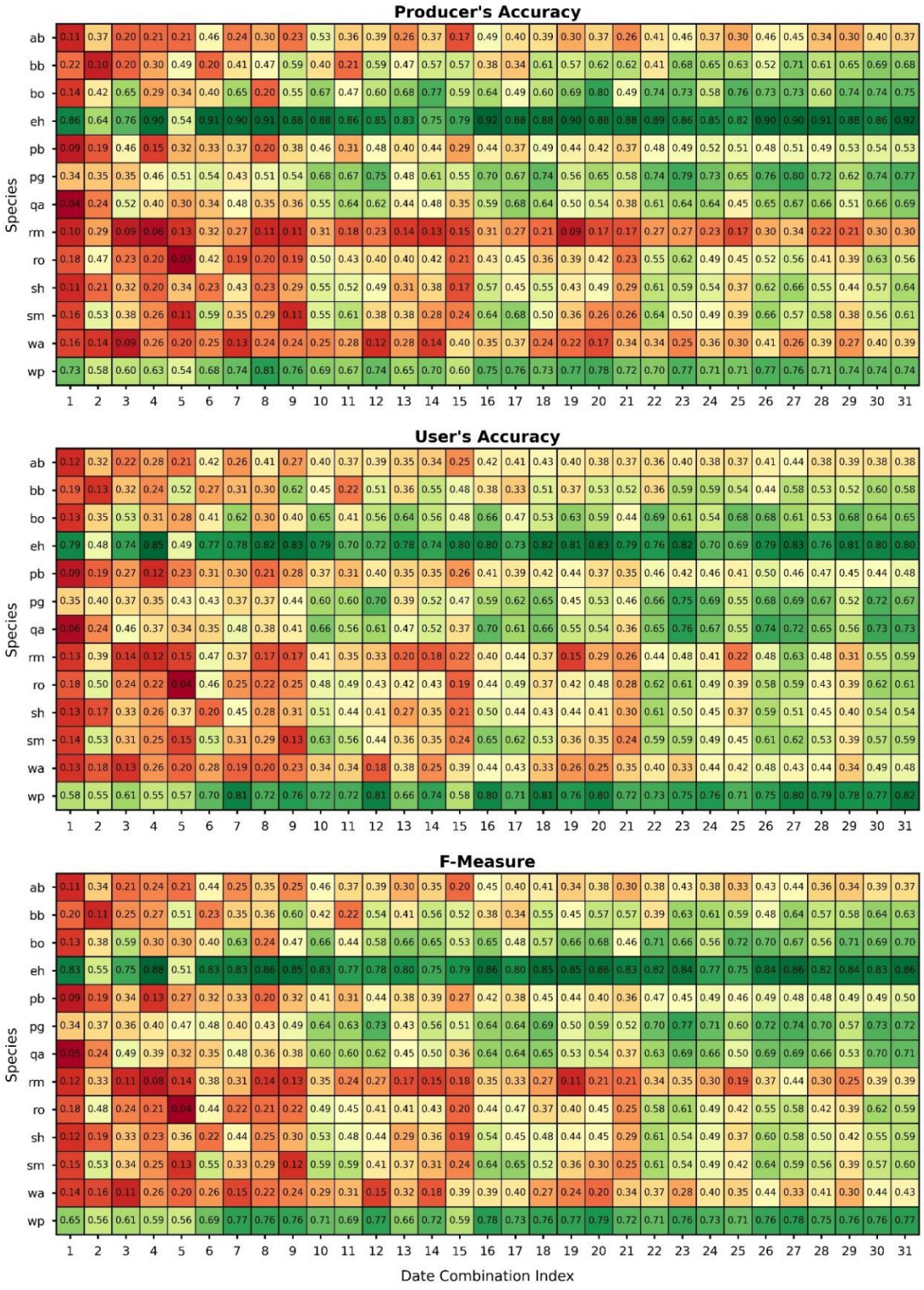

Figure 6. Producer's, User's, and F-Measure for all Aeria classifications. The values on the x-axis are the index value assigned to each classification (see. Table 10). The y-axis is the species abbreviation (see Table 9). Colors are a gradient from low accuracy(red) to higher(green).

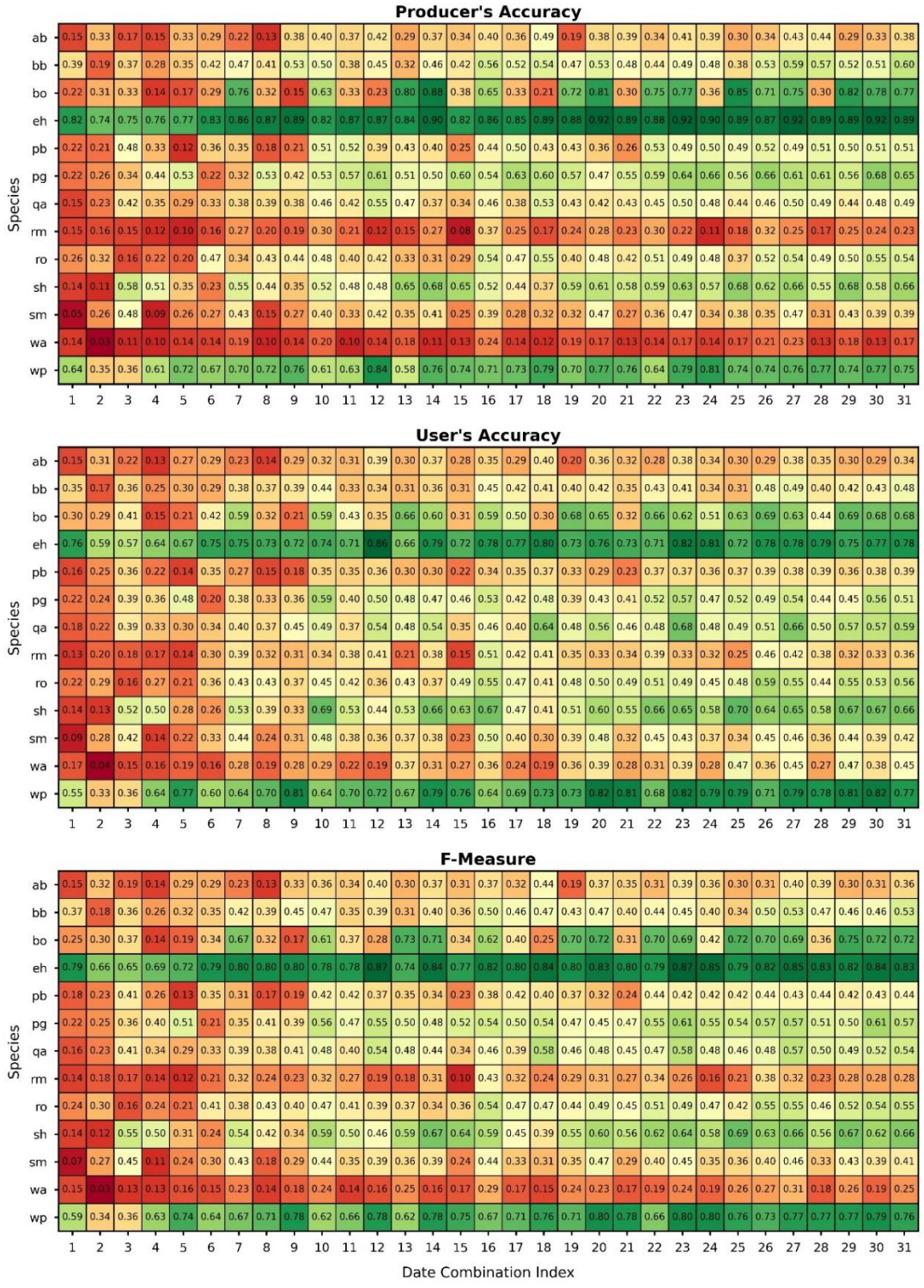

Figure 7. Producer's, User's, and F-Measure for all Sequoia classifications. The values on the x-axis are the index value assigned to each classification (see. Table 10). The y-axis is the species abbreviation (see Table 9). Colors are a gradient from low accuracy(red) to higher(green).

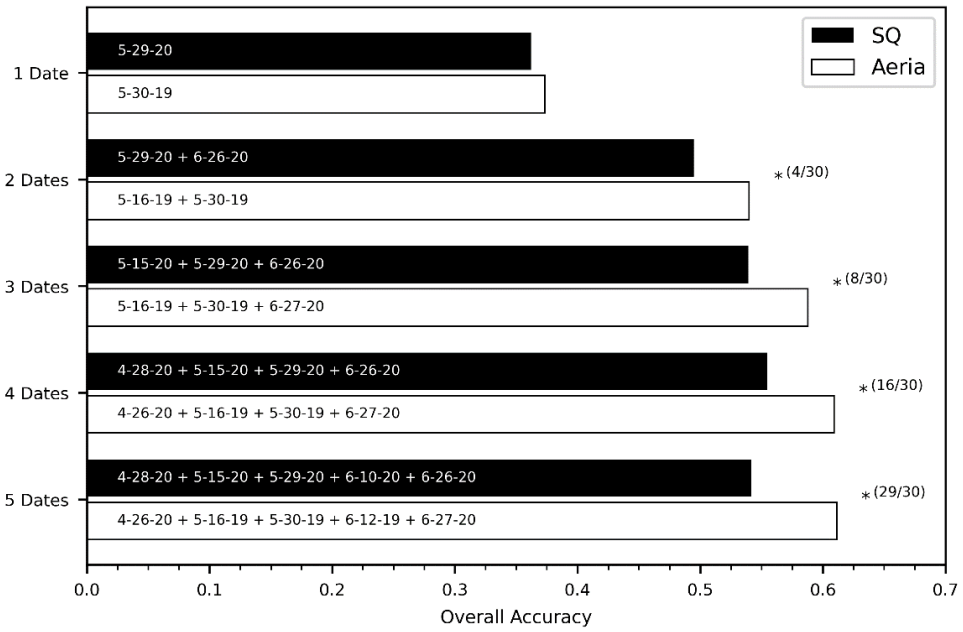

Figure 8. Comparison between the best performing Aeria and Sequoia combination, indicated on the label, within each combination group. The asterisk indicates at least one statistically significant comparison at the 95% confidence level over 30 iterations.

Mono versus Multi-temporal Classification

Both sensors employed here demonstrated a continuous increase in the overall classification accuracy as the number of dates included in the multi-temporal classification increased (Figure 5). This result falls in line with many other studies that have investigated the performance of multi-temporal classifications both with UAS (Lisein et al., 2015; Michez et al., 2016b; Gini et al., 2018) and non-UAS imagery (Key et al., 2001; Hill et al., 2010; MacLean and Congalton, 2013; Zhu and Liu, 2014). Of interest in this study was the significance of the additional benefit incurred by adding more dates. The highest accuracy was achieved with using all 5-dates of imagery for the Aeria and 4-dates for the Sequoia. From a cost-benefit perspective, one would look to achieve the highest

accuracy possible with the least number of collections. While the OA did increase with the number of dates utilized, the rate at which it increases for both sensors levels off, indicating a diminishing return. The results of the mono versus multi-temporal kappa comparisons support this conclusion (Table 11). The 2-date classification for both sensors was significantly better than the mono-temporal for all iterations. There was only a minor benefit when a third date was included and beyond three dates, there was no significant benefit. Weil et al. (2017) similarly saw little improvement in classification accuracy after 3-dates of optimal near-surface imagery using the RF classifier. These results not only reinforce the benefits of multi-temporal classifications, but also suggest that there would be no need to collect more than three dates of optimally timed imagery.

Timing of Aerial Collection

Based on the date combinations of the best performing mono and multi-temporal classifications, the mid and late-spring imagery play an important role in trees species classifications. The best mono-temporal collection date was found to be towards the end of May for both sensors. Similar studies investigating optimal phenological timing have also found the middle and end of spring to be important (Lisein et al., 2015; Weil et al., 2017). This runs counter to what one would expect which is that the accuracy would be maximized at the point where the trees are expressing their greatest phenological differences, either early spring or autumn (Lisein et al., 2015). Indeed, other studies have found autumn to be the optimal mono-temporal window for species mapping (Key et al., 2001; Hill et al., 2010; Weil et al., 2017).

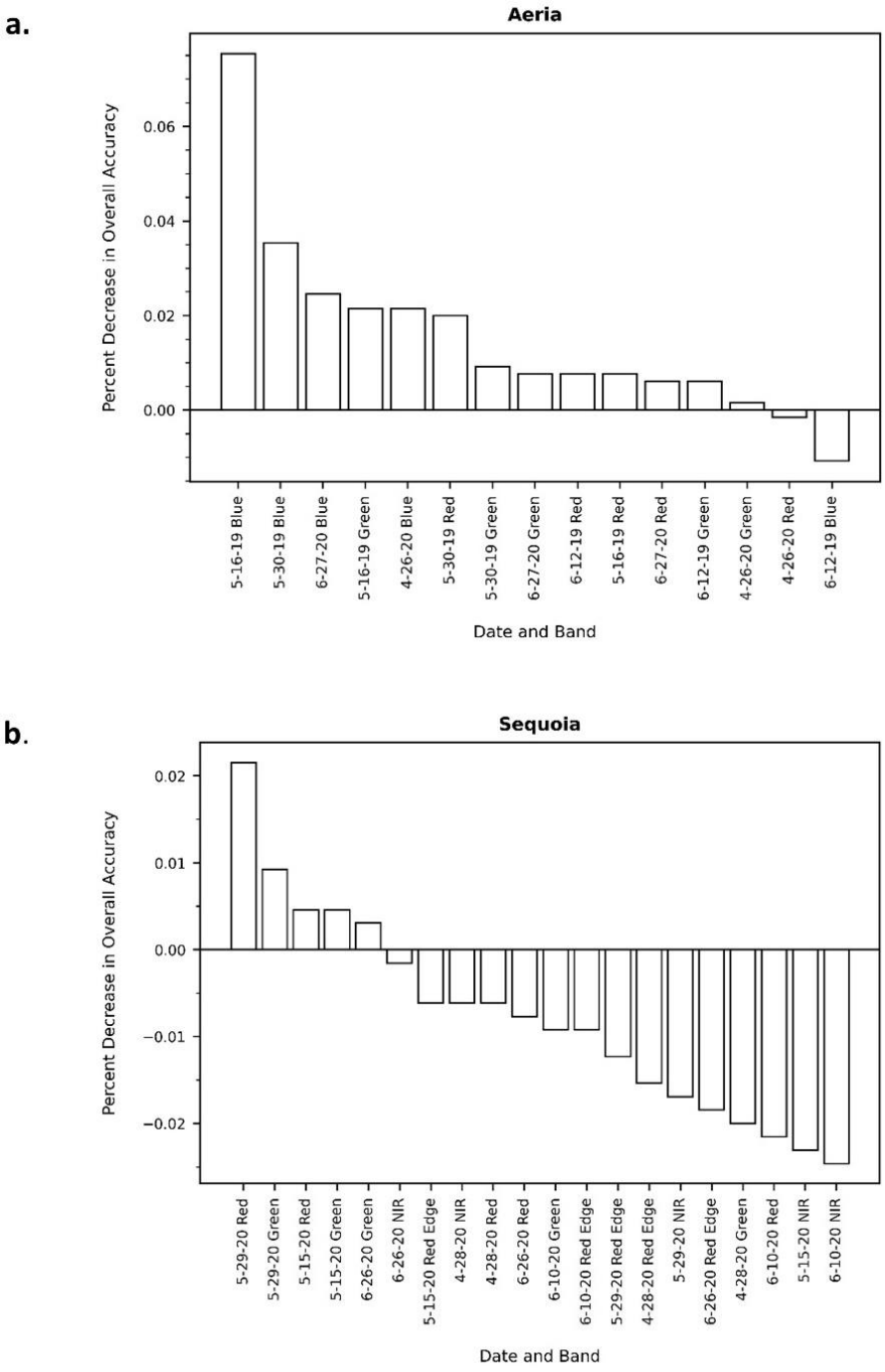

Figure 9. Feature importance values for (a) the Aeria and (b) Sequoia sensors. Feature importance is measured as the decrease in overall accuracy of the baseline model when that band is removed from the model. Positive values indicate a decrease in accuracy while negative values indicate an increase in accuracy.

Lisein (2015) suggested that this period presents a balance between inter and intra-species spectral variation, not only improving the separability between species, but the homogeneity within species. After this period, individual phenology starts to express the effects of differing microclimate, age, even health (Crimmins and Crimmins, 2008; Cole and Sheldon, 2017; Klosterman et al., 2018). It is at this point too that the spectral response of trees below the upper canopy are suppressed (full to almost full leaf-cover above), further improving the variability. This suggests that more focus should be placed on the intra-species variation when collecting phenology data for species classification.

The results of the multi-temporal classifications still demonstrate that including periods with high inter-species variation is important for achieving high classification accuracies. The best performing two and 3-date classifications included the mid- spring imagery with the late-spring imagery. Many species experienced an increase in their individual accuracies for those date combinations containing both dates (Figure 6 and Figure 7). Visually, the mid-spring imagery collected here exhibited the greatest difference between species. Unfortunately, due to equipment difficulties, the full phenological profile of the study site was not captured. Based on the results of the previously mentioned studies, the inclusion of autumn imagery along with the mid and late-spring could have significantly increased the accuracy of the three date classifications, perhaps leading to greater significance when statistically compared to the optimal 2-date classification.

While this study focused primarily on a global classification result, it is still important to investigate the accuracy of the individual species. There was a substantial difference in the performance for different species and combinations (Figure 6 and Figure 7). Most notable, the two coniferous species were consistently well classified compared to the deciduous species. Eastern hemlock exhibited accuracies > 70% within only a single date of imagery. White pine performed

better once there were two dates and then stabilized. White ash, American beech, and red maple did consistently poor, showing only a minor improvement with additional dates. Within species variation, as noted could have a significant impact on an individual species performance. Red maple naturally exhibited great variability during the important mid-springtime period, with some trees just starting to show red fluoresces to almost fully leafed out, expressing the influence of the wide variety of conditions it can tolerate (Klosterman and Richardson, 2017; Klosterman et al., 2018). American beech in the study area was much further ahead phenologically than most other species, almost completely leafed out by mid-spring, but is currently suffering from the effects of beech bark disease throughout the study area. The range of infestation is wide, with beech trees ranging from newly infected to nearing mortality, which would cause large variability in spectral response not just because of the change in vegetation health, but also the change in the structure of the canopy as well (Michez et al., 2016b). Additionally, the time series collected here may not have been dense enough to capture the specific periods within which a species becomes distinct. For example, white ash had few if any leaves by mid-spring but was fully leafed-out by late-spring. An important window may have been missed. Far more spectrally unique species, for example the aspen trees, black oak, and black birch performed well, even with just a few dates of imagery.

RGB versus Multispectral for Tree Species Classification

The multispectral sensor employed here was found to underperform compared to the consumer grade RGB sensor. The statistical comparison between the two sensors (Figure 8) suggests that for a mono-temporal classification the RGB sensor and the multispectral were not different. However, the RGB sensor becomes significantly better with each additional date added to the classification. Both Lisein et al., (2015) and Michez et al., (2016b) carried out a comparison between

multi-temporal RGB imagery and color infrared (CIR) imagery (green, red, and near infrared sensitivity only) for the purpose of forest species classification and found the RGB outperformed the CIR. Both studies suggested the poor performance from the CIR was due to the redundant sensitivity to NIR across the three bands after modifying their camera. Nijland et al., (2014) concluded the same when comparing a modified (i.e., NIR blocking filter removed) and unmodified RGB camera for monitoring plant health and phenology. This study sought to overcome the redundant sensitivity problem by utilizing a multispectral sensor designed specifically for vegetation mapping and monitoring. Not only was each band specifically designed to avoid spectral overlap, but also included an additional band in the red-edge region of the EMS, which has been found to benefit the discrimination between species (Qiu et al., 2017; Macintyre et al., 2020; Ottosen et al., 2020). The results of the feature importance testing (Figure 9) suggests that the blue band, which is lacking in the Parrot Sequoia, is of high importance for mapping tree species. Key et al., (2001) also found the blue band to be highly significant for species classification due to its sensitivity to chlorophyll and insensitivity to shadowing in canopies, a significant problem in many types of classification studies (2001; Fassnacht et al., 2016; Milas et al., 2017). The most important bands for the Sequoia also happened to be in the visible range (red and green) while the red-edge and the NIR bands were found to be the least important bands. The visible bands should thus be considered highly important when conducting future classification studies (Miyoshi et al., 2020).

This result has important implications in that users of the technology may necessarily have to buy a more expensive multispectral sensor and in-fact would achieve better results with the RGB sensor alone. However, studies comparing the consumer grade RGB sensor to multispectral sensors containing blue bands such as the Micasense RedEdge-MX (https://micasense.com) or the DJI P4 Multispectral (https://www.dji.com) should be carried out. Hyperspectral sensors with hundreds of

bands covering a visible to invisible wavelengths exist, and could very well improve the accuracy of species classifications (Nevalainen et al., 2017; Maschler et al., 2018; Miyoshi et al., 2020), but will most likely remain cost prohibitive for some time.

Conclusions

With greater focus being placed on precision forestry, there is growing need to improve our ability to generate species-level maps of forest communities. UAS, capable of achieving very high spatial and temporal resolutions, have recently become an affordable means of generating these species level maps. Hardware limitations, mainly weight, have restricted the type of sensors that can be flown. Lower spectral resolution, consumer grade RGB camera are frequently being flown due to their lower weight and affordability, but are not typically optimal for classifying vegetation down to the species level. While lightweight multispectral cameras exist, the cost of these sensors are potentially cost prohibitive. This study investigated whether taking advantage of the UAS' higher temporal resolution to track tree phenology could help to improve the species-level classification accuracy with both RGB and multispectral imagery. Additionally, the optimal phenological timing for UAS data collection was investigated and a comparison between the performances of an RGB sensor to that of a multispectral sensor carried out.

Results show that there was a considerable and statistically significant increase in accuracy when utilizing a multi-temporal classification compared to a mono-temporal classification. While accuracy increased with additional dates of imagery, there was no significant increase in accuracy beyond utilizing three dates of optimally timed imagery. Based on the accuracy of the best performing date combinations, mid and late-spring imagery was found to be crucial points in the growing to

capture, most likely due to the high inter-species spectral heterogeneity and intra-species homogeneity captured at these moments.

The multispectral sensor employed in this study consistently underperformed compared to the RGB sensor. The RGB sensor was found to perform the same as the multispectral sensor when employing a mono-temporal classification, but became statistically better as the number of dates of imagery increased. An analysis of feature importance suggests that the visual bands are important for species classification at this resolution, especially the blue band, and less significance can be placed on the non-visual bands.

This study was conducted in a highly heterogeneous forest; 14 separate species were classified. High-inter species spectral variability is to be expected, especially if they exhibit similar phenology or are natural highly variable to due growing conditions or health. Future research is needed to investigate the benefits of derivative layers such as spectral indices and texture on overall accuracy. Additionally, expansion of the UAS collection into the late summer/autumn months may present interesting results. Finally, further research is necessary on comparing consumer grade RGB sensors to multispectral sensors that employ all the visual bands if not more.

CHAPTER 5

EVALUATING THE CAPABILITY OF UNMANNED AERIAL SYSTEM (UAS) IMAGERY TO DETECT AND MEASURE THE EFFECTS OF EDGE INFLUENCE ON FOREST CANOPY COVER IN NEW ENGLAND

Abstract

Characterizing and measuring the extent of change at forest edges is important for making management decisions, especially in the face of climate change, but difficult due to the large number of factors that can modify the response. Unmanned aerial systems (UAS) imagery may serve as a tool to detect and measure the forest response at the edge quickly and repeatedly, thus allowing a larger amount of area to be covered with less work. This study is a preliminary attempt to utilize UAS imagery to detect changes in canopy cover, known to exhibit changes due to edge influences, across forest edges in a New England forest. Changes in canopy cover with increasing distance from the forest edge was measured on the ground using digital cover photography and from photogrammetric point clouds and imagery-based maps of canopy gaps produced with UAS imagery. The imagery-based canopy gap products were significantly more similar to ground estimates for canopy cover (p-value < .05) than the photogrammetric point clouds, but still suffered overestimation (RMSE of .088) due to the inability to detect small canopy openings. Both the ground and UAS data were able to detect a decrease in canopy cover to between 45-50m from the edge followed by an increase to 100m. The UAS data had the advantage of a greater sampling intensity and was thus

better able to detect a significant (p-value < .0001) edge effect of minimal magnitude in the presence of heavy variability.

Introduction

Forest fragmentation is an increasingly pervasive problem that threatens global biodiversity and decreases ecosystem services by degrading habitat quality (Murica, 1995; Harper et al., 2005; Riitters and Wickham, 2012; Haddad et al., 2015). After removal, the remaining forest is exposed to the surrounding land cover matrix leading to edge influences (EI), the effect of abiotic and biotic processes at the edge (Murica, 1995; Harper et al., 2005). Edge habitat is the area over which EIs are having an impact on forest condition. In general, there is greater light availability, temperature variability, and wind as well as increased access to organisms and materials like pollen and seeds immediately following the edge creation (Chen et al., 1992; Matlack, 1993; Didham and Ewers, 2014; Magnago et al., 2015; Hofmeister et al., 2019). These direct effects of edge creation influence ecological processes (e.g., productivity, evapotranspiration, decomposition, recruitment, and mortality) which lead to changes in the forest structure (Mascarúa López et al., 2006; Dupuch and Fortin, 2013; Wasser et al., 2015; Meeussen et al., 2020). These modifications at the edge can make the area less suitable for many of the species that once resided in and/or relied on the interior forest habitat (i.e., core area), effectively making the remaining forest patch too small to meet their needs (Murica, 1995; Riitters et al., 2012). The composition at the edges of forest patches has been found to shift towards edge-adapted, typically early-successional species in many parts of the world (Hofmeister et al., 2013; Ziter et al., 2014; Eldegard et al., 2015). Invasive species richness and cover has also been found to be positively correlated with forest edge habitat (Brothers and Spingarn, 1992; MacQuarrie and Lacroix, 2003; Pauchard and Alaback, 2006; Allen et al., 2013). Invasive plants not

only out outcompete native plants, but also support fewer insect and birds species (Frappier et al., 2003; Tallamy and Shropshire, 2009; Narango et al., 2018), further reducing biodiversity. As fragmentation continues, patches become smaller and more irregularly shaped, causing them to be increasingly dominated by edge habitat (Murica, 1995; Ries et al., 2004).

Understanding the impacts of fragmentation and the relative amount of core and edge forest habitat on the landscape requires an understanding of how far into a forest patch the edge is exerting an influence (Ranney et al., 1981; Wilcove et al., 1986; Laurance and Yensen, 1991; Didham and Ewers, 2012). A first step in accomplishing this is to estimate the depth of edge influence (DEI) (Laurance et al., 2002; Ries et al., 2004) or the distance from the edge into the forest community over which there is a substantial EI (Harper et al., 2005). Once known, edge habitat on the landscape scale can be modeled (Laurance and Yensen, 1991; Didham and Ewers, 2012). DEI is typically determined in the field by sampling along the edge to interior gradient. Transects running perpendicular from the forest edge into the interior with systematic sampling plots placed at known intervals from the edge are commonly established (Chen et al., 1992; Harper and Macdonald, 2001, 2002; Harper et al., 2007; Dupuch and Fortin, 2013; Eldegard et al., 2015). At each plot, one or more variables related to forest structure, composition, or processes that are believed to co-vary with distance (i.e., tree height, canopy cover, invasive species presence/abundance, etc.) from the edge are measured (see Harper et al., (2005) for review). Potential "edge samples", are compared to reference samples that are believed to represent interior forest conditions (MacQuarrie and Lacroix, 2003; Mascarúa López et al., 2006; Harper and Macdonald, 2011; Dupuch and Fortin, 2013; Harper et al., 2014). The DEI is measured as the sample (i.e., distance) furthest from the edge that is considered different from the interior.

DEI is a highly variable number, however, and has been found to vary with edge maintenance (i.e., is regeneration suppressed via mowing or plowing), landscape orientation, age or time since

edge creation, and stand composition (Matlack, 1993; Esseen et al., 2016; Hofmeister et al., 2019; Meeussen et al., 2020). A current review of forest edge research has further found a great deal of variation across forest biomes and edge origin (natural vs anthropogenic) (Franklin et al., 2021). One-size-fits-all DEI for landscape modeling is not appropriate (Pinto et al., 2010). Assuming a singular DEI has important implications when planning conservation areas or developing management plans with interior forest preservation in mind (Laurance et al., 2007; Pinto et al., 2010; Didham and Ewers, 2012). Additionally, the structure of the forest at the edge may have implications on modeling global carbon balances (Reinmann and Hutyra, 2017; Smith et al., 2018). However, this variability makes it difficult to accurately measure edge depth at this scale without extensive fieldwork (Dantas De Paula et al., 2016; MacLean, 2017). Moreover, it is becoming more important to assess the temporal changes across these edges in the face of climate change (Reinmann and Hutyra, 2017; Hofmeister et al., 2019), making repetitive collections necessary.

Measures of forest structure, commonly used in studies of edge influences to describe forest edge habitats, have been made from remotely sensed data for decades (Wulder et al., 2004). Remotely sensed data like satellite or aerial imagery and LiDAR have the benefit of covering large areas with repeat visitation. Given this advantage, several studies have attempted to make use of these data for investigating edge influences assessing changes in remotely sensed estimates of structure with distance. MacLean (2017) and Vaughn et al., (2015) utilized LiDAR to estimate changes in understory and over-story canopy cover, respectively, and found significant relationships between edge distance and cover. Dantas De Paula et al. (2016) utilized a Landsat Tree Cover dataset (Sexton et al., 2013) to investigate changes in canopy cover with distance from a forest edge at 11 study sites across 5 continents, finding significantly lower canopy cover near edges across all sites. These studies demonstrate the usefulness of remotely sensed data for investigating edge influences. However,

LiDAR data can be expensive to collect, outdated, or lacking the specifications (e.g., spatial resolution, leaf-on imagery) necessary to appropriately measure EIs (Brosofske et al., 2014; Colomina and Molina, 2014; Zielewska-Büttner et al., 2016). Additionally, the LANDSAT Tree Cover data or similar image products like the National Land Cover Data (NLCD) Tree Cover dataset (https://www.mrlc.gov/finddata.php) are mapped at a 30m spatial resolution. At this resolution, a pixel would cover or come close to covering the extent of most measured edge effects. For example, in a review of measured DEI for a variety of response variables, DEI, on average, was 20m to 25m for canopy and understory cover and 35m to 40m for changes in species composition (Harper et al., 2005, Franklin et al., 2021).

Imagery collected by unmanned aerial systems (UAS) have become a flexible and cost-effective means of gathering forest structural information. Recent advancement in computer vision, combined with well-established photogrammetric techniques have led to two processes known as Structure-from-Motion (SfM) (Westoby et al., 2012) and Multi-view Stereo (MVS), typically abbreviated SfM-MVS because they are often both employed together. These processes allow similar 3-dimensional information to be extracted from imagery collected by inexpensive digital cameras (Snavely et al., 2008). When the sensor is mounted on a UAS, the combination becomes a powerful tool for studying forests (Iglhaut et al., 2019). Highly dense point clouds similar to that of LiDAR data can be produced from overlapping UAS images. While it lacks the ability to capture more of the forest's internal vertical structure (Vastaranta et al., 2013; White et al., 2015; Wallace et al., 2016; Hernandez-Santin et al., 2019), UAS imagery can capture measures of canopy cover (Lisein et al., 2013; Vastaranta et al., 2013). Canopy cover has commonly been found to experience substantial effects due to EI (Chen et al., 1992; Matlack, 1993; Gehlhausen et al., 2000; Harper and Macdonald, 2001; Mascarúa López et al., 2006) and is important ecologically as it controls a number of biotic

and abiotic processes on the ground (Koukoulas and Blackburn, 2004; Bagaram et al., 2018). The very-high spatial resolution orthomosaics, with spatial resolution on the order of centimeters, produced from the UAS imagery have also been utilized to estimate foliage cover (Chianucci et al., 2016; Bagaram et al., 2018; Shin et al., 2018; Tu et al., 2019), though comparisons between cover estimates generated from the photogrammetric point clouds and orthomosaics are lacking. To date, no study has utilized the products of UAS imagery to investigate edge influences. If found to be a successful tool, the flexibility of the UAS could significantly increase data collection at the edge, especially over time due to its ability to collect imagery wherever and whenever needed at a fraction of the cost, relative to aerial or satellite imagery (Anderson and Gaston, 2013).

Forest edges in New England and, more generally, the eastern U.S. temperate broadleaved forests, deserve considerably more attention as they could potentially be important for carbon sequestration (Birdsey and Heath, 1995; Goodale et al., 2002; Zheng et al., 2011; Pugh et al., 2019; Finzi et al., 2020). Understanding the effects on forests at these edges could go on to better inform our carbon accounting (Reinmann and Hutyra, 2017; Franklin et al., 2021). The forests of New England are relatively young due to human modification following colonial settlement. In general, much of the region was completely deforested for agriculture and remained that way until they were abandoned and left to regenerate by the late 19th century (Foster, 1992; Fuller et al., 1998). This has resulted in young forests not yet facing age-related declines in growth rate and a number of disturbance-adapted species present in the area that can take advantage of the increased resources at the edges (Oliver and Larson, 1996). New Hampshire, a part of the New England region in the U.S., has long maintained the title of being the second most forested state in the U.S. However, recent data shows that the state has been experiencing a continuous decrease in forest cover (Jeon et al., 2014; Olofsson et al., 2016; Grybas et al., 2020). The increase in development due to population growth

has led to the fragmentation of large forest blocks with more predicted to occur in the future (Zankel et al., 2006), resulting in increasing exposure to edge influences. Therefore, the objective of this study was to investigate whether UAS imagery could be used to detect and assess the depth of edge influence in a New Hampshire forest. We focused on changes in canopy cover due to its strong influence on other aspects of forest structure; typically, increased light and wind at the openings (Harper et al., 2005). The measurements of canopy cover extracted from the UAS imagery were compared to ground-based measurements to determine feasibility of this method. The effects of edge influences were then modeled using both the ground and UAS-generated data to characterize and quantify the effect, if present. This study serves as an initial assessment of UAS for assessing edge habitats and should spur additional research into the effects that can be quantified with this technology.

Materials and Methods

Study Area

This research was conducted on the Blue Hills Foundation conservation lands in New Hampshire, U.S.A (Figure 10). The area covers 2946.95ha and spans five New Hampshire towns. This property is owned by the Blue Hills Foundation Inc. and managed by the Harvard Forest. This particular stand in which this study was carried out represents a natural, highly mixed, transition hardwood-hemlock-white pine forest community as described by Westveld (1956), or a Hemlock-beech-oak-pine forest as discussed in Sperduto and Nichols (2012). White pine (*Pinus strobus*) and eastern hemlock (*Tsuga canadensis*) are the dominant species in the forest followed by red maple (*Acer rubrum*), red oak (*Quercus rubra*), red pine (*Pinus resinosa*), and American beech (*Fagus*

grandifolia). Our study site and corresponding edges were located within a small subunit of the Blue Hills Foundation lands and was carefully selected due to its proximity to a suitably-sized field for UAS flying, adjacency to continuously maintained fields, because it represents a predominately southern edge exposure, and because these edges are considered older (> 30 yrs. since edge creation) (Harper et al., 2005). The latter factors were chosen in an effort to maximize the potential to detect an edge effect.

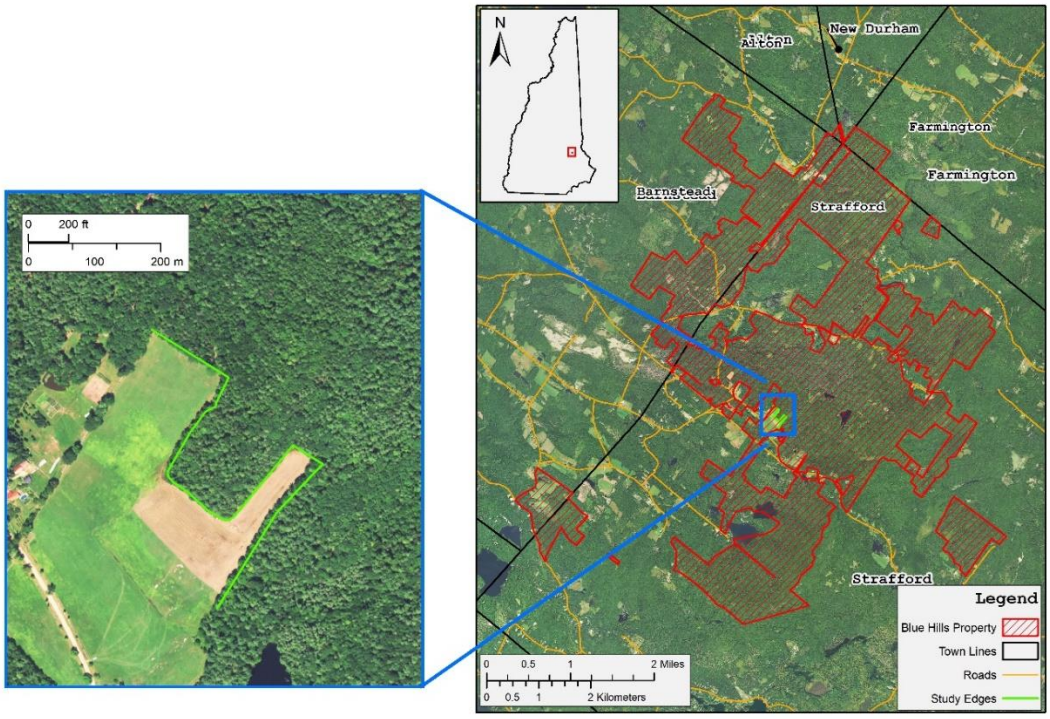

Figure 10. Study area map. The panel on the right displays the Blue Hills Foundation conservation lands. The Panel on the left shows the location of the edges (the green line) investigated in this study.

Ground Data Collection

To establish a reference for the edge effects in the study area, a traditional ground data collection of foliage cover (i.e., the vertical projection on the ground of the forest canopy including

within crown gaps) was carried out. Ground data were collected between 9/28/2019 and 9/30/2019. Nine transects running perpendicular into the forest were established along an approximately 944m length of forest edge. A random point along this edge was chosen for the placement of the first transect. Subsequent transects were spaced 100m apart and/or >50m from a corner (Chen et al., 1992; Harper and Macdonald, 2001, 2002; Wasser et al., 2015). Figure 11 shows the general sampling setup along each transect. The transect bearing was chosen as the azimuth perpendicular to the edge with the 0m distance point placed on the edge line. The edge line was considered the inside edge of any stone walls if present, or the outermost extent of the tree stems within roughly 10m of either side of the transect location. Once the starting position and bearing were established, sampling locations were placed systematically along the transect line. Sample spacing was 5m within the first 50m and then was increased to 10m between 50m – 100m. The sampling intensity was higher up to 50m because edge effects have commonly been found to extend 50m or less into the forest (Matlack, 1993; Harper et al., 2005; MacLean, 2017; Buras et al., 2018). It is important to note that not every transect line extended 100m. Transect distance was alternated between 50m and 100m due to time constraints, except in the case where a 100m distance would place the end of the transect within 50m of a second edge. In addition to a sample point being taken along the transect line at the specified distance interval, two more samples were taken 5m perpendicular on either side of the centered point, to avoid overlap between adjacent transects and DCP images. Thus, for each distance, three samples were collected.

Digital Cover Photography (DCP) was employed to estimate the foliage cover (FC) at each sample location (Macfarlane et al., 2014; Chianucci, 2020) (Figure 12). DCP is similar to traditional digital hemispherical photography, but utilizes a much narrower field-of-view (0-30° compared to 0-180°). An approximately vertical image of the canopy was collected and then processed to separate

the sky from everything else. FC was calculated as the percentage of the image not considered sky. DCP is more robust to camera parameters, lighting conditions, produces higher resolution images (Pekin and Macfarlane, 2009), and has been found to accurately measure foliage cover (Pekin and Macfarlane, 2009; Chianucci and Cutini, 2013; Chianucci, 2016). Digital canopy photos were collected at each sample site using a Canon Rebel T6i mounted to a 4m tall extension pole to capture only the upper canopy. The focal length was set to 55mm, which is approximately a 15.42° field-of-view. For each picture, the pixels were classified as either sky or vegetation using the procedures outlined in Nobis and Hunkiker (2005). FC for each image was simply the proportion of that image classified as vegetation. The three FC measurements taken at each distance on each transect were then averaged together.

UAS Data Collection and Processing

UAS imagery was collected over the study area on July 1st, 2020, with a Sensefly eBee X fixed wing and the eMotion 3 mission planning software (SenseFly, 2020). The Sensefly Aeria X camera was used to collect the imagery. The Aeria X is a standard DSLR camera and captures very high-resolution (24 mega-pixel) natural color (RGB) imagery. The weather this day was calm winds and predominately overcast which helped to maintain consistent illumination across all the images. The imagery was collected 100m above the trees (approximately 120m above the ground) with an 80% and 85% latitudinal and longitudinal overlap, respectively. The mission area for each edge of the study site was setup to collect at least 200m from the edge into the forest. In total, 1299 images were collected and used to generate the following UAS-derived products.

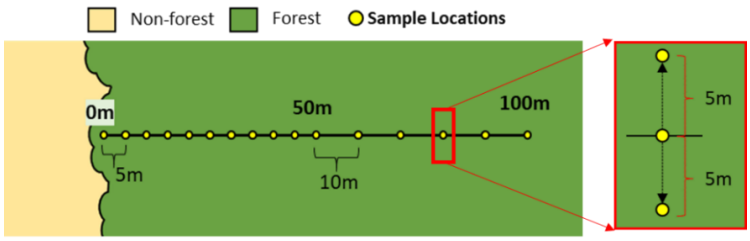

Figure 11. Ground sampling setup along transects.

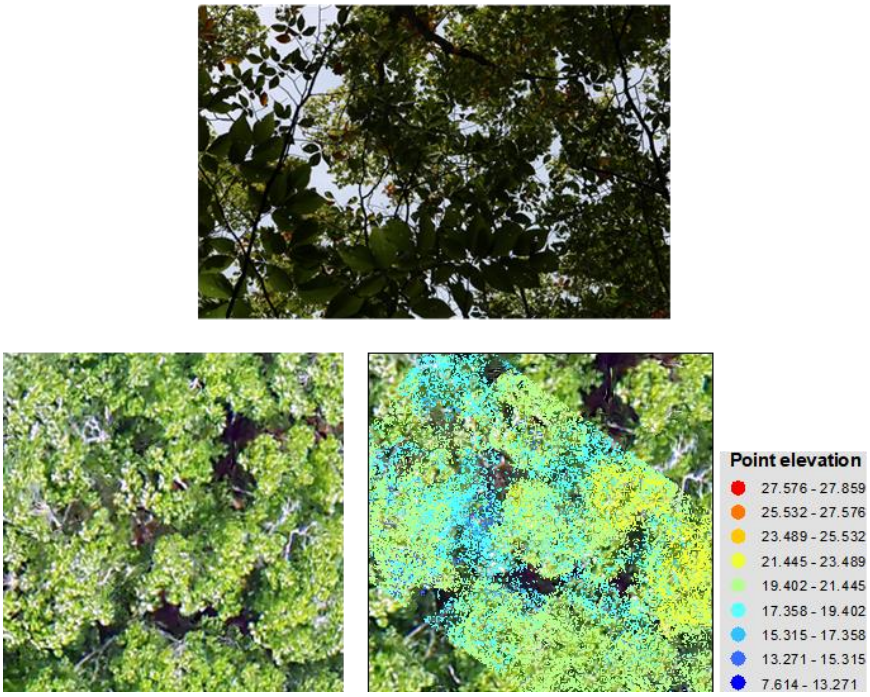

Figure 12. Comparison between digital cover photo (DCP) (Top), the 2.5cm orthomosaic (Bottom-Left) and the photogrammetric point cloud (Bottom-Right) for approximately the same location.

The eBee X is real-time kinematic (RTK) enabled, so the raw GPS positions for each image were post-process kinematic (PPK) corrected using the Sensefly Flight Data Manager included with the eMotion 3 mission planning software. Resulting positional accuracy following PPK processing was around 7cm. The UAS images were then processed in Agisoft Metashape Professional (Agisoft, 2020). Agisoft utilizes the SfM and MVS processes to produce dense, photogrammetrically generated

point clouds and orthomosaics. While a full explanation of the process is beyond the scope of this paper, it is worth noting that the point clouds are produced by automatically matching features across the multiple overlapping images and using the estimated camera interior and exterior orientation to estimate the absolute coordinate position and height for each matched feature (i.e., point). A digital surface model (DSM) was produced from the resulting point cloud which was then used to orthorectify the UAS images. The rectified images were then mosaicked together to produce an orthomosaic. The specific Agisoft processing parameters were: 1) Align Photos run with "High Accuracy" and Generic preselection, Guides Image Matching, and Adaptive model fitting turned on. 2) The dense point cloud generation was run on "Ultra-high" quality and mild filtering. 3) The UAS imagery was ortho rectified using a DSM generated from the dense point cloud and mosaicked. The dense point cloud (density of 8,264 pts/m^2) and the orthomosaic were exported from Agisoft. The spatial resolution of the orthomosaic was 2.48cm, however, for simplicity; they were exported at a 2.5cm resolution so that the spatial resolution would be a factor of the plot sizes utilized in this study. The 2mm difference was expected to have minimal impact on the canopy mapping below.

Estimating Foliage Cover from UAS Data Products

FC can be estimated two ways. The first is from the point cloud after normalizing all the point elevations to height above the ground. The percentage of the points above a certain height threshold within a defined area taken as an estimate of foliage cover. The second is an image-based method where the orthomosaic is used to map openings in the canopy creating a binary "gap map". Similar to the point clouds, the percentage of a defined area not classified as a gap is the estimated FC (Chianucci et al., 2016). It is important to note that the image-based method described here does not

employ any height threshold. Both methodologies were employed in this study, first using the UAS point cloud and then the orthomosaic.

In the first approach, the dense point cloud was normalized to height above the ground using a digital terrain model (DTM) produced in 2015-2016 from leaf-off LiDAR data. Photogrammetrically- produced point clouds typically lack points at the ground to generate an accurate DTM, especially over dense canopies. Thus, externally produced DTMs from LiDAR are often used to normalize them (Niethammer et al., 2012; Hugenholtz et al., 2013; Dandois et al., 2015). The DTM was downloaded from the GRANIT LiDAR Distribution site (https://lidar.unh.edu/map/, last accessed July 15th, 2021) at a 1m spatial resolution. The elevation of the ground estimated at the pixel within which each point fell was simply subtracted from the elevation of the point.

For the second, image-based, approach, a binary map representing gaps or openings in the canopy were mapped from the orthomosaic using a variation on the method, known as LAB2, developed by Macfarlane and Ogden (2012), and found to be well suited for estimating cover in dense forest stands (Chianucci et al., 2014, 2016). This method splits the pixels in the orthomosaic into four training groups using logical rules based on the RGB pixel values. The groups of primary importance are the foreground and background pixels representing vegetation and non-vegetation respectively. The orthomosaic is then transformed from the RGB color space to the CIE L*a*b* color space. The new bands represent a pixel's luminosity (L), hue between magenta and green (a*) and hue between yellow and blue (b*). The separation of the luminance from the pixel color helps to avoid problems associated with uneven illumination across an image (Liu et al., 2012). Additionally, the green leaf area (GLA) vegetation index was derived from the original RGB orthomosaic. The mean GLA, a*, and b* of the foreground and background groups is calculated. The pixels are then classified as either foreground or background using a minimum distance to the group mean classifier.

Based on the work of Chianucci et al., (2016), the pixels classified as foreground (vegetation) were considered the canopy while the background (non-vegetated) were considered the gaps.

The initial LAB2 results were adjusted to account for forest floor vegetation visible in canopy gaps, which should not be considered part of the upper canopy. Additionally, tree limbs and overexposed canopy pixels were classified as non-vegetated by the LAB2 methodology due to having no green reflectance and being spectrally saturated across the RGB bands, respectively, but were in fact part of the upper canopy. An assumption was made that objects in the upper canopy classified as "non-vegetation" would be bright (high L values relative to non-vegetated pixels below the canopy) due to the light being able to directly hit them. Conversely, vegetation not in the upper canopy would be dark (lower L relative to real canopy vegetation). To account for this effect, a different threshold was applied to each group of pixels (vegetation vs not vegetation) based the histogram of the L values for each. Threshold values were determined by looking for obvious breaks in the distributions. The result was similar to the LAB2 map but now considered gaps with vegetation in addition to the non-vegetated components and saturation errors above. These maps in-and-of-itself are not an estimate of FC but are used to estimate FC by summarizing the amount of gap within a defined area.

The effectiveness of the point cloud versus image-based (using the gap maps) method for estimating FC were assessed by comparing the FC estimates from method to the ground-measured FC from the DCP at the sample locations. Polygons of size 15m x 5m centered along the transects at each measured distance were generated using the GPS positions collected during ground data collection and GIS. The width of these polygons was chosen to account for the maximum distance between the outside sample plus a few meters to account for the fact that the DCP imagery at the outside samples would extend to the left and the right of the sample positions. Unfortunately, the

exact area covered by a DCP image will vary considerably with upper canopy and mid-canopy height. The accuracy of GPS positions is often highly degraded when working under the dense forest cover. For this reason, only the starting position of each of the transects, the 0m point, were recorded in the field. A Trimble Yuma, running Trimble TerraSync, was setup on a tripod in the adjacent field, away from the canopy edge with a clear view of the sky. The azimuth direction and distance from the GPS to the 0m point was recorded. The unit was set to record its position at a 1s-sampling rate during the collection of the transect. These GPS positions were then PPK-corrected in Trimble Pathfinder Office (positional error between 1-2m) and, using the azimuth and direction, utilized to calculate the coordinates of the 0m point for each transect. The coordinates of the remaining sample locations were estimated using the distance along the transect from 0m and the transect bearing. Only the points on the transect were estimated. The sample points on either side of the transect were not. The 15x by 5m polygons were centered on each point. Thus, at any given location, the polygon extended 2.5m north, south, and 7.5m east and west. The FC was calculated within each polygon first, with the normalized point cloud and then using the imagery-based gap maps. For comparison, FC with both the original LAB2 gap map and the modified LAB2 gap were calculated. The root mean squared error (RMSE) was calculated as a measure of similarity and statistically compared with a paired t-test (alpha = .05).

Investigating Edge Effects with UAS Data

Based on the results of the FC estimate comparison, the detection and modeling of edge effects using UAS data were carried out with modified LAB2 canopy gap maps. The edge line was digitized using leaf-off UAS imagery of the study site so the edge under cantilevered canopies could been seen (See inset on Figure 10). Every effort was made to mimic the edge line rules applied during

field collection. For simplicity, the digitized lines were generalized to minimize the number of vertices. A grid of points with a 5m spacing oriented to the general bearing of the digitized edge line was produced. Only those points within 200m of the edge were retained. A maximum distance of 50m was applied to the edges along the convex portion of forest in the lower edge since this area is narrow. A 2.5m radius buffer (5m diameter) was placed around each point and the perpendicular distance and bearing from the centroid to the nearest edge line, not vertex, was calculated. The FC within each 5m diameter buffer was then estimated using the canopy gap map.

Data Analysis

Generalized Additive Models (GAMs) (Wood, 2017) were used to determine where there was a significant relationship between FC and distance from an edge as well as to visualize the relationship, if present. GAMs are a powerful tool for modeling the often non-linear responses exhibited by edge effects and allows us to clearly visualize the trend between response and predictors (Lhotka and Stringer, 2013; Hofmeister et al., 2017, 2019; García-Romero et al., 2019). Unlike Generalized Linear Models (GLM), the assumption of a linear relationship between the response and a predictor variable is relaxed and is instead modeled as smooth, non-parametric function determined by fitting splines to the data. The analysis was carried out in R 4.0.2 (R Core Team, 2020) using the *mgcv* package (Wood, 2017). The GAM was fit using the image-based FC estimates. FC was modeled as a smooth function of distance from edge, fitted using penalized cubic splines. Within the specific smooth function, *k*, the basis dimension or maximum degrees of freedom the smooth function is allowed to utilize, was set to 10. Per the suggestion of Wood (2017), *k* should be large enough to ensure the underlying relationship is captured but low enough to maintain computational efficiency. The restricted maximum likelihood (REML) method was used to estimate the smoothing parameter

for the model. The smooth parameter effectively reduces the degrees of freedom to avoid overfitting. Because FC represents proportions bounded between zero and one, a beta distribution and logit link function was specified. A built-in check of the basis dimension was run to ensure *k* was set high enough. Additionally, the standard residual diagnostic plots were scrutinized to ensure the standard model assumptions were met.

A spatial term to account for spatial autocorrelation was not included in the model. A semivariogram of deviance in FC by distance between adjacent samples was checked and little to no spatial autocorrelation in the sample data was found which falls in line with the suggestion of Jennings (1999) that the sample distance be greater than the largest tree crowns in order to reduce and avoid spatial autocorrelation between estimates of canopy cover. The 5m spacing between samples is wider than the average tree crown in this stand.

Results

Ground Data Collection

In total, nine transects were measured on the ground (Figure 13). All transects extended at least 50m into the forest; three extended to 100m. The FC measurements taken at each sample location (i.e., distance) on the transect were averaged and are summarized in Figure 14. All FC estimates in this study are shown as decimal percentages between 0 (i.e., 0%) and 1 (i.e., 100%). FC was generally greater than 0.80 across the transects, potentially extending to 0.91. Two notable outliers occur at 70 and 100 meters. There is a general, decreasing trend in FC over the first 50m. After 50m, the FC increases again, coming close if not matching the FC at the edge. Variability

between and across the measured edge distances were high as indicated by the 95% confidence intervals.

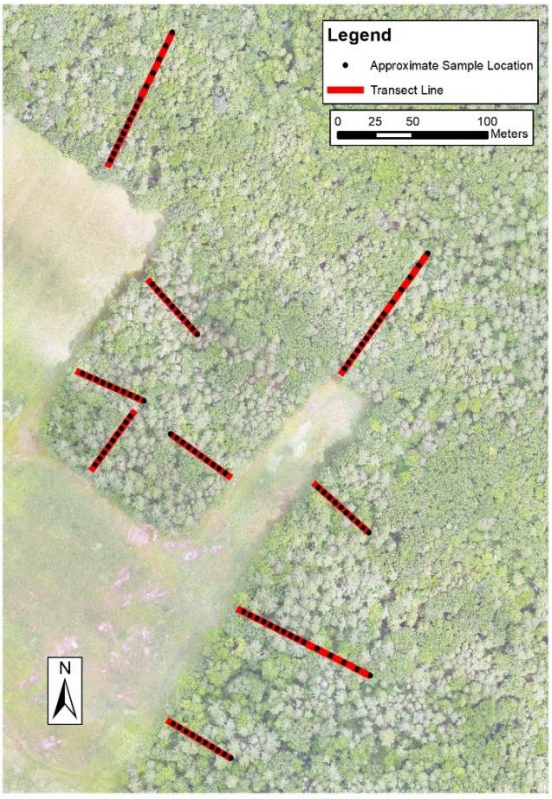

Figure 13. Estimated location of transects (red lines) and sample points (black dots) along each transect measured on the ground. Locations for transects were based on GPS position of 0m point and azimuth bearing of the transect. Sample locations are systematically placed on transect line starting at 5m and extending to either 50m or 100m. See Figure 11 for sample spacing.

Generating Foliage cover from UAS Data

Foliage cover was estimated from the UAS imagery using the normalized photogrammetric point cloud and both image-based gap maps. The similarity between the FC estimated from these methods and the ground measured FC was measured by calculating the RMSE and paired t-test between them using a 15x5m box centered on each approximate ground sample location to represent the area covered on the ground. The image-based estimates were calculated two ways. The first was

using the LAB2 method as described by Macfarlane and Ogden (2012). The second was a modified version of the LAB2 method whereby a threshold was applied to the L band to remove ground vegetation and include upper canopy features and errors. Comparison plots are presented in Figure 15. The normalized point cloud was the least similar to the ground FC (RMSE = 0.177). A paired t-test confirmed the values are significantly different (t = -17.07, df = 103, p = 0.0001 at 95% CI). The FC estimates were highly saturated close to one (i.e., 100%), suggesting continuous foliage cover. The image-based estimates were better than the point cloud estimate. The LAB2 estimates (RMSE = .141) improved the similarity by almost 4%; however, it is clear there is still significant difference (t = -10.1, df = 103, p = .0001 at 95% CI) between this estimate and the ground-based FC. The modified LAB2 approach improved the RMSE to 0.0880 and was not significantly different (t = -1.45, df = 103, p = .150 at 95% CI) from the ground. While there was still dissimilarity, the plot suggests that there was not a strong bias towards over or under estimation. When calculated, the bias for the modified LAB2 was only 0.0124 while the original LAB2 estimates was 0.099, six times greater.

Edge Effect Modeling

Generalized additive models were used to test for a significant relationship between FC and distance from the edge. Only the FC estimates from the modified LAB2 gap map were used. Figure 16 shows the results of the GAM model. The same GAM model is shown in both panels but with differing Y-axis scales. The scale of Figure 16a is set to match the scale of the ground data shown in Figure 14. The Y-axis on Figure 16b has a smaller range to better visualize the trend in the data. Distance from the edge was found to have a significant effect on FC ($p < .0001$). As with the ground data, there is a decrease in FC as distance from the edge increases. This decrease continues to around

45m from the edge before beginning to increase again, and peaks at 125m. The trend after 125m dips again, but only slightly and then levels out.

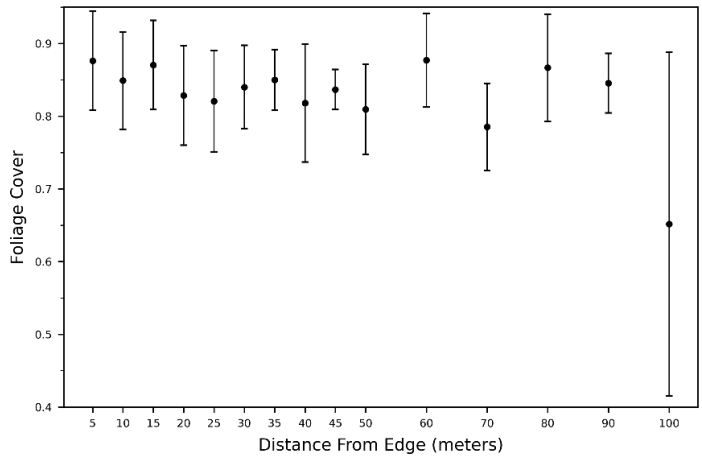

Figure 14. Average ground-based foliage cover (FC) for each sampled distance across all transects. Bars represent the 95% confidence interval around the mean. FC is shown as decimal percentages between 0 and 1 with 1 indicating 100% cover.

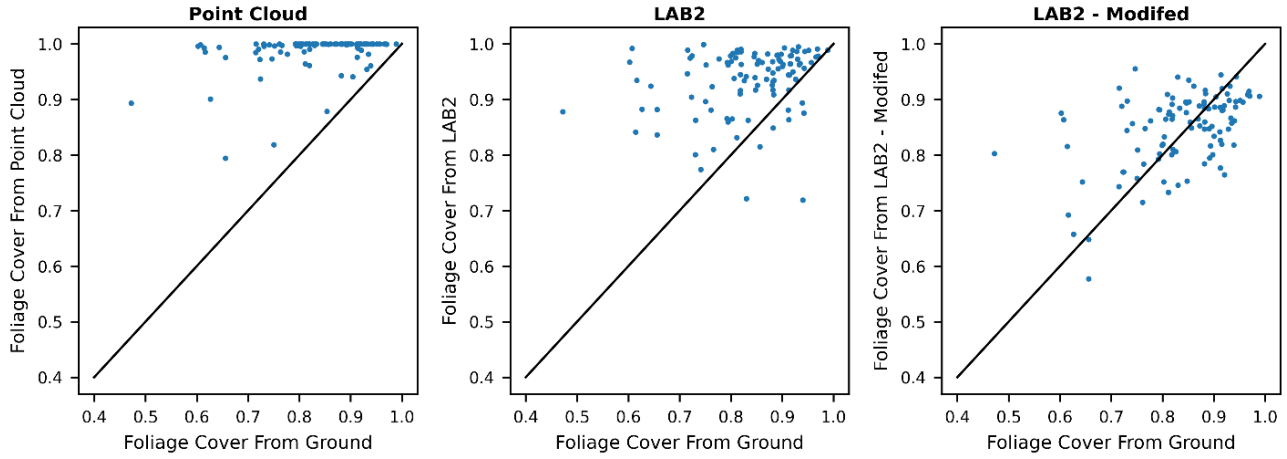

Figure 15. Comparison between the estimates of foliage cover (FC) generated from the a) normalized photogrammetric point cloud, b) the UAS orthomosaic using the LAB2 method, and c) the UAS orthomosaic using the modified LAB2 method. The solid black line indicates the 1:1 relationship. FC is shown as decimal percentages between 0 and 1 with 1 indicating 100% cover.

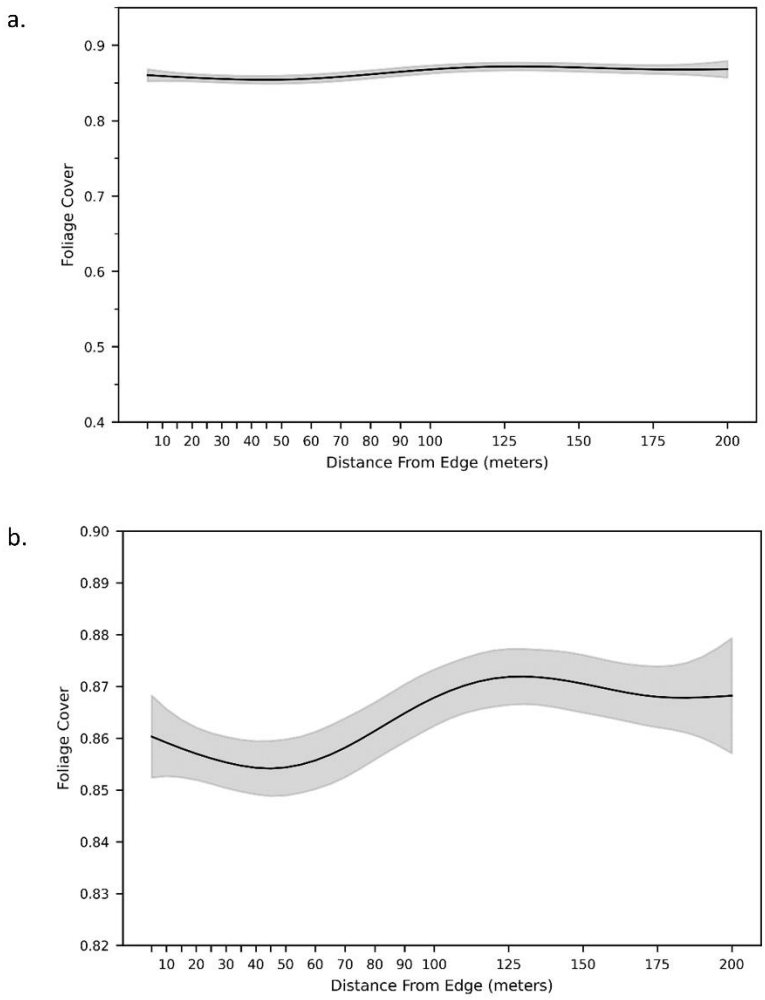

Figure 16. Results of the GAM model based on the modified LAB2 estimates of foliage cover (FC). Plots show the trend in FC with distance from edge for the same model but with different Y-axis scales. The Y-axis scale for a. matches the scale of the axis in Figure 14. The Y-axis in plot b. was narrowed to visualize the trend better. The shaded area represents the 95% confidence interval. FC is shown as decimal percentages between 0 and 1 with 1 indicating 100% cover.

Discussion

Estimating Foliage Cover with UAS Data

The ability to utilize UAS to detect and measure edge effects relies on our ability to extract the necessary information from the imagery itself. In this study, two ways to estimate foliage cover

were compared to the ground estimates of FC. The first method used the normalized photogrammetric point cloud while the second method utilized image-based gap maps derived the UAS orthomosaic. We stress here that the comparisons (i.e., RMSE) between the FC estimates from the UAS data products and the ground should not be considered measures of accuracy, rather similarity. The exact placement of the sample locations was estimated from the GPS location of the starting point due to the inability to precisely locate the positions with a GPS under dense canopy. Furthermore, unlike a camera pointed down at the ground from a known height, the area covered by an upward pointed camera is not easily known. Thus, the relative change in similarity is what was assessed.

This study found high over estimation of FC when using the normalized point cloud. An investigation of the point cloud results revealed a lack of points in small to moderate sized gaps (Figure 12). Jayathunga et al., (2018) similarly found photogrammetric point clouds from UAS imagery significantly overestimated canopy cover when compared to LiDAR produced estimates in a complex mixed forest stand. Both our study and theirs exhibited similar saturation around 1.0. They attributed their result to unreconstructed smaller gaps during the SfM-MVS processing. Other studies investigating the ability of photogrammetric point clouds to detect openings have reported similar results (Vastaranta et al., 2013; White et al., 2015; Wallace et al., 2016, 2019). The SfM-MVS method relies heavily on not only the ability to detect features in an image, but ability to match those features across a large number of images. As gap size decreases, it stands to reason the ability to "see" below the upper canopy decreases. Additionally, as the height of the upper canopy increases, it is far less likely the ground can be viewed across multiple different images (Wallace et al., 2016; Zielewska-Büttner et al., 2016). Shadows below the upper canopy can furthermore reduce feature detection, especially on sunny days when image contrast is decreased (Lisein et al., 2013; Dandois et al., 2015; Wallace et al., 2016; Iqbal et al., 2018). Zielewska-Büttner et al., (2016) attributed shadows and the

surrounding vegetation height to the high commission errors they encountered when mapping forest gaps with photogrammetric point clouds. Our imagery was flown on a predominately-overcast day to reduce the shadow occurrence; however, the upper canopy still limited light penetration to the forest floor and many of the canopy gaps were small. Increasing the overlap and lowering the flying height in order to increase the spatial resolution could help to improve the detection of these small and moderate gaps (Dandois et al., 2015; Frey et al., 2018); however, there are limitations when flying with a fixed wing UAS that may be mitigated by flying a rotary wing UAS. For example, unlike a rotary wing system, a fixed-wing system cannot stop and turn in place. Instead, it performs steep banking turns placing it closer to the canopy. The flying height must be set high enough to ensure the turns can be made without collision. Along the same line, increasing the longitudinal overlap is a simple means of increasing the image cover across a study site without increasing flight time much. However, forward overlap is limited by the time it takes the sensor to process and store the previous image and fixed-wing drones must maintain a certain air speed in order to maintain flight.

Similarity between the ground and the UAS FC estimates increased when canopy gaps were mapped using the very high-resolution orthomosaic. The original LAB2 method was simple to implement and visually performed well at separating the green vegetation from everything else. The RMSE remained high however because while it detected vegetation appropriately, many spectrally saturated pixels at the top of the canopy were mapped as non-vegetation. Additionally, without height information, vegetation that was visible in the larger canopy openings below the upper canopy were included in the non-gap category. The DCP imagery, however, was taken 4m above the ground. After testing these two components independently, the understory vegetation contributed the most to the RMSE. The LAB2 method was initially designed to separate understory vegetation from the ground

using imagery collected below upper canopy. Thus, the focus is to map vegetation versus not vegetation; height was not necessary as there was no overhead vegetation layer that had to excluded from the analysis. The primarily interest of this study however was to locate gaps in the upper canopy which may or may not contain the vegetation present in the understory. By applying the threshold to the lightness, band (L) within each group after performing the LAB2 mapping, the similarity between the ground and the UAS estimates increased considerably. It is important to note here however, that because height was not considered, the modified image-based gap was more focused on mapping shadowed gaps rather than absolute openings above a certain height (Bagaram et al., 2018). Thus, large, illuminated gaps may have been missed; however, this was of minimal concern due to flying on an overcast day.

The RMSE suggested there was still over estimation. Chianucci et al., (2016) employed the original LAB2 method to map canopy cover over a dense beech stand and found the UAS image-based estimates were consistently higher than the DCP estimates. Chianucci et al., (2021) noted that the image-based estimates of FC using 10cm UAS orthomosaics were more correlated with crown cover, canopy cover that does not consider the small with-crown gaps, most likely due to the differences in resolution. Figure 12 provides a comparison between a DCP image and the orthomosaic for the same area. The resolution of the DCP imagery is such that it is detecting small openings between leaves in the canopy that may not be detected with the UAS imagery, even with a 2.5cm spatial resolution (Chianucci et al., 2016, 2021). Furthermore, the UAS imagery is subject to motion blur due to moving treetops and “artifacts” in the orthomosaic that arise as a result of the orthorectification process that further blur the detail in the canopy (Fraser and Congalton, 2018). The DCP imagery also was collected towards the end of September. Several species, especially red

maples, had begun to senesce. We did not judge leaf-drop to be high-enough by this point to affect the results, but it could have decreased the FC estimates on the ground.

Detecting and Measuring Edge Effects Using UAS

While not directly compared to the ground estimates of FC, the trend in the FC distance from edge using the UAS estimates was very similar (Figure 14 and Figure 16). In general, both estimates detected a decrease in FC from the edge towards the interior, reaching a minimum at approximately the same distance, 50m and 45m for the ground and UAS estimates of FC, respectively. Both estimates also detected an increase in FC after 50m away from the edge. The similarity in trends is not as clear at this point due to the differences in sampling intensity. Only three transects were measured out to 100m on the ground, thus there were only three estimates of FC at each measured distance making the mean FC at those distances very susceptible to outliers. An investigation of the DCP imagery showed that some of these sample locations, especially at the 70m and 100m distances, fell in large canopy openings, which skewed the means towards lower FC. This problem highlights the advantage of the UAS-based estimates over the ground data in that sampling intensity can be much higher using remotely sensed data. High internal variability within a measured edge can complicate the process of detecting edge effects. Small, local differences in microclimate, soil type, moisture, species tolerance, etc. can cause the measured response to change frequently over small distances resulting in large variances that can mask the effect (Harper et al., 2005; Laurance, 2009; Alignier and Deconchat, 2011; Dantas De Paula et al., 2016). While the ground data shows a very slight decrease in FC, the confidence intervals suggest no real significant difference with distance. This was confirmed with an analysis of variance (ANOVA) test which found so significant difference at the 95% confidence interval. The UAS model, however, suggests that there is a significant

difference until roughly 100m. The standard error of the mean can be improved by sampling more, however ground data collection is limited by time and cost. Contrarily, the UAS data can be collected in a single day.

While the trends in FC with distance were similar for both the ground and the UAS FC modeled with the GAM, there is a notable difference in the mean FC for these methods at any of the sampled distances. We will only focus here on the FC estimated between 0m and 50m due to the high sampling intensity on the ground for these distances. The ground estimates for FC went from 0.876 at the edge to 0.809 at 50m. In contrast, the UAS FC GAM estimate was 0.860 at the edge and 0.854 at 50m, a much narrower decline. Even though it did increase after 50m, it only reached a maximum FC of 0.871, a 0.017 increase. Thus, while the GAM indicated a significant effect with the UAS FC estimates, the magnitude of this effect is very minor compared to the ground data. This difference can probably be attributed to the inability of the UAS imagery to detect small openings, predominately within the tree crowns, that are being detected in the DCP imagery (Figure 12). The UAS FC estimates tended to overestimate FC compared to the ground. Thus, as mentioned before, the estimates of FC from the UAS are most likely closer to crown cover (between crown gaps). Additionally, given the age of the edge and the suspected in-growth from the understory, it is highly likely that there are not many large canopy openings. It has been shown that edge effects diminish over time reducing the magnitude of difference from the edge into the interior (Harper et al., 2015). While it is possible to increase the resolution of the imagery, inherent limitations in the SfM-MVS process and image/orthomosaic quality may limit the use of UAS imagery for detecting small canopy openings (Jayathunga et al., 2018; Khokthong et al., 2019). For edges or conditions like the ones here, active sensors such as UAS mounted LiDAR sensors may have to be employed which have the

ability to see through the canopy openings in order to detect these finer canopy openings (Tang and Shao, 2015; Pádua et al., 2017b).

Ecology at the Edge

The FC showed a distinctive trend as distance from the edge increased. Mainly, FC decreased as distance increased to 45-50m before increasing again and reaching an equilibrium around 100m based on the trend in Figure 16. Canopy cover has frequently been reported to increase with distance from the edge due to increased mortality and wind throws (Chen et al., 1992; de Casenave et al., 1995; Braithwaite and Mallik, 2012; Harper et al., 2015; Meeussen et al., 2020). Several studies have reported, however, rapid understory release, productivity, and growth close to the forest edge in temperate broad-leaved forests, due to the vegetation taking advantage of the increased access to light from the side and above (Lhotka and Stringer, 2013; Dovčiak and Brown, 2014; Harper et al., 2015; Reinmann and Hutyra, 2017). The inverse relationship in FC is most likely the result of growth at the edge filling the openings made in the canopy. In particular, the eastern U.S forests are relatively young and not yet experiencing a decline in growth rate, thus they can quickly respond to opened resources (Briber et al., 2015; Reinmann and Hutyra, 2017; Smith et al., 2018; Finzi et al., 2020).

The fact that FC does increase again and moderates after 50m suggests that there was a decrease in canopy cover after edge creation. The land use history of this area is characterized by almost complete deforestation for agriculture followed by abandonment in the late 19th century. White pine became the dominant species in the landscape as it was able to quickly propagate and grow in these newly opened sites. Today it remains an important component of new and older forest stands (Howard and Lee, 2002). Pine trees, however, are typically taller, shallower rooted, and have

a lower wood strength relative to deciduous (hardwood) species. Therefore, the development of an edge makes them more susceptible to wind damage (Foster, 1988). The distinct pattern in FC could thus be the result of these two opposing processes occurring at the same time. Large, susceptible pines near the edge succumb to the effects of the edge. The forest understory quickly grows in, even before mortality, taking advantage of the increased access to resources; primarily light (Matlack, 1994). A meta-analysis by Franklin et al., (2021) found tree mortality typically extended to 100m from the edge while understory responses like growth and recruitment extended a little over 50m. Evidence of this process has been found in studies investigating changes in sapling density and/or diameter at breast height with edge where, in general, higher sapling density or smaller size classes have been found closer to the edge while the reverse occurs for larger size classes. (Lhotka and Stringer, 2013; Ziter et al., 2014).

Future Research

This study represents a test case for employing UAS to detect edge influences. It was conducted on the edges of one study site for one response variable, but demonstrated that UAS could potentially be used to detect large canopy openings and edge effects with a very small magnitude. This success was most likely due to the sampling intensity possible with the UAS imagery that far exceeds what is possible with fieldwork. Many other response variables known to exhibit edge effects such as tree height (Dandois and Ellis, 2013; Lisein et al., 2013), tree health and mortality (Michez et al., 2016b; Buras et al., 2018), native (Lisein et al., 2015; Michez et al., 2016b; Durgan et al., 2020) and invasive species composition (Dvořák et al., 2015; Michez et al., 2016a; Müllerová et al., 2017) have been accurately mapped with the data derived from UAS imagery. Furthermore, as lightweight LiDAR sensors for UAS become more affordable, a better picture of understory vegetation at the

edge can start to be developed (Hernandez-Santin et al., 2019). The flexibility of the UAS and the resolution at which is works will allow researchers to gain a more complete picture on how forests react to edge influences and the various mechanisms controlling edge influences across space and time. The latter becoming necessary in the face of climate change (Reinmann and Hutyra, 2017; Hofmeister et al., 2019; Franklin et al., 2021). A better understanding of edge effects may be especially important in the temperate forest regions where it is now being suggested that forest edges might be important carbon sinks due to increased growth and productivity (Reinmann and Hutyra, 2017; Smith et al., 2018).

Conclusions

Forest fragmentation is a global problem that will continue well into the future. It is clearly understood that the dynamic conditions at the forest edges ultimately lead to modifications within the forest itself. These effects are highly variable across space and time, thus methodologies that allow us to analyze these effects over larger areas repeatedly are important. Remotely sensed data collected using unmanned aerial systems may come to be a vital tool to accomplish this goal due to its quick data collection and high temporal frequency, but it has yet to be investigated for this purpose. Thus, the goal of this study was to conduct a preliminary assessment of UAS as a tool for detecting and measuring edge influences. Estimates of foliage cover were collected on the ground across several edge to interior transects. Estimates of FC were then extracted from very-high spatial resolution UAS imagery over the sight and subsequently used to model the relationship between cover and edge distance.

Limitations in the UAS imagery and processing methods resulted in higher estimates of FC compared to the ground. Normalized point clouds produced using a photogrammetric process typically failed to capture information down to the ground, especially small tree gaps, resulting in significant over estimation. Image-based mapping of canopy gaps was much more successful, but suffered from the inability to detect small openings within the tree crown that were detected by the ground data collection method.

An edge effect was detected with both the ground data collection and UAS and showed a very similar decrease in FC to between 45-50m followed by an increase. This trend was attributed to opposing effects of edge influence. Mainly the mortality of large standing pine trees at the edge, accompanied by increased growth closer to the edge due increased light availably. Due to the slight over estimation in the UAS estimates of FC, the trend suggested a much lower magnitude of difference between the edge and the suggested interior but benefitted from the much greater sample intensity of the area compared to the ground data.

Due to the success in detecting the edge effect, UAS may very well serve as an important tool for understanding edge influences. While this study only investigated the edges at a single study site and one effect, the flexibility of the platform and methods described is such that it can be implemented in other areas very easily. Additionally, numerous, different forest structural estimates, known to exhibit edge effects, can be easily and accurately collected from UAS imagery.

CHAPTER 6

OVERALL CONCLUSIONS

Here in New Hampshire, forests are an ecologically and economically important resource. However, like most of the world, they are threatened by increased development and fragmentation. The sustainable management of this resource is critical if we are to meet current needs and ensure healthy forest ecosystems into the future. To accomplish this goal, those making the management decisions must be provided the spatially and knowledge rich information they need in a timely manner. Remotely sensed data products have long served the forestry community, providing a wealth of information on forest structure and composition on time scales much narrower than traditional forest inventory. Remote sensing now is moving into a new era, marked by the arrival of highly flexible unmanned aerial systems (UAS) and powerful Structure from Motion (SfM) software. UAS will become an invaluable resource for forestry, but like the early days of any remotely sensed platform and sensor, the limitations of this technology are different from its predecessors and must be rigorously tested. Additionally, New Hampshire's complex forests serve as a nationally meaningful testing area. Therefore, the overall goal of our research was to test different, practical, methodologies for data collection that could improve the efficiency of the process while balancing the accuracy of the data products. Furthermore, UAS were tested in a unique application with ecological implications in the region.

SfM processing has allowed for the generation of highly detailed, 3-dimensional information of forest stands from UAS imagery collected with inexpensive digital cameras; a critical advancement in remotely sensed data collection. This information is similar to LiDAR data, which has been used for decades to estimate forest structural metrics, but for a fraction of the cost. The SfM process is powerful, but its sensitivity to image quality and collection methods is a very important factor that must be thoroughly studied to ensure accuracy. We assessed the effects of UAS flying height and forward overlap on the accuracy of top-of-canopy height (TCH) estimates made from the UAS SfM produced point clouds for twelve combinations of height and image overlap across four sites. We found no significant effect of flying height and a significant but minimal improvement in accuracy with increased forward overlap. The results suggests that, when estimating TCH, The UAS can be flown higher with no significant impact on the accuracy. Additionally, the highest levels of forward overlap would only lead to minor improvements and may not be necessary or even achievable at certain flying heights. These results can substantially save time in the field and processing the UAS imagery by reducing the number of images needed over an area of interest.

Forest composition is another piece of important information when making management decisions. The ability to map forests down to the species level has been limited by spatial resolution, temporal resolution, and especially cost. High spatial resolution is necessary to reduce spectral mixing within a single pixel and multi-temporal data helps to separate species based on phenology. This research tested the ability to classify 14 species in a highly heterogeneous, New England forest by taking advantage of the high (i.e., on demand) temporal resolution and very-high spatial resolution of the UAS. With operational costs in mind, we further tested the performance of a standard RGB camera to that of a higher-priced multi-spectral camera considered more suitable for vegetation mapping. Results show that the multi-temporal approach improved the accuracy of species level

classification with no additional benefit after three dates of optimal imagery. Of the dates of imagery collected for this study, mid and late spring imagery produced the highest accuracies. The RGB sensor exhibited significantly higher accuracies than the multi-spectral sensor. However, this result could be because the particular multispectral sensor employed did not measure blue spectral reflectance, which was found to be important for classification accuracy. Understanding how many acquisitions and the seasonal timing of these UAS data collections is important to understand from an efficiency standpoint. Additionally, the sensor comparison results suggest that better results can be achieved with the less expensive RGB sensor, thus reducing equipment costs.

Fragmentation of forests results in the potential modification of the remaining forests by (i.e., edge effects) exposing the forest fragment edges to new environmental conditions (e.g., more light, temperature variability, wind, etc.). These can alter the original abiotic and biotic processes in the immediate vicinity, which in turn alters the forest structure and composition. Characterizing and quantifying the extent of these changes to a forest is important but they are highly variable and the fieldwork necessary to handle this variability could be cost-prohibitive. Therefore, we assessed whether UAS data could be used to detect and measure edge effects. Change in canopy cover, measured on the ground and from UAS data, with distance from edge were compared. Both sets of data detected a decrease in cover from the edge to approximately 45m – 50m followed by an increase in cover to 100m. The ground data were highly influenced by the substantial variability in condition along the edge-to-interior gradient. The ability to intensely sample the edge with the UAS data allowed for the detection of a significant effect with a small magnitude.

The results of this dissertation will be valuable to the forestry practitioners and those in the field of landscape ecology. The results of methodological studies are invaluable to end users as it helps them ensure they are collecting accurate information on which to base their decisions while

balancing the time spent collecting and processing the UAS data. Furthermore, by demonstrating the capability of using UAS as a tool for understanding edge effects, the door is open to better understand the impacts of fragmentation over a larger area thus leading to better-informed conservation decisions. Future work should cover the effects of other factors known to influence SfM such as stand composition and lighting. The addition of fall imagery could substantially improve the classification accuracies and more testing with different multi-spectral sensors is necessary. Finally, the investigation of edge effects with UAS can be greatly expanded to include edges of different ages, orientations, and include more response variables.

LITERATURE CITED

Agisoft. (2020). *Agisoft Metashape User Manual Professional Edition, Version 1.6* (v1.6). St. Petersburg, Russia: Agisoft LLC.

Ahmed, O. S., A. Shemrock, D. Chabot, C. Dillon, G. Williams, R. Wasson, & S. E. Franklin. (2017). Hierarchical land cover and vegetation classification using multispectral data acquired from an unmanned aerial vehicle. *International Journal of Remote Sensing*, *38*(8–10), 2037–2052.

Alignier, A., & M. Deconchat. (2011). Variability of forest edge effect on vegetation implies reconsideration of its assumed hypothetical pattern. *Applied Vegetation Science*, *14*(1), 67–74.

Allen, J. M., T. J. Leininger, J. D. Hurd, D. L. Civco, A. E. Gelfand, & J. A. Silander. (2013). Socioeconomics drive woody invasive plant richness in New England, USA through forest fragmentation. *Landscape Ecology*, *28*(9), 1671–1686.

Alonzo, M., H.-E. Andersen, D. Morton, & B. Cook. (2018). Quantifying Boreal Forest Structure and Composition Using UAV Structure from Motion. *Forests*, *9*(3), 119.

Anderson, K., & K. J. Gaston. (2013). Lightweight unmanned aerial vehicles will revolutionize spatial ecology. *Frontiers in Ecology and the Environment*, *11*(3), 138–146.

Arumäe, T., & M. Lang. (2018). Estimation of canopy cover in dense mixed-species forests using airborne lidar data. *European Journal of Remote Sensing*, *51*(1), 132–141.

Baena, S., J. Moat, O. Whaley, & D. S. Boyd. (2017). Identifying species from the air: UAVs and the very high-resolution challenge for plant conservation. *PLoS ONE*, *12*(11), e0188714.

Bagaram, M. B., D. Giuliarelli, G. Chirici, F. Giannetti, A. Barbati, & A. B. Id. (2018). UAV remote sensing for biodiversity monitoring: are forest canopy gaps good covariates? *Remote Sensing*, *10*(9), 1397.

Bates, D., M. Mächler, B. M. Bolker, & S. C. Walker. (2015). Fitting linear mixed-effects models using lme4. *Journal of Statistical Software*, *67*(1).

Belgiu, Mariana, & L. Drăgu. (2016). Random forest in remote sensing: A review of applications and future directions. *ISPRS Journal of Photogrammetry and Remote Sensing*, *114*, 24–31.

Belgiu, M., & L. Drăguţ. (2014). Comparing supervised and unsupervised multiresolution segmentation approaches for extracting buildings from very high-resolution imagery. *ISPRS Journal of Photogrammetry and Remote Sensing*, *96*, 67–75.

Bhuiyan, M. A. E., C. Witharana, & A. K. Liljedahl. (2020a). Use of Very High Spatial Resolution Commercial Satellite Imagery and Deep Learning to Automatically Map Ice-Wedge Polygons across Tundra Vegetation Types. *Journal of Imaging*, *6*(12), 137.

Bhuiyan, M. A. E., C. Witharana, A. K. Liljedahl, B. M. Jones, R. Daanen, H. E. Epstein, … A. Agnew. (2020b). Understanding the effects of optimal combination of spectral bands on deep learning model predictions: A case study based on permafrost tundra landform mapping using high resolution multispectral satellite imagery. *Journal of Imaging*, *6*(9), 97.

Bianco, S., G. Ciocca, & D. Marelli. (2018). Evaluating the performance of structure from motion pipelines. *Journal of Imaging*, *4*(8), 98.

Birdsey, R. A., & L. S. Heath. (1995). Carbon Changes in U.S. Forests. In L. A. Joyce (Ed.), *Productivity of America's Forests and Climate Change. General Technical Report RM-GTR-271* (pp. 56–70). Fort Collins, Colorado: U.S. Department of Agriculture, Forest Service, Rocky Mountain Forest and Experiment Station.

Blaschke, T. (2010). Object based image analysis for remote sensing. *ISPRS Journal of Photogrammetry and Remote Sensing*, *65*(1), 2–16.

Blaschke, T., G. J. Hay, M. Kelly, S. Lang, P. Hofmann, E. Addink, … D. Tiede. (2014). Geographic Object-Based Image Analysis - Towards a new paradigm. *ISPRS Journal of Photogrammetry and Remote Sensing*, *87*, 180–191.

Bonnet, S., J. Lisein, & P. Lejeune. (2017). Comparison of UAS photogrammetric products for tree detection and characterization of coniferous stands. *International Journal of Remote Sensing*, *38*(19), 5310–5337.

Braithwaite, N. T., & A. U. Mallik. (2012). Edge effects of wildfire and riparian buffers along boreal forest streams. *Journal of Applied Ecology*, *49*(1), 192–201.

Breiman, L. (2001). Random forests. *Machine Learning*, *45*(1), 5–32.

Briber, B. M., L. R. Hutyra, A. B. Reinmann, S. M. Raciti, V. K. Dearborn, C. E. Holden, & A. L. Dunn. (2015). Tree productivity enhanced with conversion from forest to urban land covers. *PLoS ONE*, *10*(8), e0136237.

Brooks, C., C. Weinstein, A. Poley, A. Grimm, N. Marion, L. Bourgeau-Chavez, … K. Kowalski. (2021). Using Uncrewed Aerial Vehicles for Identifying the Extent of Invasive Phragmites australis in Treatment Areas Enrolled in an Adaptive Management Program. *Remote Sensing*, *13*(10), 1895.

Brosofske, K. D., R. E. Froese, M. J. Falkowski, & A. Banskota. (2014). A review of methods for mapping and prediction of inventory attributes for operational forest management. *Forest Science*, *60*(4), 733–756.

Brothers, T. S., & A. Spingarn. (1992). Forest Fragmentation and Alien Plant Invasion of Central Indiana Old-Growth Forests. *Conservation Biology*, *6*(1), 91–100.

Buras, A., C. Schunk, C. Zeitr, C. Herrmann, L. Kaiser, H. Lemme, … A. Menzel. (2018). Are Scots pine forest edges particularly prone to drought-induced mortality? *Environmental Research Letters, 13,* 025001.

Cai, Y., H. Huang, K. Wang, C. Zhang, L. Fan, & F. Guo. (2021). Selecting optimal combination of data channels for semantic segmentation in city information modelling (CIM). *Remote Sensing*, *13*(7), 1367.

Chen, J., J. F. Franklin, & T. A. Spies. (1992). Vegetation responses to edge environments in old-growth Douglas-fir forests. *Ecological Applications*, *2*(4), 387–396.

Chianucci, F. (2016). A note on estimating canopy cover from digital cover and hemispherical photography. *Silva Fennica*, *50*(1), 1518.

Chianucci, F. (2020). An overview of in situ digital canopy photography in forestry. *Canadian Journal of Forest Research*, *50*(3), 227–242.

Chianucci, F., U. Chiavetta, & A. Cutini. (2014). The estimation of canopy attributes from digital cover photography by two different image analysis methods. *IForest, 7*(4), 255–259.

Chianucci, F., & A. Cutini. (2013). Estimation of canopy properties in deciduous forests with digital hemispherical and cover photography. *Agricultural and Forest Meteorology, 168*, 130–139.

Chianucci, F., L. Disperati, D. Guzzi, D. Bianchini, V. Nardino, C. Lastri, … P. Corona. (2016). Estimation of canopy attributes in beech forests using true color digital images from a small fixed-wing UAV. *International Journal of Applied Earth Observation and Geoinformation*, *47*, 60–68.

Chianucci, F., N. Puletti, M. Grotti, C. Bisaglia, F. Giannetti, E. Romano, … C. Tattoni. (2021). Influence of image pixel resolution on canopy cover estimation in poplar plantations from field, aerial and satellite optical imagery. *Annals of Silvicultural Research*, *46*(1), 8–13.

Cole, E. F., & B. C. Sheldon. (2017). The shifting phenological landscape: Within- and between-species variation in leaf emergence in a mixed-deciduous woodland. *Ecology and Evolution*, *7*(4), 1135–1147.

Colomina, I., & P. Molina. (2014). Unmanned aerial systems for photogrammetry and remote sensing: A review. *ISPRS Journal of Photogrammetry and Remote Sensing*, *92*, 79–97.

Conchedda, G., L. Durieux, & P. Mayaux. (2008). An object-based method for mapping and change analysis in mangrove ecosystems. *ISPRS Journal of Photogrammetry and Remote Sensing*, *63*(5), 578–589.

Congalton, R. G., & K. Green. (2019). *Assessing the Accuracy of Remotely Sensed Data: Principles and Practices.* (3rd ed.). Boca Raton, FL: CRC Press.

Congalton, R. G., R. G. Oderwald, & R. A. Mead. (1983). Assessing Landsat classification accuracy using discrete multivariate analysis statistical techniques. *Photogrammetric Engineering & Remote Sensing*, *49*(12), 1671–1678.

Crimmins, M. A., & T. M. Crimmins. (2008). Monitoring plant phenology using digital repeat photography. *Environmental Management*, *41*(6), 949–958.

Cruzan, M. B., B. G. Weinstein, M. R. Grasty, B. F. Kohrn, E. C. Hendrickson, T. M. Arredondo, & P. G. Thompson. (2016). Small Unmanned Aerial Vehicles (Micro-UAVs, Drones) in Plant Ecology. *Applications in Plant Sciences*, *4*(9), 1600041.

Dainelli, R., P. Toscano, S. F. di Gennaro, & A. Matese. (2021). Recent advances in unmanned aerial vehicles forest remote sensing—a systematic review. Part i: Research applications. *Forests*, *12*(4), 327.

Dandois, J. P., & E. C. Ellis. (2010). Remote Sensing of Vegetation Structure Using Computer Vision. *Remote Sensing*, *2*(4), 1157–1176.

Dandois, J. P., & E. C. Ellis. (2013). High spatial resolution three-dimensional mapping of vegetation spectral dynamics using computer vision. *Remote Sensing of Environment*, *136*, 259–276.

Dandois, J. P., M. Olano, & E. C. Ellis. (2015). Optimal altitude, overlap, and weather conditions for computer vision UAV estimates of forest structure. *Remote Sensing*, *7*(10), 13895–13920.

Dantas De Paula, M., J. Groeneveld, & A. Huth. (2016). The extent of edge effects in fragmented landscapes: Insights from satellite measurements of tree cover. *Ecological Indicators*, *69*, 196–204.

de Casenave, J. L., J. P. Pelotto, & J. Protomastro. (1995). Edge-interior differences in vegetation structure and composition in a Chaco semi-arid forest, Argentina. *Forest Ecology and Management*, *72*(1), 61–69.

de Lima, R. S., M. Lang, N. G. Burnside, M. V. Peciña, T. Arumäe, D. Laarmann, … K. Sepp. (2021). An evaluation of the effects of UAS flight parameters on digital aerial photogrammetry processing and dense-cloud production quality in a Scots pine forest. *Remote Sensing*, *13*(6), 3–5.

Didham, R. K., & R. M. Ewers. (2012). Predicting the impacts of edge effects in fragmented habitats: Laurance and Yensen's core area model revisited. *Biological Conservation*, *155*, 104–110.

Didham, R. K., & R. M. Ewers. (2014). Edge Effects Disrupt Vertical Stratification of Microclimate in a Temperate Forest Canopy. *Pacific Science*, *68*(4), 493–508.

Didham, R. K., & J. H. Lawton. (1999). Edge Structure Determines the Magnitude of Changes in Microclimate and Vegetation Structure in Tropical Forest Fragments. *Biotropica*, *31*(1), 17–30.

Domingo, D., H. O. Ørka, E. Næsset, D. Kachamba, & T. Gobakken. (2019). Effects of UAV image resolution, camera type, and image overlap on accuracy of biomass predictions in a tropical woodland. *Remote Sensing*, *11*(8), 948.

Dovčiak, M., & J. Brown. (2014). Secondary edge effects in regenerating forest landscapes: Vegetation and microclimate patterns and their implications for management and conservation. *New Forests*, *45*(5), 733–744.

Du, M., & N. Noguchi. (2017). Monitoring of wheat growth status and mapping of wheat yield's within-field spatial variations using color images acquired from UAV-camera System. *Remote Sensing*, *9*(3), 289.

Ducey, M. J., K. M. Johnson, E. P. Belair, & M. H. Mockrin. (2016). *Forests in Flux: The Effects of Demographic Change on Forest Cover in New England and New York. Carsey Research National Issue Brief 99*. Durham, NH: University of New Hampshire Carsey School of Public Policy. 10pp

Dupuch, A., & D. Fortin. (2013). The extent of edge effects increases during post-harvesting forest succession. *Biological Conservation*, *162*, 9–16.

Durgan, S. D., C. Zhang, A. Duecaster, F. Fourney, & H. Su. (2020). Unmanned Aircraft System Photogrammetry for Mapping Diverse Vegetation Species in a Heterogeneous Coastal Wetland. *Wetlands*, *40*(6), 2621–2633.

Dvořák, P., J. Müllerová, T. Bartaloš, & J. Brůna. (2015). Unmanned Aerial Vehicles for Alien Plant Species Detection and Monitoring. *ISPRS - International Archives of the Photogrammetry, Remote Sensing and Spatial Information Sciences*, *XL-1/W4*, 83–90.

Eldegard, K., O. Totland, S. R. Moe, Ø. Totland, S. R. Moe, O. Totland, & S. R. Moe. (2015). Edge effects on plant communities along power line clearings. *Journal of Applied Ecology*, *52*(4), 871–880.

Esseen, P., A. Hedström Ringvall, K. A. Harper, P. Christensen, & J. Svensson. (2016). Factors driving structure of natural and anthropogenic forest edges from temperate to boreal ecosystems. *Journal of Vegetation Science*, *27*(3), 482–492.

Fahrig, L. (2003). Effects of Habitat Fragmentation on Biodiversity. *Annual Review of Ecology, Evolution, and Systematics*, *34*(1), 487–515.

Fassnacht, F. E., H. Latifi, K. Stereńczak, A. Modzelewska, M. Lefsky, L. T. Waser, … A. Ghosh. (2016). Review of studies on tree species classification from remotely sensed data. *Remote Sensing of Environment*, *186*, 64–87.

Feng, Q., J. Liu, & J. Gong. (2015). UAV Remote sensing for urban vegetation mapping using random forest and texture analysis. *Remote Sensing*, *7*(1), 1074–1094.

Ferreira, M. P., F. H. Wagner, L. E. O. C. Aragão, Y. E. Shimabukuro, & C. R. de Souza Filho. (2019). Tree species classification in tropical forests using visible to shortwave infrared WorldView-3 images and texture analysis. *ISPRS Journal of Photogrammetry and Remote Sensing*, *149*, 119-131.

Finzi, A. C., M. A. Giasson, A. A. Barker Plotkin, J. D. Aber, E. R. Boose, E. A. Davidson, … D. R. Foster. (2020). Carbon budget of the Harvard Forest Long-Term Ecological Research site: pattern, process, and response to global change. *Ecological Monographs*, *90*(4).

Foster, D. R. (1988). Species and Stand Response to Catastrophic Wind in Central New England, U.S.A. *The Journal of Ecology*, *76*(1), 135-151.

Foster, D. R. (1992). Land-Use History (1730-1990) and Vegetation Dynamics in Central New England, USA. *Journal of Ecology*, *80*(4), 753–771.

Franklin, C. M. A., K. A. Harper, & M. J. Clarke. (2021). Trends in studies of edge influence on vegetation at human created and natural forest edges across time and space. *Canadian Journal of Forest Research*, *51*(2), 274–282.

Franklin, S. E., & O. S. Ahmed. (2018). Deciduous tree species classification using object-based analysis and machine learning with unmanned aerial vehicle multispectral data. *International Journal of Remote Sensing*, *39*(15–16), 5236–5245.

Franklin, S. E., & M. A. Wulder. (2002). Remote sensing methods in medium spatial resolution satellite data land cover classification of large areas. *Progress in Physical Geography*, *26*(2), 173–205.

Frappier, B., R. T. Eckert, & T. D. Lee. (2003). Potential impacts of the invasive exotic shrub Rhamnus frangula L. (glossy buckthorn) on forests of southern New Hampshire. *Northeastern Naturalist*, *10*(3), 277–296.

Fraser, B. T., & R. G. Congalton. (2018). Issues in Unmanned Aerial Systems (UAS) data collection of complex forest environments. *Remote Sensing*, *10*(6), 908.

Frey, J., K. Kovach, S. Stemmler, & B. Koch. (2018). UAV photogrammetry of forests as a vulnerable process. A sensitivity analysis for a structure from motion RGB-image pipeline. *Remote Sensing*, *10*(6), 912.

Fuller, T., D. Foster, & T. McLachlan. (1998). Impact of human activity on regional forest composition and dynamics in central New England. *Ecosystems*, *1*(1), 76–95.

Ganz, S., Y. Käber, & P. Adler. (2019). Measuring tree height with remote sensing-a comparison of photogrammetric and LiDAR data with different field measurements. *Forests*, *10*(8), 694.

Gao, Y., J. F. Mas, N. Kerle, & J. A. Navarrete Pacheco. (2011). Optimal region growing segmentation and its effect on classification accuracy. *International Journal of Remote Sensing*, *32*(13), 3747–3763.

García-Romero, A., P. M. Vergara, C. Granados-Peláez, & G. Santibañez-Andrade. (2019). Landscape-mediated edge effect in temperate deciduous forest: implications for oak regeneration. *Landscape Ecology*, *34*(1), 51–62.

Gehlhausen, S. M., M. W. Schwartz, C. K. Augspurger, S. P. Ecology, M. Hall, S. G. Ave, & M. Gehlhausen. (2000). Vegetation and Microclimatic Edge Effects in Two Mixed-Mesophytic Forest Fragments. *Plant Ecology*, *147*, 21–35.

Getzin, S., R. S. Nuske, & K. Wiegand. (2014). Using unmanned aerial vehicles (UAV) to quantify spatial gap patterns in forests. *Remote Sensing*, *6*(8), 6988–7004.

Getzin, S., K. Wiegand, & I. Schöning. (2012). Assessing biodiversity in forests using very high-resolution images and unmanned aerial vehicles. *Methods in Ecology and Evolution*, *3*(2), 397–404.

Gini, R., G. Sona, G. Ronchetti, D. Passoni, & L. Pinto. (2018). Improving tree species classification using UAS multispectral images and texture measures. *ISPRS International Journal of Geo-Information*, *7*(8), 315.

Goldbergs, G. (2021). Impact of Base-to-Height Ratio on Canopy Height Estimation Accuracy of Hemiboreal Forest Tree Species by Using Satellite and Airborne Stereo Imagery. *Remote Sensing*, *13*(15), 2941.

Goodale, C. L., M. J. Apps, R. A. Birdsey, C. B. Field, L. S. Heath, R. A. Houghton et al. (2002). Forest carbon sinks in the Northern Hemisphere. *Ecological Applications*, 12(3), 891–899.

Goodbody, T. R. H., N. C. Coops, T. Hermosilla, P. Tompalski, & P. Crawford. (2018). Assessing the status of forest regeneration using digital aerial photogrammetry and unmanned aerial systems. *International Journal of Remote Sensing*, *39*(15–16), 5246–5264.

Goodbody, T. R. H., N. C. Coops, P. L. Marshall, P. Tompalski, & P. Crawford. (2017). Unmanned aerial systems for precision forest inventory purposes: A review and case study. *Forestry Chronicle*, *93*(1), 71–81.

Goodbody, T. R. H., N. C. Coops, & J. C. White. (2019). Digital Aerial Photogrammetry for Updating Area-Based Forest Inventories: A Review of Opportunities, Challenges, and Future Directions. *Current Forestry Reports*, *5*, 55–75.

Gould, W. (2000). Remote Sensing of Vegetation, Plant Species Richness, and Regional Biodiversity Hotspots. *Ecological Applications*, *10*(6), 1861–1870.

Grybas, H., R. G. Congalton, & A. F. Howard. (2020). Using Geospatial Analysis to Map Forest Change in New Hampshire: 1996-Present. *Journal of Forestry*, *118*(6), 598–612.

Guimarães, N., L. Pádua, P. Marques, N. Silva, E. Peres, & J. J. Sousa. (2020). Forestry remote sensing from unmanned aerial vehicles: A review focusing on the data, processing and potentialities. *Remote Sensing*, *12*(6), 1046.

Gülci, S. (2019). The determination of some stand parameters using SfM-based spatial 3D point cloud in forestry studies: an analysis of data production in pure coniferous young forest stands. *Environmental Monitoring and Assessment*, *191*, 495.

Haddad, N. M., L. a. Brudvig, J. Clobert, K. F. Davies, a. Gonzalez, R. D. Holt, … J. R. Townshend. (2015). Habitat fragmentation and its lasting impact on Earth's ecosystems. *Science Advances*, *1*(2), e1500052.

Hamraz, H., M. A. Contreras, & J. Zhang. (2016). A robust approach for tree segmentation in deciduous forests using small-footprint airborne LiDAR data. *International Journal of Applied Earth Observation and Geoinformation*, *52*, 532–541.

Harper, K. A., P. Drapeau, D. Lesieur, & Y. Bergeron. (2014). Forest structure and composition at fire edges of different ages: Evidence of persistent structural features on the landscape. *Forest Ecology and Management*, *314*, 131–140.

Harper, K. A., E. Macdonald, P. J. Burton, J. Chen, K. D. Brosofske, S. C. Saunder, … P.-A. Esseen. (2005). Edge influence on forest structure and composition in fragmented landscapes. *Conservation Biology*, *19*(3), 768–782.

Harper, K. A., & S. E. Macdonald. (2001). Structure and Composition of Riparian Boreal Forest: New Methods for Analyzing Edge Influence. *Ecology*, *82*(3), 649–659.

Harper, K. A., & S. E. Macdonald. (2002). Structure and composition of edges next to regenerating clear-cuts in mixed-wood boreal forest. *Journal of Vegetation Science*, *13*(4), 535–546.

Harper, K. A., & S. E. Macdonald. (2011). Quantifying distance of edge influence: a comparison of methods and a new randomization method. *Ecosphere*, *2*(8), Article 94.

Harper, K. A., S. E. Macdonald, M. S. Mayerhofer, S. R. Biswas, P. A. Esseen, K. Hylander, … Y. Bergeron. (2015). Edge influence on vegetation at natural and anthropogenic edges of boreal forests in Canada and Fennoscandia. *Journal of Ecology*, *103*(3), 550–562.

Harper, K. A., L. E. Mascarúa López, S. E. Macdonald, P. Drapeau, L. Mascarúa-López, S. E. Macdonald, … P. Drapeau. (2007). Interaction of edge influence from multiple edges: Examples from narrow corridors. *Plant Ecology*, *192*(1), 71–84.

Hawbaker, T. J., T. Gobakken, A. Lesak, E. Trømborg, & K. Contrucci. (2010). Light Detection and Ranging-Based Measures of Mixed Hardwood Forest Structure. *Forest Science*, *56*(3), 313–326.

Hawbaker, T. J., N. S. Keuler, A. A. Lesak, T. Gobakken, K. Contrucci, & V. C. Radeloff. (2009). Improved estimates of forest vegetation structure and biomass with a LiDAR-optimized sampling design. *Journal of Geophysical Research: Biogeosciences*, *114*(G2), G00E04.

Hay, G. J., & G. Castilla. (2008). *Geographic object-based image analysis (GEOBIA): A new name for a new discipline*. (T. Blaschke, S. Lang, & G. Hay, Eds.) Lecture Notes in Geoinformation and Cartography. Springer Berlin Heidelberg.

Hernandez-Santin, L., M. L. Rudge, R. E. Bartolo, & P. D. Erskine. (2019). Identifying species and monitoring understory from UAS-derived data: A literature review and future directions. *Drones*, *3*(1), 1–18.

Hilker, T., M. A. Wulder, & N. C. Coops. (2008). Update of forest inventory data with lidar and high spatial resolution satellite imagery. *Canadian Journal of Remote Sensing*, *34*(1), 5–12.

Hill, R. A., A. K. Wilson, M. George, & S. A. Hinsley. (2010). Mapping tree species in temperate deciduous woodland using time-series multi-spectral data. *Applied Vegetation Science*, *13*(1), 86–99.

Hofmeister, J., J. Hošek, M. Brabec, R. Hédl, & M. Modrý. (2013). Strong influence of long-distance edge effect on herb-layer vegetation in forest fragments in an agricultural landscape. *Perspectives in Plant Ecology, Evolution and Systematics*, *15*(6), 293–303.

Hofmeister, J., J. Hošek, M. Brabec, & R. Kočvara. (2017). Spatial distribution of bird communities in small forest fragments in central Europe in relation to distance to the forest edge, fragment size and type of forest. *Forest Ecology and Management*, *401*, 255–263.

Hofmeister, J., J. Hošek, M. Brabec, R. Střalková, P. Mýlová, M. Bouda, … M. Svoboda. (2019). Microclimate edge effect in small fragments of temperate forests in the context of climate change. *Forest Ecology and Management*, *448*(June), 48–56.

Howard, L. F., & T. D. Lee. (2002). Upland Old-Field Succession in Southeastern New Hampshire. *Journal of the Torrey Botanical Society*, *129*(1), 60–76.

Hugenholtz, C. H., K. Whitehead, O. W. Brown, T. E. Barchyn, B. J. Moorman, A. LeClair, … T. Hamilton. (2013). Geomorphological mapping with a small, unmanned aircraft system (sUAS): Feature detection and accuracy assessment of a photogrammetrically-derived digital terrain model. *Geomorphology*, *194*, 16–24.

Hunt, E. R., W. Dean Hively, S. J. Fujikawa, D. S. Linden, C. S. T. Daughtry, & G. W. McCarty. (2010). Acquisition of NIR-green-blue digital photographs from unmanned aircraft for crop monitoring. *Remote Sensing*, *2*(1), 290–305.

Hyyppä, J., X. Yu, H. Hyyppä, M. Vastaranta, M. Holopainen, A. Kukko, … P. Alho. (2012). Advances in forest inventory using airborne laser scanning. *Remote Sensing*, *4*(5), 1190–1207.

Ibáñez, I., D. S. W. Katz, D. Peltier, S. M. Wolf, B. T. Connor Barrie, & B. T. C. Barrie. (2014). Assessing the integrated effects of landscape fragmentation on plants and plant communities: The challenge of multiprocess-multiresponse dynamics. *Journal of Ecology*, *102*(4), 882–895.

Iglhaut, J., C. Cabo, S. Puliti, L. Piermattei, J. O'Connor, & J. Rosette. (2019). Structure from Motion Photogrammetry in Forestry: A Review. *Current Forestry Reports*, *5*(3), 155–168.

Immitzer, M., C. Atzberger, & T. Koukal. (2012). Tree species classification with Random Forest using very high spatial resolution 8-band worldView-2 satellite data. *Remote Sensing*, *4*(9), 2661–2693.

Iqbal, I. A., J. Osborn, C. Stone, A. Lucieer, M. Dell, & C. McCoull. (2018). Evaluating the robustness of point clouds from small format aerial photography over a Pinus radiata plantation. *Australian Forestry*, *81*(3), 162–176.

Jakubowski, M. K., Q. Guo, & M. Kelly. (2013). Tradeoffs between lidar pulse density and forest measurement accuracy. *Remote Sensing of Environment*, *130*, 245–253.

Jayathunga, S., T. Owari, & S. Tsuyuki. (2018). Evaluating the performance of photogrammetric products using fixed-wing UAV imagery over a mixed conifer-broadleaf forest: Comparison with airborne laser scanning. *Remote Sensing*, *10*(2), 187.

Jennings, S. (1999). Assessing forest canopies and understory illumination: canopy closure, canopy cover and other measures. *Forestry*, *72*(1), 59–74.

Jensen, J. R. (2016). *Introductory Digital Image Processing: A Remote Sensing Perspective* (4th ed.). Upper Saddle River, NJ: Pearson Prentice Hall.

Jeon, S. B., P. Olofsson, & C. E. Woodcock. (2014). Land use change in New England: A reversal of the forest transition. *Journal of Land Use Science*, *9*(1), 105–130.

Johansen, K., S. Phinn, & C. Witte. (2010). Mapping of riparian zone attributes using discrete return LiDAR, QuickBird and SPOT-5 imagery: Assessing accuracy and costs. *Remote Sensing of Environment*, *114*(11), 2679–2691.

Justice, D., A. K. Deely, & F. Rubin. (2002). *New Hampshire land cover assessment: final report*. Durham, NH.

Kameyama, S., & K. Sugiura. (2020). Estimating tree height and volume using unmanned aerial vehicle photography and SfM technology, with verification of result accuracy. *Drones*, *4*(2), 19.

Kameyama, S., & K. Sugiura. (2021). Effects of differences in structure from motion software on image processing of unmanned aerial vehicle photography and estimation of crown area and tree height in forests. *Remote Sensing*, *13*(4), 626.

Kattenborn, T., J. Eichel, S. Wiser, L. Burrows, F. E. Fassnacht, & S. Schmidtlein. (2020). Convolutional Neural Networks accurately predict cover fractions of plant species and communities in Unmanned Aerial Vehicle imagery. *Remote Sensing in Ecology and Conservation*, *6*(4), 472-486.

Kerr, J. T., & M. Ostrovsky. (2003). From space to species: Ecological applications for remote sensing. *Trends in Ecology and Evolution*, *18*(6), 299–305.

Ke, Y., & L. J. Quackenbush. (2011). A review of methods for automatic individual tree-crown detection and delineation from passive remote sensing. *International Journal of Remote Sensing*, *32*(17), 4725–4747.

Key, T., T. A. Warner, J. B. McGraw, & M. A. Fajvan. (2001). A comparison of multispectral and multitemporal information in high spatial resolution imagery for classification of individual tree species in a temperate hardwood forest. *Remote Sensing of Environment*, *75*(1), 100–112.

Khokthong, W., D. C. Zemp, B. Irawan, L. Sundawati, H. Kreft, & D. Hölscher. (2019). Drone-Based Assessment of Canopy Cover for Analyzing Tree Mortality in an Oil Palm Agroforest. *Frontiers in Forests and Global Change*, *2*, 12.

Khosravipour, A., A. K. Skidmore, M. Isenburg, T. Wang, & Y. A. Hussin. (2014). Generating Pit-free Canopy Height Models from Airborne Lidar. *Photogrammetric Engineering & Remote Sensing*, *80*(9), 863–872.

Klosterman, S., E. Melaas, J. Wang, A. Martinez, S. Frederick, J. O'Keefe, … A. D. Richardson. (2018). Fine-scale perspectives on landscape phenology from unmanned aerial vehicle (UAV) photography. *Agricultural and Forest Meteorology, 248*, 397–407.

Klosterman, S., & A. D. Richardson. (2017). Observing spring and fall phenology in a deciduous forest with aerial drone imagery. *Sensors (Switzerland), 17*(12), 1–17.

Klouček, T., J. Komárek, P. Surový, K. Hrach, P. Janata, & B. Vašíček. (2019). The use of UAV mounted sensors for precise detection of bark beetle infestation. *Remote Sensing*, *11*(13), 1561.

Knoth, C., B. Klein, T. Prinz, & T. Kleinebecker. (2013). Unmanned aerial vehicles as innovative remote sensing platforms for high-resolution infrared imagery to support restoration monitoring in cut-over bogs. *Applied Vegetation Science*, *16*(3), 509–517.

Kohv, M., E. Sepp, & L. Vammus. (2017). Assessing multitemporal water-level changes with UAS-based photogrammetry. *Photogrammetric Record*, *32*(160), 424–442.

Komárek, J., T. Klouček, & J. Prošek. (2018). The potential of Unmanned Aerial Systems: A tool towards precision classification of hard-to-distinguish vegetation types? *International Journal of Applied Earth Observation and Geoinformation*, *71*, 9–19.

Koukoulas, S., & G. A. Blackburn. (2004). Quantifying the spatial properties of forest canopy gaps using LiDAR imagery and GIS. *International Journal of Remote Sensing*, *25*(15), 3049–3071.

Kükenbrink, D., F. D. Schneider, R. Leiterer, M. E. Schaepman, & F. Morsdorf. (2017). Quantification of hidden canopy volume of airborne laser scanning data using a voxel traversal algorithm. *Remote Sensing of Environment*, *194*, 424–436.

Laliberte, A. S., J. E. Herrick, A. Rango, & C. Winters. (2010). Acquisition, Orthorectification, and Object-based Classification of Unmanned Aerial Vehicle (UAV) Imagery for Rangeland Monitoring. *Photogrammetric Engineering Remote Sensing*, *76*(6), 661–672.

Laliberte, A. S., & A. Rango. (2011). Image Processing and Classification Procedures for Analysis of Sub-decimeter Imagery Acquired with an Unmanned Aircraft over Arid Rangelands. *GIScience & Remote Sensing*, *48*(1), 4–23.

Lang, S., A. Baraldi, D. Tiede, G. Hay, & T. Blaschke. (2018). Towards a (GE)OBIA 2.0 manifesto - achievements and open challenges in information & knowledge extraction from big Earth data. In *GEOBIA 2018 - From pixels to ecosystems and global sustainability* (pp. 0–15).

Laurance, W. F. (2009). Hyperdynamism in fragmented habitats. *Journal of Vegetation Science*, *13*(4), 595–602.

Laurance, W. F., T. E. Lovejoy, H. L. Vasconcelos, E. M. Bruna, R. K. Didham, P. C. Stouffer, … E. Sampaio. (2002). Ecosystem decay of Amazonian forest fragments: a 22-years investigation. *Conservation Biology*, *16*(3), 605–618.

Laurance, W. F., H. E. M. Nascimento, S. G. Laurance, A. Andrade, R. M. Ewers, K. E. Harms, … J. E. Ribeiro. (2007). Habitat fragmentation, variable edge effects, and the landscape-divergence hypothesis. *PLoS ONE*, *2*(10), e1017.

Laurance, W. F., & E. Yensen. (1991). Predicting the impacts of edge effects in fragmented habitats. *Biological Conservation*, *55*(1), 77–92.

Leckie, D. G., F. A. Gougeon, S. Tinis, T. Nelson, C. N. Burnett, & D. Paradine. (2005). Automated tree recognition in old growth conifer stands with high resolution digital imagery. *Remote Sensing of Environment*, *94*(3), 311–326.

Leduc, M. B., & A. J. Knudby. (2018). Mapping wild leek through the forest canopy using a UAV. *Remote Sensing*, *10*(1), 70.

Lefsky, M. A., W. B. Cohen, S. A. Acker, G. G. Parker, T. A. Spies, & D. Harding. (1999). Lidar remote sensing of the canopy structure and biophysical properties of Douglas-fir western hemlock forests. *Remote Sensing of Environment*, *70*(3), 339–361.

Lhotka, J. M., & J. W. Stringer. (2013). Forest edge effects on Quercus reproduction within naturally regenerated mixed broadleaf stands. *Canadian Journal of Forest Research*, *43*(10), 911–918.

Li, D., Y. Ke, H. Gong, & X. Li. (2015). Object-based urban tree species classification using bi-temporal worldview-2 and worldview-3 images. *Remote Sensing*, *7*(12), 16917–16937.

Li, L., X. Mu, C. Macfarlane, W. Song, J. Chen, K. Yan, & G. Yan. (2018). A half-Gaussian fitting method for estimating fractional vegetation cover of corn crops using unmanned aerial vehicle images. *Agricultural and Forest Meteorology*, *262*, 379–390.

Lim, K., P. M. Treitz, M. A. Wulder, B. St-Onge, & M. Flood. (2003). LiDAR remote sensing of forest structure. *Progress in Physical Geography*, *27*(1), 88–106.

Li, M., Z. Li, & Q. Liu. (2021). Comparison of Coniferous Plantation Heights Using Unmanned Aerial Vehicle (UAV) Laser Scanning and Stereo Photogrammetry.

Linchant, J., J. Lisein, J. Semeki, P. Lejeune, & C. Vermeulen. (2015). Are unmanned aircraft systems (UASs) the future of wildlife monitoring? A review of accomplishments and challenges. *Mammal Review*, *45*(4), 239–252.

Lisein, J., A. Michez, H. Claessens, & P. Lejeune. (2015). Discrimination of deciduous tree species from time series of unmanned aerial system imagery. *PLoS ONE*, *10*(11), e0141006.

Lisein, J., M. Pierrot-Deseilligny, S. Bonnet, & P. Lejeune. (2013). A photogrammetric workflow for the creation of a forest canopy height model from small unmanned aerial system imagery. *Forests*, *4*(4), 922–944.

Liu, Y., X. Mu, H. Wang, & G. Yan. (2012). A novel method for extracting green fractional vegetation cover from digital images. *Journal of Vegetation Science*, *23*(3), 406–418.

Loarie, S. R., L. N. Joppa, & S. L. Pimm. (2007). Satellites miss environmental priorities. *TRENDS in Ecology and Evolution*, *22*(12), 630–632.

Lu, B., & Y. He. (2017). Species classification using Unmanned Aerial Vehicle (UAV)-acquired high spatial resolution imagery in a heterogeneous grassland. *ISPRS Journal of Photogrammetry and Remote Sensing*, *128*, 73–85.

Lucieer, A., S. M. de Jong, & D. Turner. (2014). Mapping landslide displacements using Structure from Motion (SfM) and image correlation of multi-temporal UAV photography. *Progress in Physical Geography*, *38*(1), 97–116.

MacDicken, K. G., P. Sola, J. E. Hall, C. Sabogal, M. Tadoum, & C. de Wasseige. (2015). Global progress toward sustainable forest management. *Forest Ecology and Management*, *352*, 47–56.

Macfarlane, C., & G. N. Ogden. (2012). Automated estimation of foliage cover in forest understory from digital nadir images. *Methods in Ecology and Evolution*, *3*(2), 405–415.

Macfarlane, C., Y. Ryu, G. N. Ogden, & O. Sonnentag. (2014). Digital canopy photography: Exposed and in the raw. *Agricultural and Forest Meteorology*, *197*, 244–253.

Macintyre, P., A. van Niekerk, & L. Mucina. (2020). Efficacy of multi-season Sentinel-2 imagery for compositional vegetation classification. *International Journal of Applied Earth Observation and Geoinformation*, *85*, 101980.

MacLean, M. G. (2017). Edge influence detection using aerial LiDAR in Northeastern US deciduous forests. *Ecological Indicators*, *72*, 310–314.

MacLean, M.G., & R. G. Congalton. (2013). Applicability of Multi-date Land Cover Mapping using Landsat-5 TM Imagery in the Northeastern US. *Photogrammetric Engineering & Remote Sensing*, *79*(4), 359–368.

MacQuarrie, K., & C. Lacroix. (2003). The upland hardwood component of Prince Edward Island's remnant Acadian forest: determination of depth of edge and patterns of exotic plant invasion. *Canadian Journal of Botany*, *81*(11), 1113–1128.

Mafanya, M., P. Tsele, J. Botai, P. Manyama, B. Swart, & T. Monate. (2017). Evaluating pixel and object-based image classification techniques for mapping plant invasions from UAV derived aerial imagery: Harrisia pomanensis as a case study. *ISPRS Journal of Photogrammetry and Remote Sensing*, *129*, 1–11.

Magnago, L. F. S., M. F. Rocha, L. Meyer, S. V. Martins, & J. A. A. Meira-Neto. (2015). Microclimatic conditions at forest edges have significant impacts on vegetation structure in large Atlantic forest fragments. *Biodiversity and Conservation*, *24*(9), 2305–2318.

Maltamo, M., O. M. Bollandsås, E. Næsset, T. Gobakken, & P. Packalén. (2011). Different plot selection strategies for field training data in ALS-assisted forest inventory. *Forestry*, *84*(1), 23–31.

Maltamo, M., P. Packalén, X. Yu, K. Eerikäinen, J. Hyyppä, & J. Pitkänen. (2005). Identifying and quantifying structural characteristics of heterogeneous boreal forests using laser scanner data. *Forest Ecology and Management*, *216*, 41–50.

Manfreda, S., M. F. McCabe, P. E. Miller, R. Lucas, V. P. Madrigal, G. Mallinis, … B. Toth. (2018). On the use of unmanned aerial systems for environmental monitoring. *Remote Sensing*, *10*(4).

Mascarúa López, L. E., K. a. Harper, & P. Drapeau. (2006). Edge influence on forest structure in large forest remnants, cutblock separators, and riparian buffers in managed black spruce forests. *Ecoscience*, *13*(2), 226–233.

Maschler, J., C. Atzberger, & M. Immitzer. (2018). Individual tree crown segmentation and classification of 13 tree species using Airborne hyperspectral data. *Remote Sensing*, *10*(8), 1218.

Matlack, G. R. (1993). Microenvironment variation within and among forest edge sites in the eastern United States. *Biological Conservation*, *66*(3), 185–194.

Matlack, G. R. (1994). Vegetation dynamics of the forest edge--trends in space and successional time. *Journal of Ecology*, *82*(1), 113–123.

McGlone, J. C. (2013). *Manual of Photogrammetry*. (J. C. McGlone & G. Y. G. Lee, Eds.) (6th ed.). Bethesda, MD: American Society for Photogrammetry and Remote Sensing.

Meeussen, C., S. Govaert, T. Vanneste, K. Calders, K. Bollmann, J. Brunet, … P. de Frenne. (2020). Structural variation of forest edges across Europe. *Forest Ecology and Management*, *462*, 117929.

Micheletti, N., J. H. Chandler, & S. N. Lane. (2015). Structure from Motion (SfM) Photogrammetry. In S. J. Cook, L. E. Clarke, & J. M. Nield (Eds.), *Geomorphological Techniques* (Online Edi). London, UK: British Society for Geomorphology.

Michez, A., H. Piégay, L. Jonathan, H. Claessens, & P. Lejeune. (2016a). Mapping of riparian invasive species with supervised classification of Unmanned Aerial System (UAS) imagery. *International Journal of Applied Earth Observation and Geoinformation*, *44*, 88–94.

Michez, A., H. Piégay, J. Lisein, H. Claessens, & P. Lejeune. (2016b). Classification of riparian forest species and health condition using multi-temporal and hyperspatial imagery from unmanned aerial system. *Environmental Monitoring and Assessment*, *188*, 146.

Mickelson, J. G., D. L. Civco, & J. a Silander. (1998). Delineating Forest Canopy Species in the Northeastern United States Using Multi-Temporal TM Imagery. *Photogrammetric Engineering & Remote Sensing*, *64*, 891–904.

Milas, A. S., K. Arend, C. Mayer, M. A. Simonson, A. Simic, K. Arend, … M. A. Simonson. (2017). Different colors of shadows: classification of UAV images. *International Journal of Remote Sensing*, *38*(8–10), 3084–3100.

Mitchell, M. G. E., A. F. Suarez-Castro, M. Martinez-Harms, M. Maron, C. McAlpine, K. J. Gaston, … J. R. Rhodes. (2015). Reframing landscape fragmentation's effects on ecosystem services. *Trends in Ecology and Evolution*, *30*(4), 190–198.

Miyoshi, G. T., N. N. Imai, A. M. G. Tommaselli, M. V. A. de Moraes, & E. Honkavaara. (2020). Evaluation of hyperspectral multitemporal information to improve tree species identification in the highly diverse Atlantic forests. *Remote Sensing*, *12*(2), 244.

Morsdorf, F., B. Kötz, E. Meier, K. I. Itten, & B. Allgöwer. (2006). Estimation of LAI and fractional cover from small footprint airborne laser scanning data based on gap fraction. *Remote Sensing of Environment*, *104*(1), 50–61.

Müllerová, J., T. Bartaloš, J. Brůna, P. Dvořák, & M. Vítková. (2017). Unmanned aircraft in nature conservation: an example from plant invasions. *International Journal of Remote Sensing*, *38*(8–10), 2177–2198.

Müllerová, J., J. Brůna, T. Bartaloš, P. Dvořák, M. Vítková, & P. Pyšek. (2017). Timing Is Important: Unmanned Aircraft vs. Satellite Imagery in Plant Invasion Monitoring. *Frontiers in Plant Science*, *8*, 887.

Müllerová, J., J. Brůna, P. Dvořák, T. Bartaloš, & M. Vítková. (2016). Does the data resolution/origin matter? Satellite, airborne and UAV imagery to tackle plant invasions. *International Archives of the Photogrammetry, Remote Sensing and Spatial Information Sciences - ISPRS Archives*, *41*, 903–908.

Murica, C. (1995). Edge Effects in Fragmented Forests: Implications for Conservation. *Trends in Ecology & Evolution*, *10*(2), 58–62.

Næsset, E. (2002). Predicting forest stand characteristics with airborne scanning laser using a practical two-stage procedure and field data. *Remote Sensing of Environment*, *80*(1), 88–99.

Næsset, E. (2004). Practical large-scale forest stand inventory using a small-footprint airborne scanning laser. *Scandinavian Journal of Forest Research*, *19*(2), 164–179.

Næsset, E. (2005). Assessing sensor effects and effects of leaf-off and leaf-on canopy conditions on biophysical stand properties derived from small-footprint airborne laser data. *Remote Sensing of Environment*, *98*(2–3), 356–370.

Næsset, E., & T. Okland. (2002). Estimating tree height and tree crown properties using airborne scanning laser in a boreal. *Remote Sensing of Environment*, *79*(1), 105–115.

Nagendra, H., R. Lucas, J. P. Honrado, R. H. G. Jongman, C. Tarantino, M. Adamo, & P. Mairota. (2013). Remote sensing for conservation monitoring: Assessing protected areas, habitat extent, habitat condition, species diversity, and threats. *Ecological Indicators*, *33*, 45–59.

Narango, D. L., D. W. Tallamy, & P. P. Marra. (2018). Nonnative plants reduce population growth of an insectivorous bird. *Proceedings of the National Academy of Sciences of the United States of America*, *115*(45), 11549–11554.

Nevalainen, O., E. Honkavaara, S. Tuominen, N. Viljanen, T. Hakala, X. Yu, … A. M. G. Tommaselli. (2017). Individual tree detection and classification with UAV-Based photogrammetric point clouds and hyperspectral imaging. *Remote Sensing*, *9*(3), 185.

Niethammer, U., M. R. James, S. Rothmund, J. Travelletti, & M. Joswig. (2012). UAV-based remote sensing of the Super-Sauze landslide: Evaluation and results. *Engineering Geology*, *128*, 2–11.

Nijland, W., R. de Jong, S. M. de Jong, M. A. Wulder, C. W. Bater, & N. C. Coops. (2014). Monitoring plant condition and phenology using infrared sensitive consumer grade digital cameras. *Agricultural and Forest Meteorology*, *184*, 98–106.

Ni, W., J. Liu, Z. Zhang, G. Sun, & A. Yang. (2015). Evaluation of UAS-Based Forest Inventory System Compared with Lidar Data. In *IEEE International Geoscience and Remote Sensing Symposium, 2015. IGARSS '15. Proceedings* (pp. 3874–3877).

Ni, W., G. Sun, Y. Pang, Z. Zhang, J. Liu, A. Yang, … D. Zhang. (2018). Mapping Three-Dimensional Structures of Forest Canopy Using UAV Stereo Imagery: Evaluating Impacts of Forward Overlaps and Image Resolutions with LiDAR Data as Reference. *IEEE Journal of Selected Topics in Applied Earth Observations and Remote Sensing*, *11*(10), 3578–3589.

Nobis, M., & U. Hunziker. (2005). Automatic thresholding for hemispherical canopy-photographs based on edge detection. *Agricultural and Forest Meteorology*, *128*(3–4), 243–250.

Oliver, C. D., & B. C. Larson. (1996). *Forest Stand Dynamics: Updated Edition*. *Forest stand dynamics*. New York, New York: John Wiley and Sons.

Olofsson, P., C. E. Holden, E. L. Bullock, & C. E. Woodcock. (2016). Time series analysis of satellite data reveals continuous deforestation of New England since the 1980s. *Environmental Research Letters*, *11*, 064002.

Ota, T., M. Ogawa, K. Shimizu, T. Kajisa, N. Mizoue, S. Yoshida, … N. Ket. (2015). Aboveground biomass estimation using structure from motion approach with aerial photographs in a seasonal tropical forest. *Forests*, *6*(11), 3882–3898.

Ottosen, T.-B., G. Petch, M. Hanson, & C. A. Skjøth. (2020). Tree cover mapping based on Sentinel-2 images demonstrate high thematic accuracy in Europe. *International Journal of Applied Earth Observation and Geoinformation*, *84*, 101947.

Pádua, L., J. Hruška, J. Bessa, T. Adão, L. Martins, J. Gonçalves, … J. Sousa. (2017a). Multi-Temporal Analysis of Forestry and Coastal Environments Using UASs. *Remote Sensing*, *10*(1), 24.

Pádua, L., J. Vanko, J. Hruška, T. Adão, J. J. Sousa, E. Peres, & R. Morais. (2017b). UAS, sensors, and data processing in agroforestry: a review towards practical applications. *International Journal of Remote Sensing*, *38*(8–10), 2349–2391.

Pasquarella, V. J., C. E. Holden, & C. E. Woodcock. (2018). Improved mapping of forest type using spectral-temporal Landsat features. *Remote Sensing of Environment*, *210*, 193–207.

Pekin, B., & C. Macfarlane. (2009). Measurement of crown cover and leaf area index using digital cover photography and its application to remote sensing. *Remote Sensing*, *1*(4), 1298–1320.

Penner, M., D. G. Pitt, & M. E. Woods. (2013). Parametric vs. nonparametric LiDAR models for operational forest inventory in boreal Ontario. *Canadian Journal of Remote Sensing*, *39*(5), 426–443.

Pinto, S. R. R., G. Mendes, A. M. M. Santos, M. Dantas, M. Tabarelli, & F. P. L. Melo. (2010). Landscape attributes drive complex spatial microclimate configuration of Brazilian Atlantic forest fragments. *Tropical Conservation Science*, *3*(4), 389–402.

Pitt, D. G., M. Woods, & M. Penner. (2014). A comparison of point clouds derived from stereo imagery and airborne laser scanning for the area-based estimation of forest inventory attributes in boreal Ontario. *Canadian Journal of Remote Sensing*, *40*(3), 214–232.

Pugh, T. A. M., M. Lindeskog, B. Smith, B. Poulter, A. Arneth, V. Haverd, & L. Calle. (2019). Role of forest regrowth in global carbon sink dynamics. *Proceedings of the National Academy of Sciences of the United States of America*, 116(10), 4382–4387.

Puliti, S., H. Olerka, T. Gobakken, E. Næsset, H. O. Ørka, T. Gobakken, … E. Næsset. (2015). Inventory of Small Forest Areas Using an Unmanned Aerial System. *Remote Sensing*, *7*(8), 9632–9654.

Puliti, S., S. Solberg, & A. Granhus. (2019). Use of UAV photogrammetric data for estimation of biophysical properties in forest stands under regeneration. *Remote Sensing*, *11*(3), 233.

Pu, R., & S. Landry. (2012). A comparative analysis of high spatial resolution IKONOS and WorldView-2 imagery for mapping urban tree species. *Remote Sensing of Environment*, *124*, 516–533.

Qiu, S., B. He, C. Yin, & Z. Liao. (2017). Assessments of Sentinel-2 vegetation red-edge spectral bands for improving land cover classification. *International Archives of the Photogrammetry, Remote Sensing and Spatial Information Sciences - ISPRS Archives*, *42*, 871–874.

Ranney, J. W., M. C. Bruner, & J. B. Levenson. (1981). The importance of edge in the structure and dynamics of forest islands. In R. L. Burgess & D. M. Sharpe (Eds.), *Forest Island Dynamics in Man-Dominated Landscapes* (1st ed., pp. 67–95). New York, New York: Springer-Verlag New York.

R Core Team. (2020). *R: A Language and Environment for Statistical Computing*. Vienna, Austria: R Foundation for Statistical Computing.

Reinmann, A. B., & L. R. Hutyra. (2017). Edge effects enhance carbon uptake and its vulnerability to climate change in temperate broadleaf forests. *Proceedings of the National Academy of Sciences of the United States of America*, *114*(1), 107–112.

Ries, L., R. J. Fletcher, J. Battin, & T. D. Sisk. (2004). Ecological Responses to Habitat Edges: Mechanisms, Models, and Variability Explained. *Annual Review of Ecology, Evolution, and Systematics, 35*, 491–522.

Riitters, K. H., J. W. Coulston, & J. D. Wickham. (2012). Fragmentation of forest communities in the eastern United States. *Forest Ecology and Management, 263*, 85–93.

Riitters, K. H., & J. D. Wickham. (2012). Decline of forest interior conditions in the conterminous United States. *Scientific Reports, 2*.

Riitters, K. H., J. D. Wickham, R. V. O. Neill, K. B. Jones, R. Smith, J. W. Coulston, … E. R. Smith. (2002). Fragmentation of Continental Fragmentation United Forests. *Ecosystems*, *5*(8), 815–822.

Rodriguez-Galiano, V. F., M. Chica-Olmo, F. Abarca-Hernandez, P. M. Atkinson, & C. Jeganathan. (2012). Random Forest classification of Mediterranean land cover using multi-seasonal imagery and multi-seasonal texture. *Remote Sensing of Environment*, *121*, 93–107.

Roth, L., & B. Streit. (2018). Predicting cover crop biomass by lightweight UAS-based RGB and NIR photography: an applied photogrammetric approach. *Precision Agriculture, 19*, 93–114.

Roussel, J. R., D. Auty, N. C. Coops, P. Tompalski, T. R. H. Goodbody, A. S. Meador, … A. Achim. (2020). lidR: An R package for analysis of Airborne Laser Scanning (ALS) data. *Remote Sensing of Environment, 251*, 112061.

Ruiz, L. A., T. Hermosilla, F. Mauro, & M. Godino. (2014). Analysis of the influence of plot size and LiDAR density on forest structure attribute estimates. *Forests, 5*(5), 936–951.

Rustad, L., J. Campbell, J. S. Dukes, T. Huntington, K. F. Lambert, J. Mohan, & N. Rodenhouse. (2012). *Changing climate, changing forests: the impacts of climate change on forests of the Northeastern United States and Eastern Canada*. Newtown Square, PA.

Saarinen, N., M. Vastaranta, R. Näsi, T. Rosnell, T. Hakala, E. Honkavaara, … J. Hyyppä. (2018). Assessing biodiversity in boreal forests with UAV-based photogrammetric point clouds and hyperspectral imaging. *Remote Sensing*, *10*(2), 338.

Saunders, D. A., R. J. Hobbs, & C. R. Margules. (1991). Biological Consequences of Ecosystem Fragmentation - a Review. *Conservation Biology*, *5*(1), 18–32.

Seifert, E., S. Seifert, H. Vogt, D. Drew, J. van Aardt, A. Kunneke, & T. Seifert. (2019). Influence of drone altitude, image overlap, and optical sensor resolution on multi-view reconstruction of forest images. *Remote Sensing*, *11*(10), 1252.

SenseFly. (2020). *eMotion User Manual Revision 3.1* (v3.1). Cheseaux-sur-Lausanne, Switzerland: SenseFly SA.

Sexton, J. O., X. P. Song, M. Feng, P. Noojipady, A. Anand, C. Huang, … J. R. Townshend. (2013). Global, 30-m resolution continuous fields of tree cover: Landsat-based rescaling of MODIS

vegetation continuous fields with lidar-based estimates of error. *International Journal of Digital Earth*, *6*(5), 427–448.

Shin, P., T. Sankey, M. M. Moore, & A. E. Thode. (2018). Evaluating unmanned aerial vehicle images for estimating forest canopy fuels in a ponderosa pine stand. *Remote Sensing*, *10*(8), 1266.

Smith, I. A., L. R. Hutyra, A. B. Reinmann, J. K. Marrs, & J. R. Thompson. (2018). Piecing together the fragments: elucidating edge effects on forest carbon dynamics. *Frontiers in Ecology and the Environment*, *16*(4), 213–221.

Smith, M. W., J. L. Carrivick, & D. J. Quincey. (2016). Structure from motion photogrammetry in physical geography. *Progress in Physical Geography*, *40*(2), 247–275.

Snavely, N., S. M. Seitz, & R. Szeliski. (2008). Modeling the world from Internet photo collections. *International Journal of Computer Vision*, *80*(2), 189–210.

Song, W., X. Mu, G. Yan, & S. Huang. (2015). Extracting the green fractional vegetation cover from digital images using a shadow-resistant algorithm (SHAR-LABFVC). *Remote Sensing*, *7*(8), 10425–10443.

Sperduto, D. D., & W. F. Nichols. (2012). Natural Communities of New Hampshire, 266.

Story, M., & R. G. Congalton. (1986). Accuracy Assessment: A User's Perspective. *Photogrammetric Engineering & Remote Sensing*, *52*(3), 397–399.

Sugumaran, R., M. K. Pavuluri, & D. Zerr. (2003). The use of high-resolution imagery for identification of urban climax forest species using traditional and rule-based classification approach. *IEEE Transactions on Geoscience and Remote Sensing*, *41*(9), 1933–1939.

Swayze, N. C., W. T. Tinkham, J. C. Vogeler, & A. T. Hudak. (2021). Influence of flight parameters on UAS-based monitoring of tree height, diameter, and density. *Remote Sensing of Environment*, *263*, 112540.

Tallamy, D. W., & K. J. Shropshire. (2009). Ranking lepidopteran use of native versus introduced plants. *Conservation Biology*, *23*(4), 941–947.

Tang, L., & G. Shao. (2015). Drone remote sensing for forestry research and practices. *Journal of Forestry Research*, *26*(4), 791–797.

Tigges, J., T. Lakes, & P. Hostert. (2013). Urban vegetation classification: Benefits of multitemporal RapidEye satellite data. *Remote Sensing of Environment*, *136*, 66–75.

Tinkham, W. T., & N. C. Swayze. (2021). Influence of Agisoft Metashape parameters on UAS structure from motion individual tree detection from canopy height models. *Forests*, *12*(2), 250.

Tmušić, G., S. Manfreda, H. Aasen, M. R. James, G. Gonçalves, E. Ben-Dor, … M. F. McCabe. (2020). Current practices in UAS-based environmental monitoring. *Remote Sensing*, *12*(6), 1001.

Tomaštík, J., M. Mokroš, P. Surový, A. Grznárová, & J. Merganič. (2019). UAV RTK/PPK method-An optimal solution for mapping inaccessible forested areas? *Remote Sensing*, *11*(6), 721.

Torres-Sánchez, J., F. López-Granados, I. Borra-Serrano, & J. M. Peña. (2017). Assessing UAV-collected image overlap influence on computation time and digital surface model accuracy in olive orchards. *Precision Agriculture*, *19*(1), 115–133.

Turner, W., S. Spector, N. Gardiner, M. Fladeland, E. Sterling, & M. Steininger. (2003). Remote sensing for biodiversity science and conservation. *Trends in Ecology and Evolution*, *18*(6), 306-314.

Tu, Y. H., K. Johansen, S. Phinn, & A. Robson. (2019). Measuring canopy structure and condition using multi-spectral UAS imagery in a horticultural environment. *Remote Sensing*, *11*(3), 269.

van Leeuwen, M., & M. Nieuwenhuis. (2010). Retrieval of forest structural parameters using LiDAR remote sensing. *European Journal of Forest Research*, *129*(4), 749–770.

Vastaranta, M., M. A. Wulder, J. C. White, A. Pekkarinen, S. Tuominen, C. Ginzler, … H. Hyyppa. (2013). Airborne laser scanning and digital stereo imagery measures of forest structure: Comparative results and implications to forest mapping and inventory update. *Canadian Journal of Remote Sensing*, *39*(5), 382–395.

Vaughn, N. R., G. P. Asner, & C. P. Giardina. (2014). Centennial impacts of fragmentation on the canopy structure of tropical montane forest. *Ecological Applications*, *24*(7), 1638–1650.

Vaughn, N. R., G. P. Asner, & C. P. Giardina. (2015). Long-term fragmentation effects on the distribution and dynamics of canopy gaps in a tropical montane forest. *Ecosphere*, *6*(12), 271.

Vega, C., A. Hamrouni, A. el Mokhtari, M. Morel, J. Bock, J. P. Renaud, … S. Durrieue. (2014). PTrees: A point-based approach to forest tree extraction from lidar data. *International Journal of Applied Earth Observation and Geoinformation*, *33*(1), 98–108.

ver Planck, N. R., A. O. Finley, J. A. Kershaw, A. R. Weiskittel, & M. C. Kress. (2018). Hierarchical Bayesian models for small area estimation of forest variables using LiDAR. *Remote Sensing of Environment*, *204*, 287–295.

Vierling, K. T., L. A. Vierling, W. A. Gould, S. Martinuzzi, & R. M. Clawges. (2008). Lidar: Shedding new light on habitat characterization and modeling. *Frontiers in Ecology and the Environment*, *6*(2), 90–98.

Villikka, M., P. Packalén, & M. Maltamo. (2012). The suitability of leaf-off airborne laser scanning data in an area-based forest inventory of coniferous and deciduous trees. *Silva Fennica*, *46*(1), 99–110.

Vogelmann, J. E. (1995). Assessment of Forest Fragmentation in Southern New England Using Remote Sensing and Geographic Information Systems Technology. *Conservation Biology*, *9*(2), 439–449.

Wallace, L., C. Bellman, B. Hally, J. Hernandez, S. Jones, & S. Hillman. (2019). Assessing the Ability of Image Based Point Clouds Captured from a UAV to Measure the Terrain in the Presence of Canopy Cover. *Forests*, *10*(3), 284.

Wallace, L., A. Lucieer, Z. Malenovský, D. Turner, P. Vopěnka, Z. Malenovskỳ, … P. Vopěnka. (2016). Assessment of forest structure using two UAV techniques: A comparison of airborne laser scanning and structure from motion (SfM) point clouds. *Forests*, *7*(3), 62.

Wasser, L., L. Chasmer, R. Day, & A. Taylor. (2015). Quantifying land use effects on forested riparian buffer vegetation structure using LiDAR data. *Ecosphere*, *6*(1), 10.

Wasser, L., R. Day, L. Chasmer, & A. Taylor. (2013). Influence of Vegetation Structure on Lidar-derived Canopy Height and Fractional Cover in Forested Riparian Buffers During Leaf-Off and Leaf-On Conditions. *PLoS ONE*, *8*(1), e54776.

Weil, G., I. M. Lensky, Y. S. Resheff, & N. Levin. (2017). Optimizing the timing of unmanned aerial vehicle image acquisition for applied mapping of woody vegetation species using feature selection. *Remote Sensing*, *9*(11). 1130.

Westoby, M. J., J. Brasington, N. F. Glasser, M. J. Hambrey, & J. M. Reynolds. (2012). "Structure-from-Motion" photogrammetry: A low-cost, effective tool for geoscience applications. *Geomorphology*, *179*, 300–314.

Westveld, M. (1956). Natural forest vegetation zones of New England. *Journal of Forestry*, *54*, 332–338.

Whitehead, K., & C. H. Hugenholtz. (2014a). Remote sensing of the environment with small, unmanned aircraft systems (UASs), part 1: A review of progress and challenges Remote sensing of the environment with small, unmanned aircraft systems (UASs), part 1: a review of progress and challenges. *Journal of Unmanned Vehicle Systems*, *2*, 69–85.

Whitehead, K., & C. H. Hugenholtz. (2014b). Remote sensing of the environment with small, unmanned aircraft systems (UASs), part 2: scientific and commercial applications. *Journal of Unmanned Vehicle Systems*, *2*, 86–102.

White, J. C., J. T. T. R. Arnett, M. A. Wulder, P. Tompalski, & N. C. Coops. (2015). Evaluating the impact of leaf-on and leaf-off airborne laser scanning data on the estimation of forest inventory attributes with the area-based approach. *Canadian Journal of Forest Research*, *45*(11), 1498–1513.

White, J. C., N. C. Coops, M. A. Wulder, M. Vastaranta, T. Hilker, & P. Tompalski. (2016). Remote Sensing Technologies for Enhancing Forest Inventories: A Review. *Canadian Journal of Remote Sensing*, *42*(5), 619–641.

White, J. C., C. Stepper, P. Tompalski, N. C. Coops, & M. A. Wulder. (2015). Comparing ALS and image-based point cloud metrics and modelled forest inventory attributes in a complex coastal forest environment. *Forests*, *6*(10), 3704–3732.

White, J. C., M. A. Wulder, A. Varhola, M. Vastaranta, N. C. Coops, B. D. Cook, … M. Woods. (2013). *A best practices guide for generating forest inventory attributes from airborne laser scanning data using an area-based approach* (Vol. FI-X-010). Victoria, British Columbia The: Natural Resources Canada, Canadian Forest Service, Canadian Wood Fibre Centre.

White, J. C., M. A. Wulder, M. Vastaranta, N. C. Coops, D. Pitt, & M. Woods. (2013). The utility of image-based point clouds for forest inventory: A comparison with airborne laser scanning. *Forests*, *4*(3), 518–536.

Wiens, J., R. Sutter, M. Anderson, J. Blanchard, A. Barnett, N. Aguilar-Amuchastegui, … S. Laine. (2009). Selecting and conserving lands for biodiversity: The role of remote sensing. *Remote Sensing of Environment*, *113*(7), 1370–1381.

Wijesingha, J., T. Astor, D. Schulze-Brüninghoff, & M. Wachendorf. (2020). Mapping Invasive Lupinus polyphyllus Lindl. in Semi-natural Grasslands Using Object-Based Image Analysis of UAV-borne Images. *PFG - Journal of Photogrammetry, Remote Sensing and Geoinformation Science*, *88*, 391–406.

Wilcove, D. S., C. H. McLellan, & A. P. Dobson. (1986). Habitat Fragmentation in the temperate zone. *Conservation Biology: The Science of Scarcity and Diversity*.

Wolter, P. T., D. J. Mladenoff, G. E. Host, & T. R. Crow. (1995). Improved forest classification in the northern Lake States using multi-temporal Landsat imagery. *Photogrammetric Engineering and Remote Sensing*, *61*(9), 1129–1143.

Wood, S. N. (2017). *Generalized additive models: An introduction with R, second edition* (2nd ed.). Boca Raton, FL: CRC Press.

Wulder, M. A., C. W. Bater, N. C. Coops, T. Hilker, & J. C. White. (2008). The role of LiDAR in sustainable forest management. *Forestry Chronicle*, *84*(6), 807–826.

Wulder, M. A., R. J. Hall, N. C. Coops, & S. E. Franklin. (2004). High Spatial Resolution Remotely Sensed Data for Ecosystem Characterization. *BioScience*, *54*(6), 511–521.

Wulder, M. A., J. C. White, R. F. Nelson, E. Næsset, H. O. Ørka, N. C. Coops, … T. Gobakken. (2012). Lidar sampling for large-area forest characterization: A review. *Remote Sensing of Environment*, *121*, 196–209.

Yaney-Keller, A., P. S. Tomillo, J. M. Marshall, & F. v. Paladino. (2019). Using unmanned aerial systems (UAS) to assay mangrove estuaries on the pacific coast of Costa Rica. *PLoS ONE*, *14*(6), e0217310.

Yan, G., L. Li, A. Coy, X. Mu, S. Chen, D. Xie, … H. Zhou. (2019). Improving the estimation of fractional vegetation cover from UAV RGB imagery by color unmixing. *ISPRS Journal of Photogrammetry and Remote Sensing*, *158*, 23–34.

Zankel, M., C. Copeland, J. Robinson, C. Sinnott, D. Sundquist, T. Walker, & J. Alford. (2006). *The Land Conservation Plan for New Hampshire's Coastal Watersheds*. Concord, NH: New Hampshire Estuaries Project.

Zhang, J., J. Hu, J. Lian, Z. Fan, X. Ouyang, & W. Ye. (2016). Seeing the forest from drones: Testing the potential of lightweight drones as a tool for long-term forest monitoring. *Biological Conservation*, *198*, 60–69.

Zheng, D., L. S. Heath, M. J. Ducey, & B. Butler. (2010). Relationships between major ownerships, forest aboveground biomass distributions, and landscape dynamics in the New England region of USA. *Environmental Management*, 45(2), 377–386.

Zheng, D., L. S. Heath, M. J. Ducey, & J. E. Smith. (2011). Carbon changes in conterminous US forests associated with growth and major disturbances: 1992-2001. *Environmental Research Letters*, 6, 014012.

Zhu, X., & D. Liu. (2014). Accurate mapping of forest types using dense seasonal Landsat time-series. *ISPRS Journal of Photogrammetry and Remote Sensing*, *96*, 1–11.

Zielewska-Büttner, K., P. Adler, M. Ehmann, & V. Braunisch. (2016). Automated detection of forest gaps in spruce dominated stands using canopy height models derived from stereo aerial imagery. *Remote Sensing*, *8*(3), 175.

Ziter, C., E. M. Bennett, & A. Gonzalez. (2014). Temperate forest fragments maintain aboveground carbon stocks out to the forest edge despite changes in community composition. *Oecologia*, *176*(3), 893–902.

APPENDIX

APPENDIX

Table 12. Accuracy for all Aeria classifications. Overall accuracy (OA) is reported here as the average OA of the 30 classification iterations performed for each combination. The standard deviations (STDs) are given. The results are sorted by the number of dates included in the combination and the average OA.

		Date Combination	Average OA	STD
One Date	1	4-26-20	0.248	0.004
	5	6-27-20	0.313	0.005
	4	6-12-19	0.332	0.005
	2	5-16-19	0.346	0.004
	3	5-30-19	0.373	0.005
Two Dates	8	4-26-20 + 6-12-19	0.370	0.005
	15	6-12-19 + 6-27-20	0.391	0.006
	9	4-26-20 + 6-27-20	0.404	0.006
	7	4-26-20 + 5-30-19	0.429	0.005
	6	4-26-20 + 5-16-19	0.437	0.004
	13	5-30-19 + 6-12-19	0.440	0.006
	14	5-30-19 + 6-27-20	0.466	0.005
	11	5-16-19 + 6-12-19	0.479	0.006
	12	5-16-19 + 6-27-20	0.511	0.005
	10	5-16-19 + 5-30-19	0.540	0.005
Three Dates	21	4-26-20 + 6-12-19 + 6-27-20	0.430	0.005
	19	4-26-20 + 5-30-19 + 6-12-19	0.479	0.006
	25	5-30-19 + 6-12-19 + 6-27-20	0.501	0.006
	20	4-26-20 + 5-30-19 + 6-27-20	0.507	0.006
	17	4-26-20 + 5-16-19 + 6-12-19	0.524	0.005
	18	4-26-20 + 5-16-19 + 6-27-20	0.534	0.005
	24	5-16-19 + 6-12-19 + 6-27-20	0.550	0.004
	16	4-26-20 + 5-16-19 + 5-30-19	0.555	0.006
	22	5-16-19 + 5-30-19 + 6-12-19	0.567	0.005
	23	5-16-19 + 5-30-19 + 6-27-20	0.588	0.005
Four Dates	29	4-26-20 + 5-30-19 + 6-12-19 + 6-27-20	0.513	0.005
	28	4-26-20 + 5-16-19 + 6-12-19 + 6-27-20	0.554	0.004
	26	4-26-20 + 5-16-19 + 5-30-19 + 6-12-19	0.598	0.006
	30	5-16-19 + 5-30-19 + 6-12-19 + 6-27-20	0.604	0.006
	27	4-26-20 + 5-16-19 + 5-30-19 + 6-27-20	0.609	0.006
All	31	4-26-20 + 5-16-19 + 5-30-19 + 6-12-19 + 6-27-20	0.611	0.005

Table 13. Accuracy for all Sequoia classifications. Overall accuracy (OA) is reported here as the average OA of the 30 classification iterations performed for each combination. The standard deviations (STDs) are given. The results are sorted by the number of dates included in the combination and the average OA.

		Date Combination	Average OA	STD
One Date	2	5-15-20	0.270	0.005
	1	4-28-20	0.272	0.005
	4	6-10-20	0.315	0.006
	5	6-26-20	0.333	0.006
	3	5-29-20	0.362	0.006
Two Dates	6	4-28-20 + 5-15-20	0.362	0.004
	8	4-28-20 + 6-10-20	0.375	0.004
	9	4-28-20 + 6-26-20	0.393	0.005
	15	6-10-20 + 6-26-20	0.405	0.005
	11	5-15-20 + 6-10-20	0.431	0.006
	7	4-28-20 + 5-29-20	0.450	0.005
	13	5-29-20 + 6-10-20	0.455	0.004
	12	5-15-20 + 6-26-20	0.457	0.006
	10	5-15-20 + 5-29-20	0.489	0.005
	14	5-29-20 + 6-26-20	0.495	0.007
Three Dates	21	4-28-20 + 6-10-20 + 6-26-20	0.437	0.005
	17	4-28-20 + 5-15-20 + 6-10-20	0.452	0.007
	18	4-28-20 + 5-15-20 + 6-26-20	0.462	0.006
	19	4-28-20 + 5-29-20 + 6-10-20	0.470	0.007
	24	5-15-20 + 6-10-20 + 6-26-20	0.479	0.005
	25	5-29-20 + 6-10-20 + 6-26-20	0.494	0.006
	22	5-15-20 + 5-29-20 + 6-10-20	0.502	0.005
	20	4-28-20 + 5-29-20 + 6-26-20	0.513	0.006
	16	4-28-20 + 5-15-20 + 5-29-20	0.515	0.006
	23	5-15-20 + 5-29-20 + 6-26-20	0.539	0.005
Four Dates	28	4-28-20 + 5-15-20 + 6-10-20 + 6-26-20	0.478	0.005
	29	4-28-20 + 5-29-20 + 6-10-20 + 6-26-20	0.523	0.008
	30	5-15-20 + 5-29-20 + 6-10-20 + 6-26-20	0.528	0.005
	26	4-28-20 + 5-15-20 + 5-29-20 + 6-10-20	0.528	0.006
	27	4-28-20 + 5-15-20 + 5-29-20 + 6-26-20	0.555	0.006
All	31	4-28-20 + 5-15-20 + 5-29-20 + 6-10-20 + 6-26-20	0.542	0.007